Observed Characteristics of Turbulence in the Atmospheric Boundary Layer over Mountainous Terrain

by
David C. Hahn

Department of Atmospheric Science
Colorado State University
Fort Collins, Colorado

Colorado State University

Department of Atmospheric Science

Paper No. 332

OBSERVED CHARACTERISTICS OF TURBULENCE IN THE ATMOSPHERIC BOUNDARY LAYER OVER MOUNTAINOUS TERRAIN

by

David C. Hahn

Research Supported by the

National Science Foundation

under Grant ATM76-83361

Department of Atmospheric Science

Colorado State University

Fort Collins, Colorado

December, 1980

Atmospheric Science Paper No. 332

ABSTRACT OF THESIS

entitled

OBSERVED CHARACTERISTICS OF TURBULENCE IN
THE ATMOSPHERIC BOUNDARY LAYER OVER MOUNTAINOUS TERRAIN

This study examines the location and development of turbulence in the morning hours of boundary layer development over mountainous terrain. Four case study days are presented which illustrate important features on two types of days observed in the mountains of central Colorado.

The study site is located on a broad and elevated plain called South Park which is bordered on the north and west by relatively high mountain ranges. Smaller mountains are present to the south and east. This area is thought to be an important genesis area of convective systems that migrate out onto the plains of eastern Colorado.

These case studies use data taken during the 1977 South Park Area Cumulus Experiment (SPACE). The primary source of data is the NCAR Queenair aircraft. Supporting data sources include a surface network of 19 meteorological stations located throughout the study area and rawinsondes launched 3 or 4 times per day. The data are analyzed through the use of the clear air conservative variables, mixing ratio and potential temperature. Various terms of the turbulent kinetic energy (TKE) equation, thought to be important on the different days, are analyzed in a spatially varying sense which allows for horizontal variability to be detected.

One type of case study day is characterized by extensive cumulus convection. The winds aloft are generally light and moisture is available, especially to the southeast at lower surface levels. The clouds

originate over the mountainous areas apparently the result of the convergence of upslope winds. They can then act as a coupling mechanism between the above-ridge-top and below-ridge-top air masses. Turbulent mixing and associated evaporational cooling creates downdrafts which allow for the downward movement of higher momentum air aloft. The formation of surface gust fronts and convergence zones, and their concomitant precipitating cloud systems, results.

The second type of case study day is characterized by strong dry westerly winds at mountain ridgetop that, by midafternoon, work their way down to the surface of South Park and the boundary layer becomes well-mixed and dry. The strong, upper-level winds reach the surface when below-ridge-top air, being well-mixed due to surface heating, and the above-ridge-top air, being well-mixed due to shear instability, approach the same potential temperature. As a result of this the moisture, initially available in South Park and also advected in from the southeast as morning upslope and upvalley winds, is flushed out of the Park and limited cloud development occurs.

David C. Hahn
Department of Atmospheric Science
Colorado State University
Fort Collins, Colorado 80523
December, 1980

ACKNOWLEDGMENTS

The author would like to express his deep gratitude to Robert M. Banta for his support throughout the preparation of this paper, Prof. William R. Cotton for his review and suggestions, Dr. Donald Lenschow for his helpful suggestions regarding various methods of calculations, Prof. Peter C. Sinclair for his helpful comments about aircraft data, Raymond L. George and Kevin R. Knupp for their fruitful conversations, and Lucy McCall and Mark Howes for the drafting of many complex figures. A special thanks is extended to Polly Laun Cletcher for typing the manuscript.

This research was sponsored by National Science Foundation (NSF) Grant #ATM76-83361. Computer time was provided by the National Center for Atmospheric Research computing facility, which is sponsored by NSF, and located in Boulder, Colorado.

TABLE OF CONTENTS

LIST OF TABLES

LIST OF FIGURES

1.0 INTRODUCTION

This study describes the location and development of turbulence in and slightly above the evolving unstable atmospheric boundary layer over mountainous terrain. Terrain is shown to substantially influence the localization of highly turbulent areas.

The spatial variability of turbulence is analyzed through the use of terms in the turbulent kinetic energy (TKE) equation which is evaluated on two scales of motion. Averaged deviations from the large-scale mean flow are used, representing all scales of motion discernible by the aircraft, as well as averaged deviations from the smoothed data representing small-scale motion.

NCAR Queenair aircraft data from the 1977 South Park Area Cumulus Experiment of Colorado State University were used. The aircraft flight legs were centered over and around a broad, elevated plain called South Park. The plain is bordered on the north and west by relatively high mountain ranges. East-west flight patterns were flown above and to the lee of the north-south mountain range bordering the Park on its western edge. The flights occurred in the morning hours when surface heating begins. Three to four different flight elevations were flown at various levels of the boundary layer from 200 m AGL upward.

Two types of case study days were chosen which illustrate important features of the boundary layer on different types of days in South Park. The first set of days, July 14 and July 15, represent features typical of days when cumulus convection originates over the mountain peaks resulting in the formation of many clouds or cloud systems that precipitate. Winds at and just above mountain ridgetop are light and have little vertical

shear. The air is fairly moist. These conditions, and a favorable surface pressure gradient that allows low-level moisture to reach South Park from the south or east, were generally observed to be necessary for significant cumulus development.

The second type of day has strong dry winds at mountain ridgetop that eventually work their way down to the surface of South Park. There is limited cumulus cloud development and the formation of precipitation is either delayed or suppressed throughout the day.

Cross-sectional plots of the clear air conservative variables, mixing ratio and potential temperature, made primarily from the aircraft data, are used to discern the basic characteristics of the boundary layer to the lee of the mountain crest. Supplemental data sources include surface meteorological stations, rawinsondes, and a tethered balloon. Analysis of the TKE field allows elucidation of the nature of the turbulent flow. Calculations of buoyancy production were made on the convective days as this was considered to be the term of greatest importance. On windy days, calculations of buoyancy production, shear production, horizontal convergence of TKE, and advection of TKE were made. An estimation of dissipation was done for both types of days. Additionally, attempts were made to draw streamlines characteristic of the flow on the windy days.

The study represents a somewhat unique examination of the boundary layer since it takes place in a mountainous environment. Previous studies have focused on the boundary layer over flat surfaces or on individual aspects of mountain circulations such as wave flow or slope-valley winds. This study attempts to integrate these mountainous features with features of the developing convective boundary layer.

2.0 BACKGROUND

2.1 General Characteristics of the ABL Over Flat Surfaces

The general characteristics of the unstable planetary boundary layer over flat surfaces have been examined for over a decade now. Several experiments and models derived from them suggest that we are arriving at a good conceptual picture of the developing unstable boundary layer. Most experimenters have interpreted their data in terms of the turbulent kinetic energy budget equation. Turbulence is defined as deviations from mean quantities and partitioned into various production and transport modes. These are used to describe the development of the boundary layer.

In high Reynolds number atmospheric turbulence, the budget of turbulent kinetic energy per unit mass is expressed by (Lumley and Panofsky, 1964)

$$\frac{1}{2}\frac{\partial \overline{u_i u_i}}{\partial t} + \frac{U_j}{2}\frac{\partial \overline{u_i u_i}}{\partial x_j} = -\overline{u_i u_j}\frac{\partial U_i}{\partial x_j} + \frac{g\overline{T_v' u_3}}{T_v}$$

$$-\frac{1}{2}\frac{\partial \overline{u_i u_i u_j}}{\partial x_j} - \nu\frac{\partial u_i}{\partial x_j}\frac{\partial u_i}{x_j} - \frac{1}{\rho_o}\frac{\partial \overline{pu_i}}{\partial x_i} \quad . \tag{1}$$

U_i and u_i are the mean and fluctuating parts, respectively, of velocity in the x_i direction, and repeated indices are summed; T_v and T_v' are the mean and fluctuating virtual temperature; ρ_o is the mean density; p the fluctuating pressure; and g the acceleration of gravity. The equation is greatly simplified in horizontally homogeneous conditions and most studies have been performed under these conditions. If it is assumed that mean quantities vary only in the vertical direction, the mean velocity U

is unidirectional and aligned with the mean wind, turbulence is isotropic, and the TKE budget is in equilibrium (i.e., the left-hand side of (1) is zero), the simplified turbulent kinetic energy budget equation becomes:

$$\overline{uw}\ \frac{\partial U}{\partial z} - \frac{g}{T_v}\overline{wT'_v} + \frac{\partial \overline{wq^2}}{\partial z} + 15\nu\ \overline{\frac{\partial u}{\partial x}^2} + \frac{1}{\rho}\frac{\overline{\partial pw}}{\partial z} = 0 \quad , \tag{2}$$

where $q^2 = u^2 + v^2 + w^2$.

The remaining terms are (in order) shear or mechanical production, buoyant production, vertical turbulent transport, dissipation, and transport by pressure. The first four terms are measurable and are often the considerations of experimental design. The last term represents the transfer of kinetic energy from one region in space to another due to correlations between fluctuating pressure and velocity. It cannot be accurately measured by present technology and is usually assumed to be small and calculated as a remainder or residual in budget considerations.

The 1968 Kansas Surface Layer Experiment concentrated on the first 32 m of the boundary layer. The results showed an unstable surface layer transports turbulence vertically to balance production due to heating and wind shear near the surface. Generally speaking, this layer of air provides the turbulent input that drives the developing boundary layer. It is a relatively thin layer of air being on the order of tens of meters thick.

The 1973 Minnesota Boundary Layer Experiment provided an extension of the Kansas surface layer data to the mixed layer above it. The generalized structure is revealed by Kaimel et al. (1976). The mixed layer is considered to be an efficient zone of turbulent mixing as evidenced by the constancy of potential temperature in that layer. A

later paper by Caughey et al. (1979) analyzed the turbulent kinetic energy budget of the surface and mixed layers. The energy balance terms showed a buoyantly-driven turbulent boundary layer. Shear production was significant in the surface layer but unimportant in the mixed layer where the vertical wind gradient was small.

Aircraft measurements have greatly expanded boundary layer experimental capabilities. Both the Kansas and Minnesota experiments were based on fixed-point sensor measurements and were of necessity one-dimensional and generally within the surface layer. Generally, the aircraft results (e.g., Zubkovsky, 1970) have shown comparable results, but have also provided observations over a greater depth of the ABL. In addition, aircraft data have allowed the elucidation of certain two-dimensional features of the boundary layer. Lenschow (1970), examining the characteristics of the mixed layer over relatively flat (and treeless) terrain in southeastern Colorado, revealed the presence of elongated thermals stretched in the direction of the mean wind. The turbulent kinetic energy budget showed similar features to the Minnesota experiment. Nicholls (1978) has revealed semiorganized motion in the boundary layer over the North Sea involving convective rolls.

Recently, a few studies have focused on the spatial variability of the boundary layer due to horizontal inhomogeneities in surface vegetation, soil type, and in a limited sense, topography. Wood (1977) compared surface layer flux densities of heat and moisture from various sites in southern England, yet detected minimal differences. The 1974 Cooperative Atmospheric Boundary Layer Experiment also over England had as one of its objectives: "to investigate the spatial variation of heat flux profile and boundary layer development". The results generally

showed minimal horizontal variation in heat flux. However, these experiments still represented fairly uniform terrain features.

The general conclusions to be drawn from these studies of the unstable boundary layer on a clear sunny day are that over flat surfaces low-level buoyant production of turbulent kinetic energy drives the evolving boundary layer by the generation of warm thermals near the surface which mix upwards into the boundary layer. The mixing is balanced by the vertical turbulent transport of TKE. Dissipation of turbulent kinetic energy is relatively constant with respect to height, and shear generation, important in the surface layer, tends to fall to minimal levels in the mixed layer. Some structural organization may also be present.

A summary of the TKE budget terms is given in Fig. 2.1.

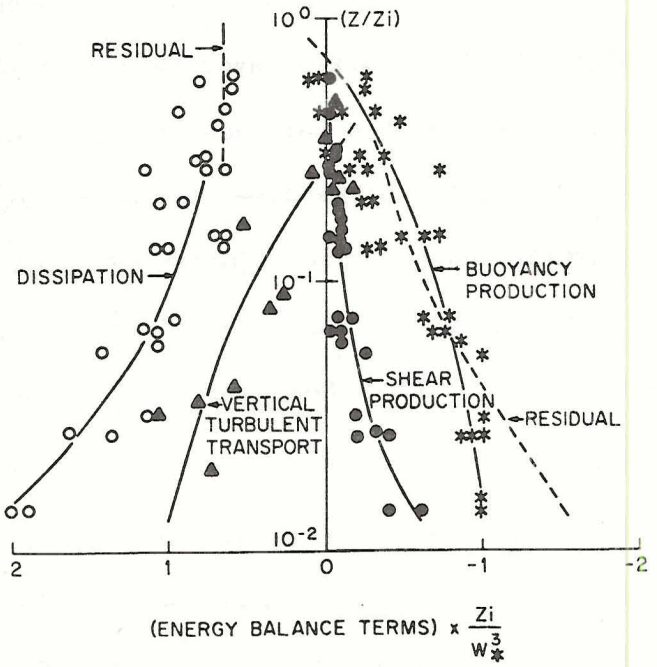

Figure 2.1 Summary of terms of the TKE budget equation. Terms of the TKE equation nondimensionalized with respect to surface layer heat flux. The dimensionless terms are expected to be functions of surface heat flux (included in W_*) and boundary layer height Z_i. Note that the vertical scale is logarithmic. Data is from the Minnesota Boundary Layer Experiment. From Caughey and Wyngaard (1979).

2.2 Studies over Inhomogeneous Terrain

Various additional terms in the TKE equation become important when terrain inhomogeneities are considered. In the surface layer, Peterson (1972) has shown through a numerical model that for a surface roughness change, advection and flux divergence become significant and greater than mechanical production. Surface inhomogeneities, however, are expressed as anything from vegetation changes to large terrain variations.

Recently Lenschow et al. (1979) has presented data that illustrates the developmental characteristics of an evolving boundary layer over marginally hilly terrain in which potentially cooler air (4°K) has drained into the valleys (10 km wide). The data are taken from two separate sites in eastern Colorado where topographic variations as high as 100 m/10 km are common. The localized pockets of potentially cool air result from radiational cooling and drainage during the night. As surface heating begins the air above the ridgetops becomes well-mixed earlier than air in the valley due to its higher potential temperature. Higher momentum air from aloft can then mix down near the ridgetops. Above the valleys, stability decreases due to this higher momentum air being brought down. The resulting shear stress then becomes large enough to effectively pull the potentially cool air out of the valley and aid in the subsequent advection of warmer upstream air associated with the ridgetop. A sudden rise in temperature preceding a rise in wind speed by 20 to 40 minutes is the result. This type of boundary layer development is different from that occurring over flat terrain in that buoyant production is not a major source of TKE in the valleys.

These features of the ABL occurring over inhomogeneous terrain are the direct result of topographical variations. As the terrain becomes more varied additional considerations are necessary. Steeper slopes allow the development of upslope winds and more organized upvalley winds. Forced air flow over a mountain barrier can result in the formation of gravity waves and the possiblity of turbulence associated with them.

2.3 Additional Considerations of a Mountainous Boundary Layer

We know little of the boundary layer over truly inhomogeneous terrain such as mountains. Additional factors must be considered such as slope-valley winds and the formation of gravity waves induced by terrain features.

2.3.1 Slope-valley winds

Slope-valley winds have been studied for a long time and are an important consideration in the study of the unstable ABL over mountainous terrain. Defant (1951) provides a good summary of this flow (Fig. 2.2). Basically, upslope winds are caused by the heating of air next to the mountain slope. This results in the formation of potentially warm air (relative to adjacent areas that are at the same height and not under the influence of a mountain) which begins to flow (rise) 1/4 to 3/4 of an hour after sunrise. The depth of the upslope flow is typically 100-200 m with speeds of about 3-5 m/s.

On the larger scale, valley winds also show this diurnal variation. The term valley wind is used here to designate flow occurring on a scale greater than that of an individual slope. Hence valley winds represent a more organized flow not necessarily in the local terrain fall line.

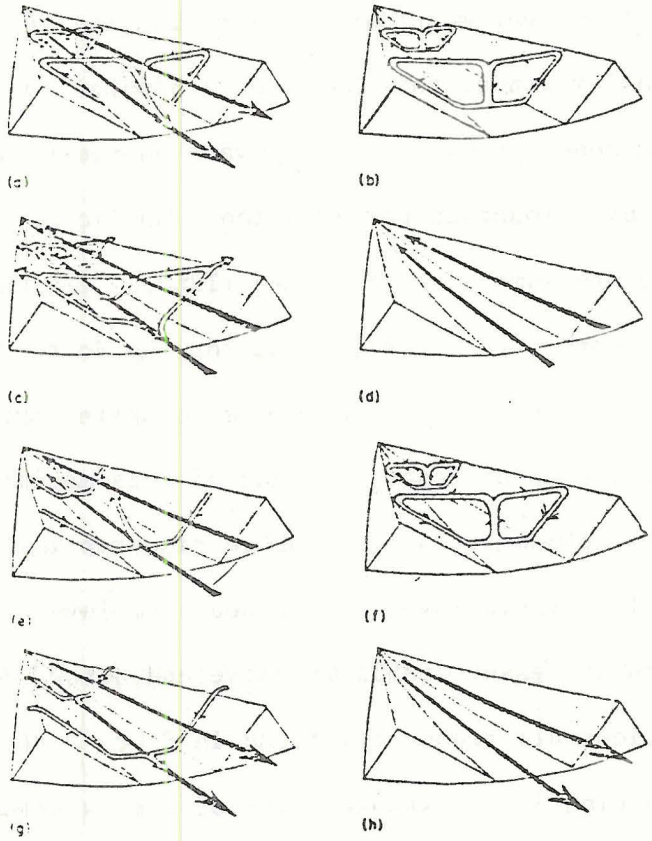

Schematic illustration of the normal diurnal variations of the air currents in a valley. (After F. Defant [17].)
(a) Sunrise; onset of upslope winds (white arrows), continuation of mountain wind (black arrows). Valley cold, plains warm.
(b) Forenoon (about 1900); strong slope winds, transition from mountain wind to valley wind. Valley temperature same as plains.
(c) Noon and early afternoon; diminishing slope winds, fully developed valley wind. Valley warmer than plains.
(d) Late afternoon; slope winds have ceased, valley wind continues. Valley continues warmer than plains.
(e) Evening; onset of downslope winds, diminishing valley wind. Valley only slightly warmer than plains.
(f) Early night; well-developed downslope winds, transition from valley wind to mountain wind. Valley and plains at same temperature.
(g) Middle of night; downslope winds continue, mountain wind fully developed. Valley colder than plains.
(h) Late night to morning; downslope winds have ceased, mountain wind fills valley. Valley colder than plains.

Figure 2.2 Schematic of the interactions between valley winds and slope winds for a complete 24 hour diurnal cycle. From Defant (1951).

Mountain valley winds usually begin somewhat after slope winds, according to the size, shape, and aspect of the valley.

Both slope and valley winds are indirectly the result of solar heating and commence earlier on slopes which face eastward to receive a maximal amount of solar radiation.

Banta and Cotton (1979) have provided a summary of these effects pertaining to the particular mountain location of this study.

2.3.2 Mountain barrier flow

The effects of airflow over mountain barriers is also of relevant concern. Like slope-valley winds, this has been a popular area of research resulting in the description of gravity wave phenomena (5-25 km wavelengths) initiated by a mountain perturbation. Applicable requirements for gravity waves are summarized by Alaka (1960). The wind direction must be within 30^{o} normal to the ridge and for the South Park area, which is bordered on its western edge by a 1300 m mountain barrier, a windspeed of at least 7 m/s is necessary. Winds of this magnitude and direction are common in the summertime just above ridgetop in Colorado. In addition, a "statically stable layer of air near the level of the mountain top with layers of lesser stability above and below" is required. These conditions are frequently found in South Park. Also, as will be discussed in Section 3.3, a stable layer of air is frequently observed about 1800 m above the apex of the Mosquito mountain range. It is to some extent the result of the previous days boundary layer top but seems to be accentuated over mountainous terrain during the night.

Finally, for large amplitude waves to occur, wind speed should increase steadily with height to values of approximately 30 m s^{-1} at the tropopause with little vertical change in direction.

2.4 Interpretation of the TKE Equation

Previous boundary layer studies have relied on horizontal homogeneity as a simplifying assumption. This allowed an easy "1st order" interpretation of the TKE equation. Perturbations about a mean quantity could be considered as spatially equivalent in the horizontal and calculated as averaged properties of a particular height. However, in

a horizontally varying turbulent field, one is forced to abandon this approach. The localization of turbulence is important.

It becomes desirable to display the data in such a way that the spatial variability of TKE is shown. This was accomplished by computing deviations from a flight leg mean value and displaying the data in their proper spatial location. All turbulent calculations were smoothed with a low pass filter with a cutoff wavelength of 4 km. The actual method is outlined in Appendix A.

Further, it is desirable to partition the turbulence into size ranges such that the contribution of different wavelengths can be explored. Power spectral analysis (Appendix B) showed that most of the variance occurs on scales of motion greater than 1 km, so two size ranges were chosen. First, deviations were calculated which represent motion occurring at all wavelengths by taking deviations from the mean value of a variable on a particular flight leg. Due to the distribution of turbulent energy, this represented motion primarily at wavelengths greater than 1 km. Secondly, the smaller scale turbulence was calculated by taking deviations from the data after it was low pass filtered to a cutoff wavelength of 1 km. This method had the added attraction of filtering out unwanted deviations in the mean flow caused by the mountainous topography. Airflow will sometimes conform with the terrain features and cause a turbulent interpretation of a semi-stationary flow regime occurring at the longer wavelengths. In actuality, the motion is not turbulence in the strict sense of the word.

For purposes of this study, buoyant production is calculated on all four case study days. Shear production is calculated on July 28 and July 30 when the mean vertical wind gradient was significant. No

attempt was made to calculate vertical turbulent transport. It is difficult to measure for several reasons. There were a limited number of observation levels (3 to 4) which were often separated by 500 m elevation or more and in time by as much as 30 minutes. An accurate vertical gradient would therefore be difficult to measure. Further, the flight legs were of varying lengths as necessitated by the topography which meant that only one-half of the study domain contained all of the flight legs. Also, the flight legs are not always vertically aligned, differing by as much as 1 km. Pressure transport of turbulence is not accurately measurable by the aircraft sensor system, and is generally assumed to be small.

The dissipation of turbulence is sometimes estimated from the longitudinal (along the axis of the aircraft) velocity spectrum. In this study, it is estimated from the variance of the longitudinal velocity. The data are first filtered with a high pass Lanceos (1956) filter so that only wavelengths less than 250 m (and greater than 40 m) are considered. If this spectral band is assumed to be in the inertial subrange, where TKE per unit wavenumber, or spectral density, is predicted to vary according to the Kolmogorov-Obukhov 2/3 law for the structure function, it is possible to obtain an estimation of dissipation. Although this is somewhat crude, it allows a representation of the horizontal variability of dissipation. The actual method of computing dissipation and the other measurable terms is included in Appendix C.

On July 30, an attempt was made to calculate two additional transport TKE terms not usually measured under horizontally homogeneous conditions. These were the horizontal advection of TKE

$$-\frac{U}{2}\frac{\partial \overline{q^2}}{\partial x} \quad ,$$

and horizontal u-diverge of TKE

$$-\frac{1}{2}\frac{\partial \overline{uq^2}}{\partial x} \quad .$$

The divergence of TKE is difficult to accurately portray in only one direction, especially when the uncalculated vertical divergence is of comparable magnitude, yet an attempt is made to calculate it.

This study does not represent an attempt to calculate a TKE budget. Rather, it is an attempt to illustrate the relative importance and localization of various terms of the TKE equation on two different types of days in the boundary layer over mountainous terrain.

3.0 DATA SET

3.1 South Park Area Cumulus Experiment

The 1977 Colorado State University South Park Area Cumulus Experiment (SPACE) was a comprehensive summertime meteorological program. The field portion of the program was located in central Colorado on a broad, elevated, and largely treeless plain called South Park (Fig. 3.1). The area is relatively flat and averages about 2.9 km MSL. South Park is bordered on its wesetern edge by the Mosquito Mountain Range running north-south. Previous field programs conducted in 1973, 1974, and 1975 have identified this range as a strong genesis region for cumulus and cumulonimbus clouds. For 1977, the scope of the SPACE was expanded. Attention was focused on the role of the mountains and South Park in influencing the mesoscale circulation and precipitation patterns on the eastern plains of Colorado.

A large variety of field equipment was deployed in the study. Much of it was located at the main SPACE base station on the western side of South Park. Rawinsondes were launched from the base daily at 0600 MDT (Mountain Daylight Time), or 1200 GMT (Greenwich Mean Time), 1000 MDT, and 1300 MDT. A micrometeorological subexperimental system was located at the base. Included were UVW anemometers and thermistors at various levels on two towers, two Boundary Layer Profilers (BLP) tethered balloons, and a Doppler acoustic sounder. A Lidar system was also present.

The National Center for Atmospheric Research (NCAR) Portable Automated Mesonet (PAM) was deployed in South Park (Cotton and George, 1978). Twenty remote weather stations were spaced roughly on a 10x10 km grid, with three (later reduced to two) remote stations located high on the

ridge top of the Mosquito Range. A station was located on a lower mountain top between ridgetop and South Park and the remaining stations in South Park proper. Each station measured various meteorological variables including wind speed and direction 4 m above the ground and wet and dry-bulb temperatures from 2 m above the ground. The PAM base van was located at the SPACE base station. The data were obtained from the remote stations by radio telemetry once per minute, and were instantly available for display by a computer graphics terminal located in the van.

Aircraft measurements were obtained over South Park and the Mosquito Mountain Range with the NCAR Queenair (304D) aircraft. The aircraft was equipped with an inertial navigation system (INS), gust probes, and other basic meteorological instruments. The characteristics of functioning system are analyzed in a subsequent section.

Additionally, other experimental systems were available. Triple-Doppler radar were centered in South Park as were sailplane flight operations and other cloud physics aircraft.

In this study, focus is primarily on the larger-scale features of the mixed layer of the developing boundary layer. Rawinsonde data and PAM data supplement the major data source: the NCAR Queenair. Tethered balloon data is available early in the morning on July 30.

3.2 Aircraft Flight Patterns

The NCAR Queenair 304D was the primary source of data for this study. A series of "butterfly" patterns were flown at various altitudes above the South Park area centering over the SPACE base site. The heights at which the aircraft flew were determined on the morning of

the flight from the 0600 MDT rawinsonde. On 14 JUL and 15JUL (two of four case study days) three levels were chosen. The first height was chosen to be in the cloud layer just above the expected cloud base. The second flight leg was just below cloud base and the third leg, confined to South Park proper, was approximately 200 m above the surface. On 28JUL and 30JUL four lower flight levels were chosen, all below the middle flight leg of 14JUL and 15JUL. Two were above mountain ridge-top level and two in the confines of South Park. Again the lowest flight leg was flown at about 200 m above ground level. On 30JUL two extra lower level flight legs were flown.

This study focused only on the portion of the flight legs flown over the SPACE base station and mountains directly to the west. This is shown in Fig. 3.1. The flight legs chosen were generally separated by about 1/2 hour. A summary of the flight leg times and elevations is given in Table 3.1.

As evidenced by the concomitant rawinsondes, most of these flight legs were in the mixed layer of the boundary layer. The exception to this is the highest flight legs on 14JUL and 15JUL. The surface layer was probably not sampled. The lowest flight legs were 200 m above the surface and the surface layer does not normally extend to this height.

3.3 Observed Characteristics of the Aircraft Data

The NCAR Queenair 304D aircraft is the primary source of data for this study. Data from NCAR's Portable Automated Mesonet system (PAM) were also used, as were coincident rawinsondes. However, both of these systems were used largely in a supportive role. The aircraft data

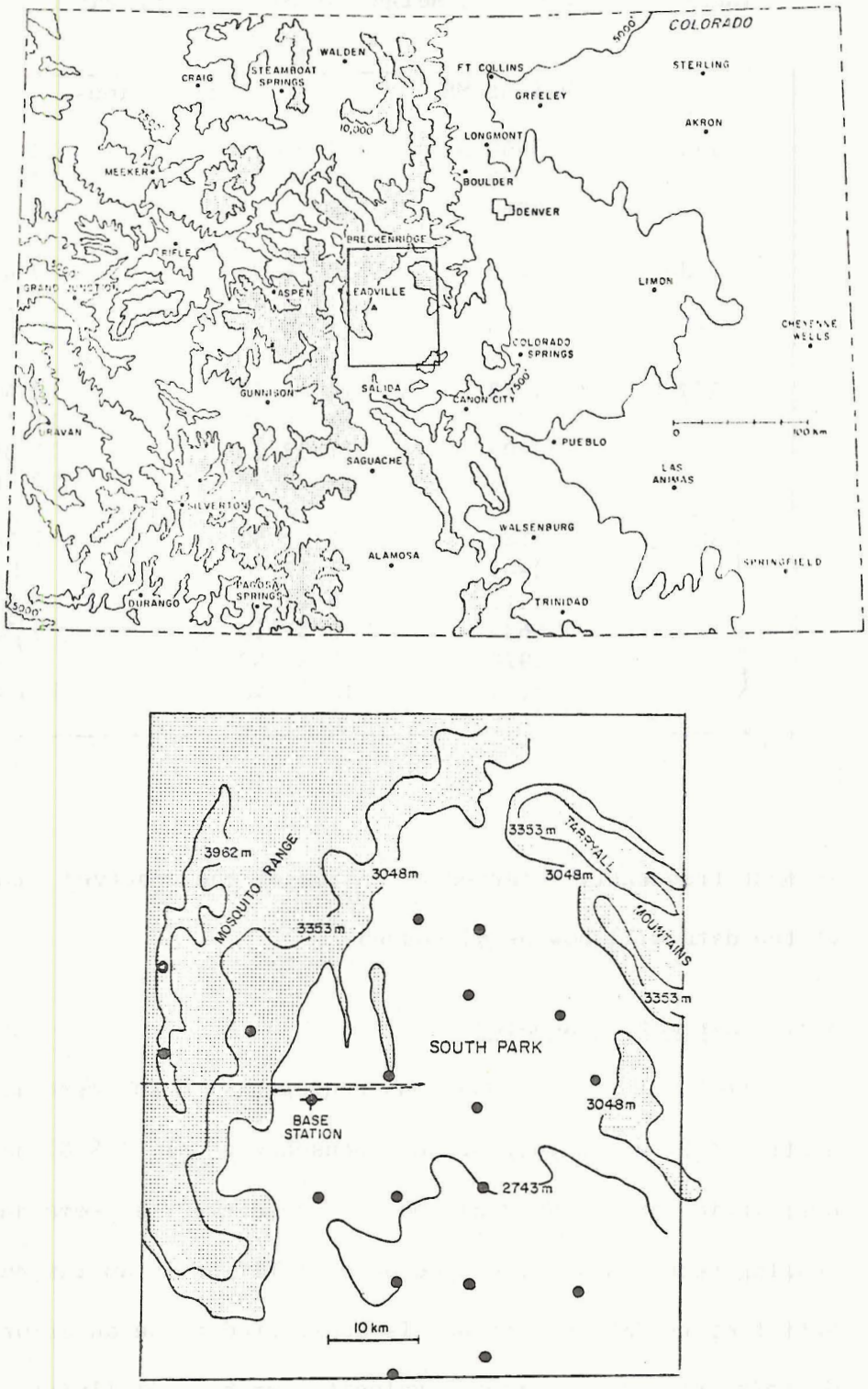

Figure 3.1 Topographic map of Colorado and South Park area. Upper illustration indicates location in Colorado of the lower enlargement of the South Park area. Black dots represent the location of the PAM surface stations. The dashed lines indicate aircraft flight patterns. Rawinsondes were launched from the base station.

Table 3.1 Times and Height of Aircraft Flight Legs

	Height MSL	Flight Times		
14JUL	5960 m	11 55 25	to	12 3 4
	4900	12 28 25		12 35 24
	3060	13 0 5		13 4 44
15JUL	5750	10 38 25		10 45 4
	5121	11 8 45		11 15 4
	3170	11 39 45		11 44 44
28JUL	4572	10 40 58		10 46 29
	4254	11 8 58		11 13 57
	3906	11 32 30		11 36 29
	3137	11 56 58		12 0 57
30JUL	3144	7 33 50		7 38 9
	3969	7 57 30		8 2 9
	4312	8 21 50		8 27 49
	4635	8 51 50		8 57 29
	3976	9 34 50		9 38 49
	3139	10 0 40		10 4 19

is most frequently referred to. Some of the observed characteristics of the data will now be discussed.

3.3.1 Air motion sensing

The NCAR Queenair 304D was equipped with an inertial navigation system (INS) and a gust probe. Lenschow et al. (1978) have presented a description of the NCAR air motion measurement systems and data processing techniques. Included on each flight is an instrument check. Satisfactory INS performance is considered to be an error less than 0.5 m/s drift in horizontal velocity per hour of flying time. This combined with a $\pm$1.0 m/s sensitivity error in the gust probe means a time dependent error of $\pm(1.0 + 0.5t)$ m/sec in horizontal wind where t is the flight time in hours. Most flights were on the order of 2

hours giving a horizontal error of ± 2 m/s. On calm days, this error can be as large as the wind itself disallowing the measurement of horizontal winds in an absolute sense. According to the rawinsonde, two of the case study days, 14JUL and 15JUL, had winds in the flight domain of this magnitude (3 m/s). The data on these days can therefore be strictly interpreted in a turbulent sense only. However, 28JUL and 30JUL were very windy days so that the horizontal error was relatively small. On these days, aircraft measured horizontal winds were considered to be quite accurate. They matched up well with the rawinsonde derived winds. Vertical velocity can usually be measured in a relative sense to within ± 0.5 m/s. In an absolute sense mean vertical motion over a 10 km flight domain is usually less than 0.1 m/s (if no intense convection and no large amplitude gravity waves are present). Since all flight legs are from 15-35 km, we have assumed zero absolute vertical motion. Thus, while absolute vertical velocity cannot be measured directly, it can be estimated to a greater accuracy than horizontal wind due to the inherent drift in that system.

28JUL and 30JUL showed evidence of gravity waves covering much of the flight legs. Assuming zero absolute vertical motion, relative vertical velocities on the order of 3 m/s (occasionally as high as 4 m/s) were associated with the waves. Zero absolute vertical velocity is thought to be a good assumption on these days for two reasons. First, the amplitude of the wave is small, and second, most of the wave seems to be within the domain of the flight leg where small net vertical motion would be expected.

Taken together, vertical and horizontal wind velocities can be used to construct a flow field on 28JUL and 30JUL. This will prove very helpful in discerning flow features on these days.

There was some problem with icing. The constrained vanes of the gust probe are not deiced and should not be expected to give accurate readings in icing conditions. Icing occurred on one of our case study days (14JUL) upon penetration of 6.5 km of a cloud at subfreezing levels. The average w-gust component appeared to rise by about 0.7 m/s and lessen the quality of data on this leg. However, the basic cloud structure, involving vertical velocities on the order of 3 m/s is still discernible. The 24th of July (not specifically included in this study) also showed this same effect of similar magnitude for about 7 km of cloud penetration. Vertical velocities again were on the order of 3 m/s which allowed a good estimate of the clouds' structure. However, at this level, turbulent calculations must be interpreted with caution. July 15 also had a cloud penetration with these same subfreezing conditions. However, the penetration was only for 3.5 km and no icing was evident.

Despite the fact that aircraft-derived winds on low wind days are relatively inaccurate in an absolute sense, certain consistencies within the error limits would be expected with the wind derived from the rawinsonde. This was indeed the case on 14JUL despite the above mentioned INS error where aircraft winds of 6 m/s at 270^{o} could be compared with rawinsonde derived winds of 3 m/s at 270^{o} taken 2 hours earlier. However, on 15JUL a larger absolute wind error was noted. The aircraft measured winds of 5.5 m/s at 340^{o} whereas the rawinsonde indicated winds

of 3.5 m/s at 250°. This translates to an error of about 6.3 m/s in the y-direction which is much larger than would be expected. No readily apparent reason for this discrepancy was found. A comparison of the wind direction at a common point passed by the aircraft before and after the upper flight leg which included cloud penetrations gave the same wind value. It was therefore decided to adjust the y-component on 15JUL so as to be more consistent with the known rawinsonde wind direction. The adjustment does not affect any calculations to be done for that day.

The gust probes were considered to be responsive to wind fluctuations occurring at 4Hz. This translates to a spatial resolution of 20 m at typical Queenair speeds. Therefore, the time response associated with measurements of air motion is negligible.

3.3.2 Temperature measurements

Temperature is measured by two separate sensors on the aircraft, a Rosemount 25μm platinum wire resistance thermometer and a reverse-flow temperature sensor. The Rosemount temperature sensor is generally considered to have an absolute error of $\pm 0.5^{\circ}C$ in clear air and $\pm 1^{\circ}C$ in cloudy air (Lenschow and Pennell, 1974). Its response time is 1 sec which indicates that it takes that long to respond to 63.2% of a temperature discontinuity. In this study, the greatest differences in temperature detected on any one flight leg (constant height) were $1.5^{\circ}C$. If in the unrealistic event this were a sharp discontinuity, it would take the Rosemount temperature sensor 2 sec to respond to $1.3^{\circ}C$ of this temperature change. At typical Queenair speeds this translates to a horizontal lag of 160 m. A discontinuity this sharp seems somewhat unrealistic but serves to illustrate an upper limit to this type of

error. For most data presentations in this study this lag effect is unimportant where 500 m and 1 km horizontal averages of potential temperature are often used. However, correlations of vertical velocity and temperature are computed and for higher frequencies this effect can be important.

It is possible to correct for this temperature lag with a numerical scheme developed by McCarthy (1973). The scheme allows for both the response of the sensing element, as well as conduction between the element and its supporting structure. A finite-difference, iterative solution is used. The technique was tried on a sample of data from one of the case study days; the largest correction noted was 0.05^{o}; the average was 0.01^{o}. This roughly translates to an error in buoyancy of as much as 6%, or an average of about 1% depending on the assumed conditions. Since there was a relatively small amount of TKE at the shorter wavelengths and the correction small, the data were not adjusted. However, in a more rigorous study, this correction might be desirable.

The reverse-flow temperature sensor is considered to be accurate to within $\pm 0.5\ ^{o}C$ independent of cloud water. To achieve this, a protective housing is necessary which lengthens the response time to 4 or 5 sec. Hence the reverse-flow sensor was more capable of measuring temperature independent of cloud water but less capable of measuring temperature variations. Only two cloud penetrations occur in this study and both sensors seemed to be in agreement. That is, both sensors were usually within 0.3^{o} of each other, independent of the presence of cloud water. Throughout the study, differences in the two sensors only rarely would reach 0.6^{o}. The slower response of the reverse-flow sensor was obvious upon cloud penetration on 15JUL. The two instruments differed

by 0.5^{o} at the discontinuities in potential temperature associated with the cloud whereas in and around the cloud they only differed by 0.2^{o} to 0.3^{o} at the most.

There was one cloud penetration on July 23 (not included in the case study presented here) where the reverse-flow sensor proved to be more accurate than the Rosemount. The Rosemount sensor measured an actively growing cumulus cloud as colder than the environment and hence negatively buoyant. However, the reverse-flow sensor measured warm air in this cloud which seemed to be more reasonable. Apparently liquid water was cooling the Rosemount sensor. This was generally an infrequent phenomenon and not observed during any of the periods of observation in this study. Therefore the Rosemount derived temperature was used throughout this study.

3.3.3 Estimation of potential temperature

In order to illustrate the thermal structure of the air it is desirable to use potential temperature. However, the calculation of potential temperature requires the use of pressure, which has its own error. This error is generally less than 0.1 kPa. For typical conditions of this case study a 0.1 kPa error in pressure will cause a 0.15^{o} error in potential temperature. Considering both sources of error (temperature and pressure) we expect to measure potential temperature in an absolute sense to within an error of $\pm 0.65^{o}$. However, the relative difference between two adjacent points would be much smaller.

In addition to the advantages of displaying the thermal structure of the atmosphere with a conservative variable we are implicitly correcting for another source of error. That is, changes in aircraft

elevation due to pilot error or turbulence can introduce an inferred horizontal temperature fluctuation due to the variability of temperature in the vertical direction. The data are considered to be representative of a specific height and if the air is not isothermal an error is introduced. This is especially important in spectral analysis of temperature. By using potential temperature, however, we are implicitly assuming the air is adiabatic in this region. This is generally a better estimate of temperature because the air is not usually isothermal. For South Park, variations in aircraft flight elevation were usually within $\pm$15 m. Occasionally, on highly turbulent days, variations as high as $\pm$30 m were observed. We are effectively assuming that the air in our sample is isentropic 30 m above and below our designated aircraft height.

3.3.4 Humidity measurements

Humidity is measured by two separate sensors on the aircraft, a dewpoint hygrometer, and a microwave refractometer (Bulletin #22 NCAR). The dewpoint hygrometer is good for absolute humidity measurements corresponding to dewpoints within $\pm 1^{o}$C above freezing and $\pm 2^{o}$C below freezing. For typical South Park conditions, this translates to an error in mixing ratio of $\pm$0.5 gm/kg to $\pm$1 gm/kg,respectively. Comparison of predicted saturation mixing ratio and measured saturation mixing ratio in clouds revealed that our estimate was well within these bounds. In fact, variations to within one-half of these error limits were almost always met. The dewpoint hygrometer, however, has a much slower response time than the microwave refractometer. The reflecting surface of the dewpoint hygrometer is cooled or heated at a rate of 2^{o}C/sec so that

sharp moisture discontinuties are difficult to detect. In this study, the greatest variation in dewpoint occurring on one aircraft flight leg (one elevation) was about 7°C. If in the unlikely situation that this was a sharp discontinuity the aircraft would take 3.5 sec to respond to the correct dewpoint. At typical Queenair speeds this would translate to a horizontal error of 280 m. This delay is an absolute upper limit for the data herein analyzed. Cross-sectional plots of mixing ratio have been made with 500 m averages so that the effect should be minimal.

The microwave refractometer has a much faster response time than the dewpoint hygrometer. However it is not effective for in-cloud measurements and tends to wander making absolute measurements difficult. But due to its faster response time it can be used in non-cloudy conditions to measure humidity fluctuations. This was done to a limited degree in this study.

3.3.5 Aircraft height determination

The heights at which the aircraft flew were interpolated from the concomitant rawinsonde. That is, the aircraft measured pressure was matched to the appropriate pressure surface (height) as determined from the rawinsonde output. This rawinsonde derived height more closely fit with known features of the flight paths which required the clearance of certain topographical features. When the plane was within 763.5 m of the ground and hence above these features, the geometric (radio) altitude could be measured. When the geometric altitude was compared with the new rawinsonde derived altitude agreement was to within 40 m. This error could be partially explained by local variations in topography.

It was evident that the aircraft-derived heights were in error on all case study days. Gross underestimations of as much as 200 m at 70 kPa frequently put the aircraft below ground level. The error increased with height as the 50 kPa height was underestimated by as much as 480 m on 14JUL.

To conclude, heights have been corrected so that any error in height should be less than 40 m. For the resolution used to display the data in cross-sectional plots, this is very small.

3.3.6 Data sampling

Some of the instruments on the Queenair were capable of "fast response" measurements. These included the gust probes (u,v,w wind components) and the microwave refractometer humidity sensor. These instruments were sampled at 8 times per second. Since the speed of the aircraft was generally about 80 m/s this translates to a point every 10 m. However, due to a lack of coupling between the INS pallet and probe, the data bandwidth for the air motion system was limited to 4 Hz or 20 m. The Rosemount temperature sensor, reverse-flow temperature sensor, dewpoint hygrometer, and the pressure sensor were measured once per second.

4.0 CASE STUDY DAYS

Four case study days were chosen to illustrate the development of turbulence in the ABL over South Park. They were July 14, July 15, July 28, and July 30, hereafter abbreviated as 14JUL, 15JUL, 28JUL, and 30JUL. As a group, these days represent two entirely different types of boundary layer development seen in South Park. One type, represented by 14JUL and 15JUL, illustrates the initial development of the boundary layer on a day in which vigorous convective activity resulting in precipitation occurs throughout the day. The other type of day, represented by 28JUL and 30JUL, illustrates the features of boundary layer development on a day when cumulus activity is suppressed or delayed and dry westerly winds reach the surface. Precipitation was either absent or occurred to a lesser extent later in the day.

4.1 July 14

As observed throughout the 1977 SPACE program the general synoptic conditions favorable for the occurrence of cumulus convection over the central Colorado mountains were threefold:

1) a favorable surface pressure pattern for maintaining the supply of surface moisture to the mountains,

2) a flux of moisture at 50 kPa and below, and

3) weak flow aloft (at least at levels near mountain tops and several thousand feet above) so as to suppress the dynamic interaction of the mountain barriers with the westerly airstream.

These conditions were met on 14JUL. A surface low was analyzed on the 0600 MDT surface map centered over the Utah-Colorado border. A high was also analyzed over New Mexico. Hence a favorable pressure gradient

was set up which could supply moisture from the southeast (due to topographical considerations, low-level moisture must generally enter South Park from the south or east). The 50 kPa pattern for this entire time period including 15JUL was dominated by a large subtropical high centered over the southeastern United States (Fig. 4.1a). This situation brought upper level moisture in from sources to the south such as the Gulf of California or the Gulf of Mexico. The winds on 14JUL were very light at and above ridgetop. The 1000 MDT rawinsonde showed winds of about 3 m/s from just above the surface up to 45 kPa or 6300 m MSL (Fig. 4.2a). Thus all three criteria for cumulus convection were satisfied on 14JUL.

In addition to the above-mentioned features, the lower edge of a weak, slow-moving, upper-level short wave passed over South Park during the morning. Associated with this was a weak cold front analyzed at the surface. General backing of the wind with height from 3730 m to 7660 m (MSL) was noted on the 1000 MDT rawinsonde and assumed to be associated with the weak cold front. This system aided in the early development of cumuli in South Park by 0900 MDT. Precipitation shafts were observed by 1030 MDT. Thus, by the time the aircraft had reached South Park on this day, convective activity was well developed.

Vertical cross-sectional contour plots of the conservative variables potential temperature and mixing ratio were made for 14JUL (Fig. 4.3). Averages of 500 m length of these variables, as derived from the aircraft, were plotted in the appropriate spatial locations for each flight leg. The terrain is indicated below, accentuating the Mosquito Mountain Range over which the aircraft flew. The horizontal dotted lines indicate

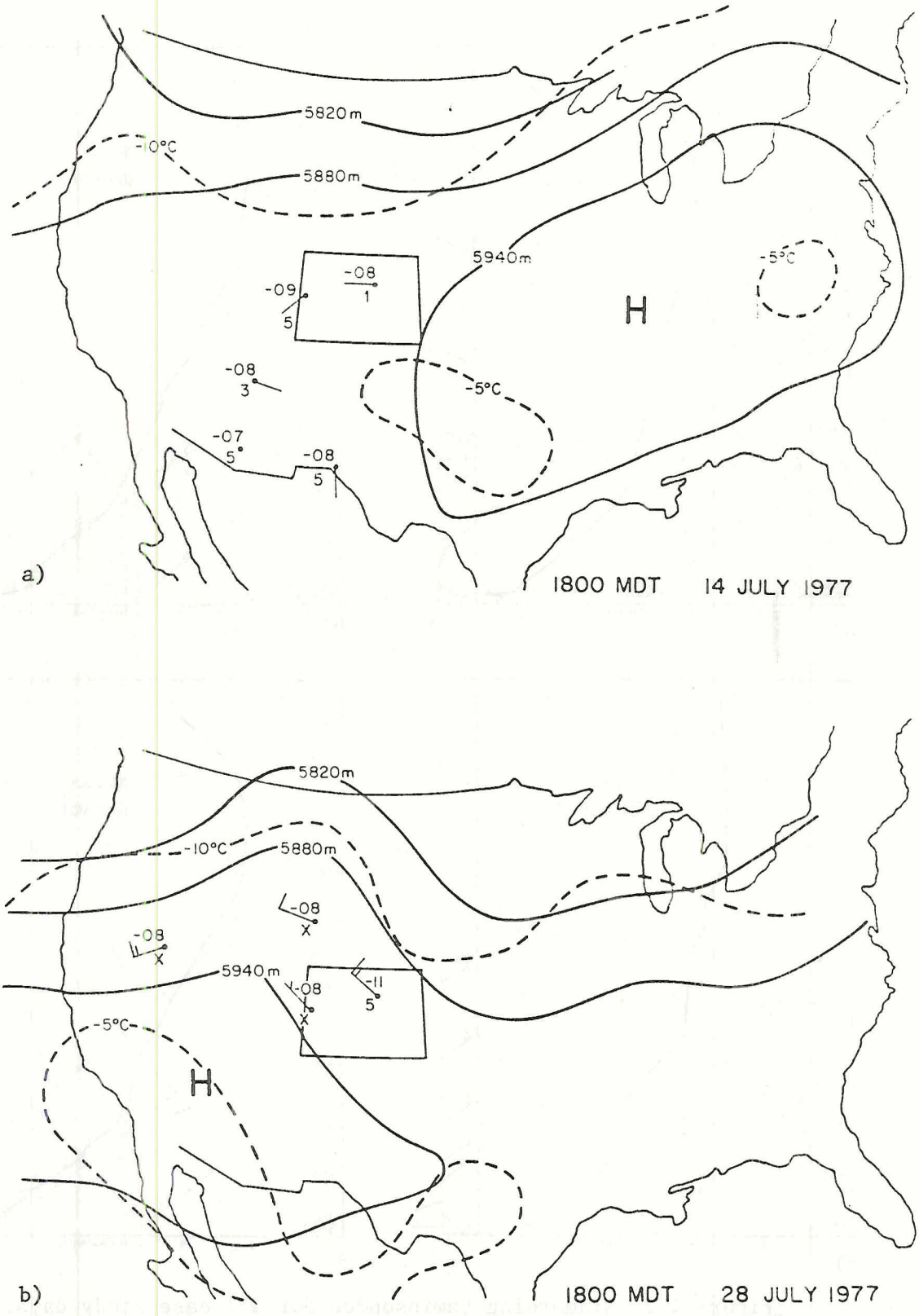

Fig. 4.1 50 kPa synoptic patterns. Height of 50 kPa surface for two different case study days. Upper-level station data for selected up-wind sites includes temperature, dewpoint depression, and winds in meters per second.

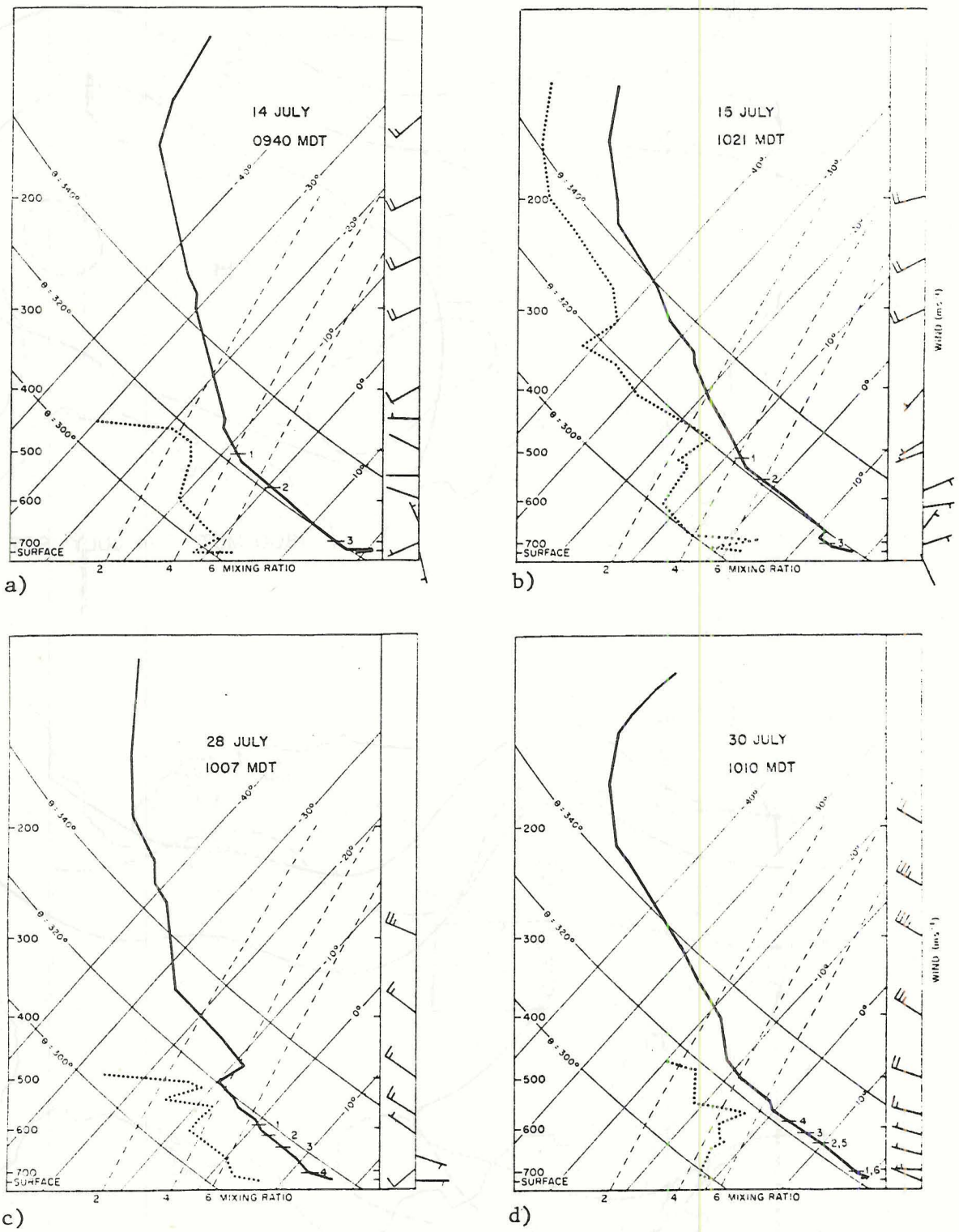

Figure 4.2 Midmorning rawinsondes for all case study days. Pressure is in mb on left; temperature is represented by diagonal lines running to upper right and are in ^{o}C; winds are in meters per second.

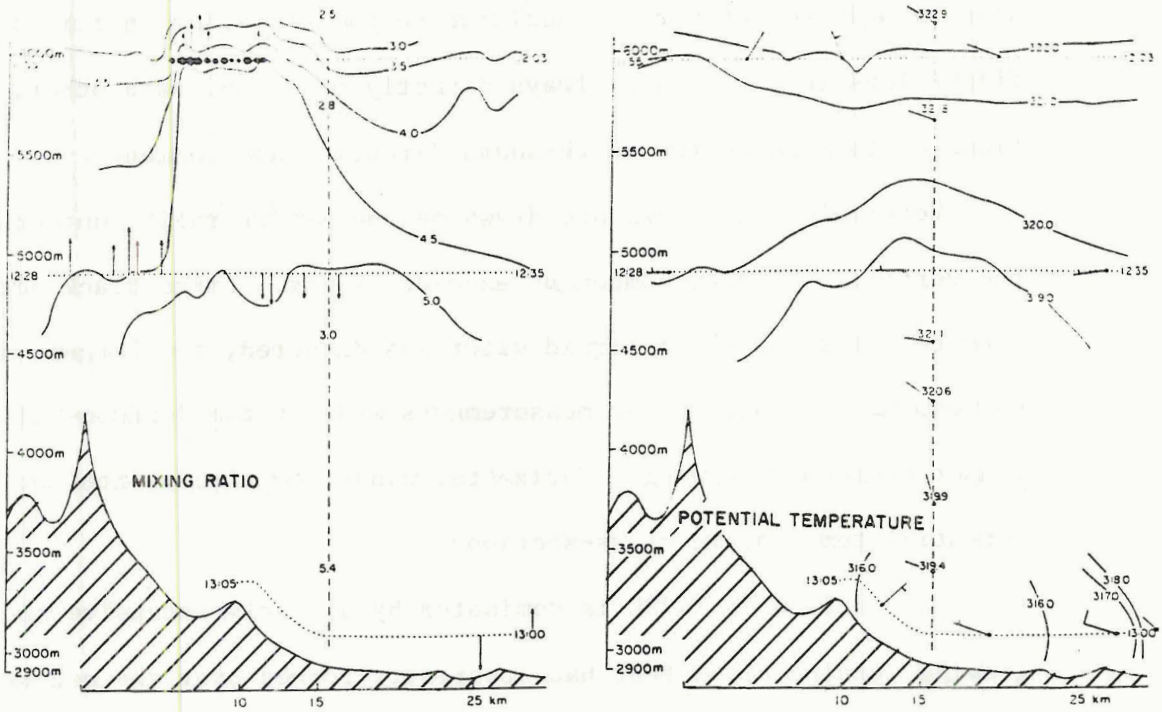

Figure 4.3 Cross sections of mixing ratio and potential temperature for July 14. Horizontal dotted lines are aircraft flight legs with times included at the ends. Vertical dashed line represents the path of the 0940 MDT rawinsonde and includes data points from it. Note that it occurred ∿3 hours earlier. Vertical velocities greater than |2 m/s| are recorded on the mixing ratio plot where 1 cm = 6 m/s. Cloud water is also indicated as blackened circles where the largest circles equal .4 gm/kg. Winds in m/s are displayed on the potential temperature plots.

the path of the aircraft with the corresponding times at the ends of the flight legs. The vertical dashed line indicates the path of the rawinsonde nearest in time of the flight legs Also included are surface data from three PAM sites which were in the plane of the cross-section. These stations were located at 0, 16, and 27 km downwind of the mountain crest.

Contours were drawn primarily from the aircraft data. Where discrepancies arose in the different data sources, usually the result of a temporal inconsistency, the aircraft data were used. Generally, all three sources of data corresponded within their error limits. It should

also be pointed out that in addition to the variation in time of the flight legs they were not always directly on top of each other. Variations up to 1 km in the north-south direction are common.

Vertical wind arrows are drawn on the mixing ratio contours where the vertical velocity component exceeded 2 m/s. Large black dots correspond to points at which liquid water was detected, the largest dots correspond to liquid water measurements made by the Johnson-Williams sensor of about 0.4 gm/kg. Horizontal winds are also plotted on the potential temperature cross-sections.

The airflow on 14JUL is dominated by a fairly extensive and actively growing cumulus cloud that had apparently formed over the mountains. The cloud was penetrated during the upper flight leg. Mixing ratios about 1.5 gm/kg higher than the surrounding air supported the assumption that the cloud air mass had originated from lower levels where more moisture was available. Potential temperatures in the cloud are higher than the surrounding air apparently due to the release of latent heat from the condensing moisture.

The cloud slowly drifted to the east and had begun precipitating before 1230 MDT as shown by aircraft camera film. In the figure it is evident as negative vertical velocities in the center of the middle-level flight leg. Regions of upward moving, locally warm and moist air were evident directly over the mountains. This suggests the presence of thermals originating on the mountain which, presumably, would lead to future cumulus development in that area.

The lower flight leg was also under the influence of rain and drizzle as shown by the aircraft camera film and evident on these figures as potentially cool air over the base station and much of South Park.

This cooler mass of air appeared to be working its way out onto the Park as a small gust front as evidenced by the potential temperature cross-section. Low-level winds were diverging over the base station and converging further to the east at about the 30 km marker.

The development of the boundary layer on 14JUL is displayed as successive profiles of potential temperature (Fig. 4.4a). The data are taken from rawinsondes launched from the base station. They are subject to an absolute error of about $\pm 1^{o}$ which makes specific intercomparison

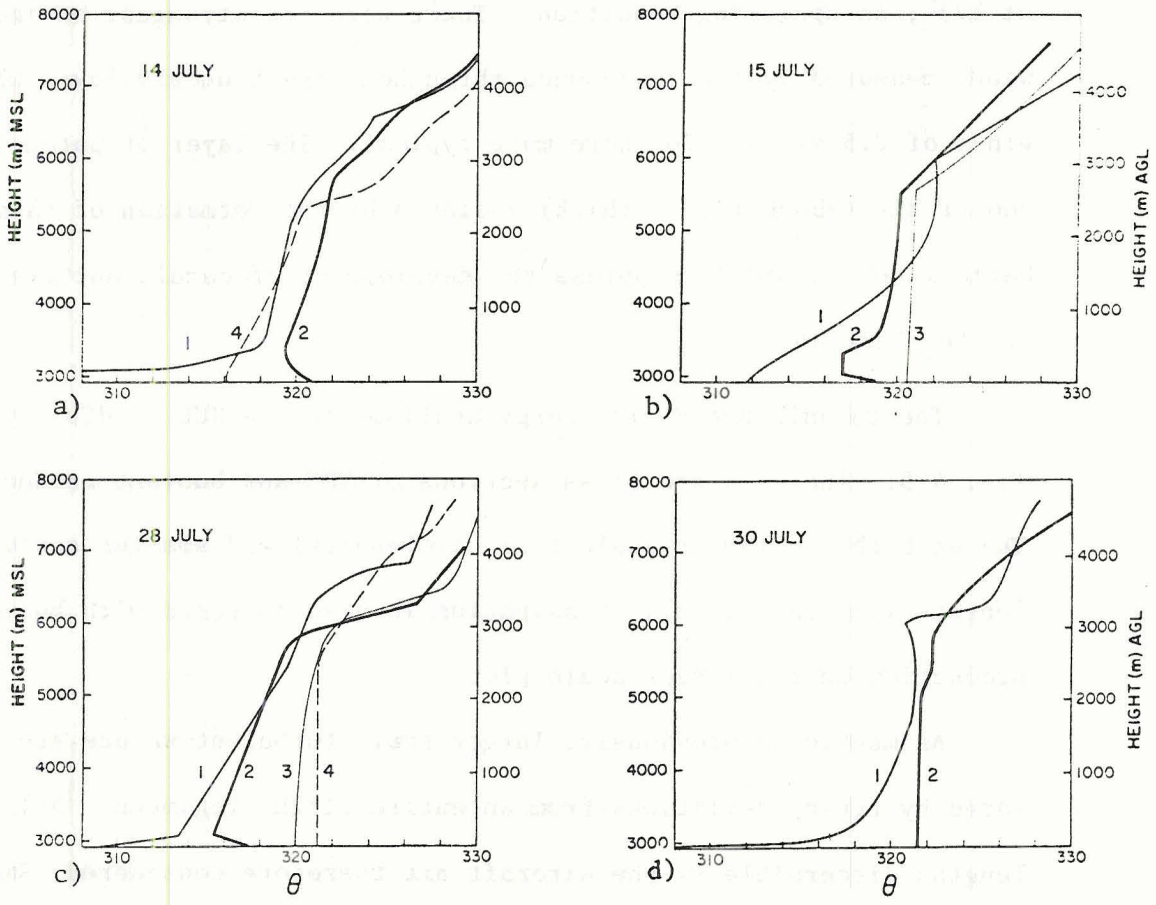

Figure 4.4 Successive profiles of potential temperature for all case study days. They are based on rawinsondes taken at ∿0600 MDT (1), ∿1000 MDT (2), ∿1300 MDT (3), and ∿1700 MDT (4).

difficult. Each sounding, however, by itself represents well the structure of the developing boundary layer.

On 14JUL a morning surface inversion is evident from the first rawinsonde taken at ~0600 MDT. The previous days boundary layer is evident above this layer extending to about 3000 m AGL. The second sounding, taken after cumulus activity had started, reveals the presence of a superadiabatic layer near the surface. The formation of this warm layer can then feed the developing cumulus cloud already mentioned through the mechanism of upslope-valley winds. Winds measured by the rawinsonde near the surface at this time, and extending up to 100 m AGL, were 5 m/s at 175°, an upsloping condition. These were the strongest horizontal winds measured by the rawinsonde throughout the boundary layer where winds of 2.5 m/s at 270° were more typical. The layer of potentially cooler air (about 1000 m thick) isolated by the formation of this adiabatic layer seemed to suppress the development of cumuli out over the flatter Park area.

The turbulent kinetic energy analysis for 14 JUL is displayed in Fig. 4.5. Included are cross sections of TKE and buoyant production of TKE at both the larger scale (all wavelengths) and smaller scale (wavelengths less than 1 km). Dissipation is also included with buoyancy production on the larger scale plot.

As mentioned previously, larger scale turbulent values are calculated by taking deviations from an entire flight leg mean. All wavelengths discernible by the aircraft are therefore considered. Smaller scale turbulence is calculated by taking deviations from the data after it has been smoothed to a cutoff wavelength of about 1 km. Therefore wavelengths less than 1 km are considered. Finally, both the larger

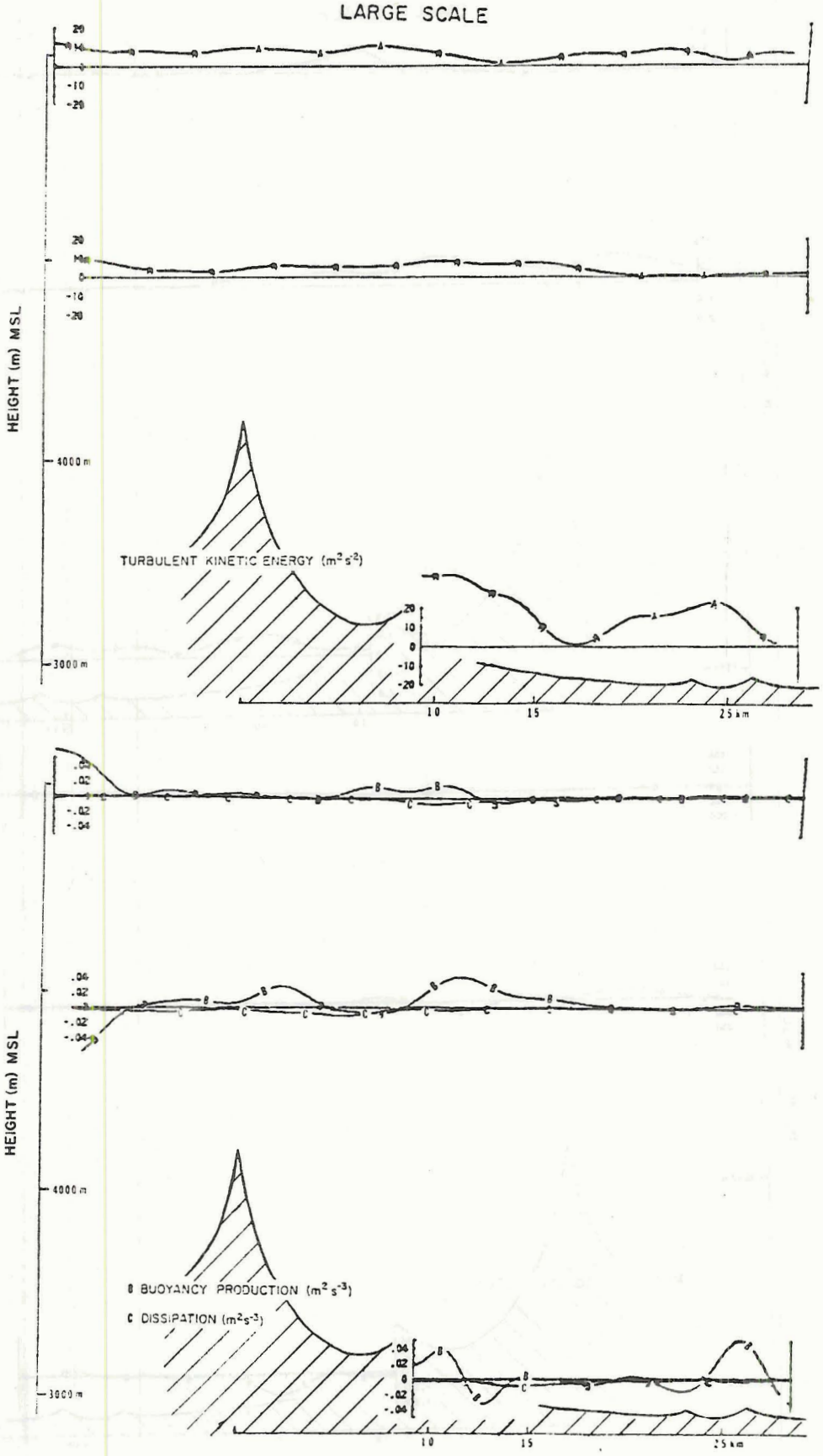

Fig. 4.5 14JUL TKE analysis.

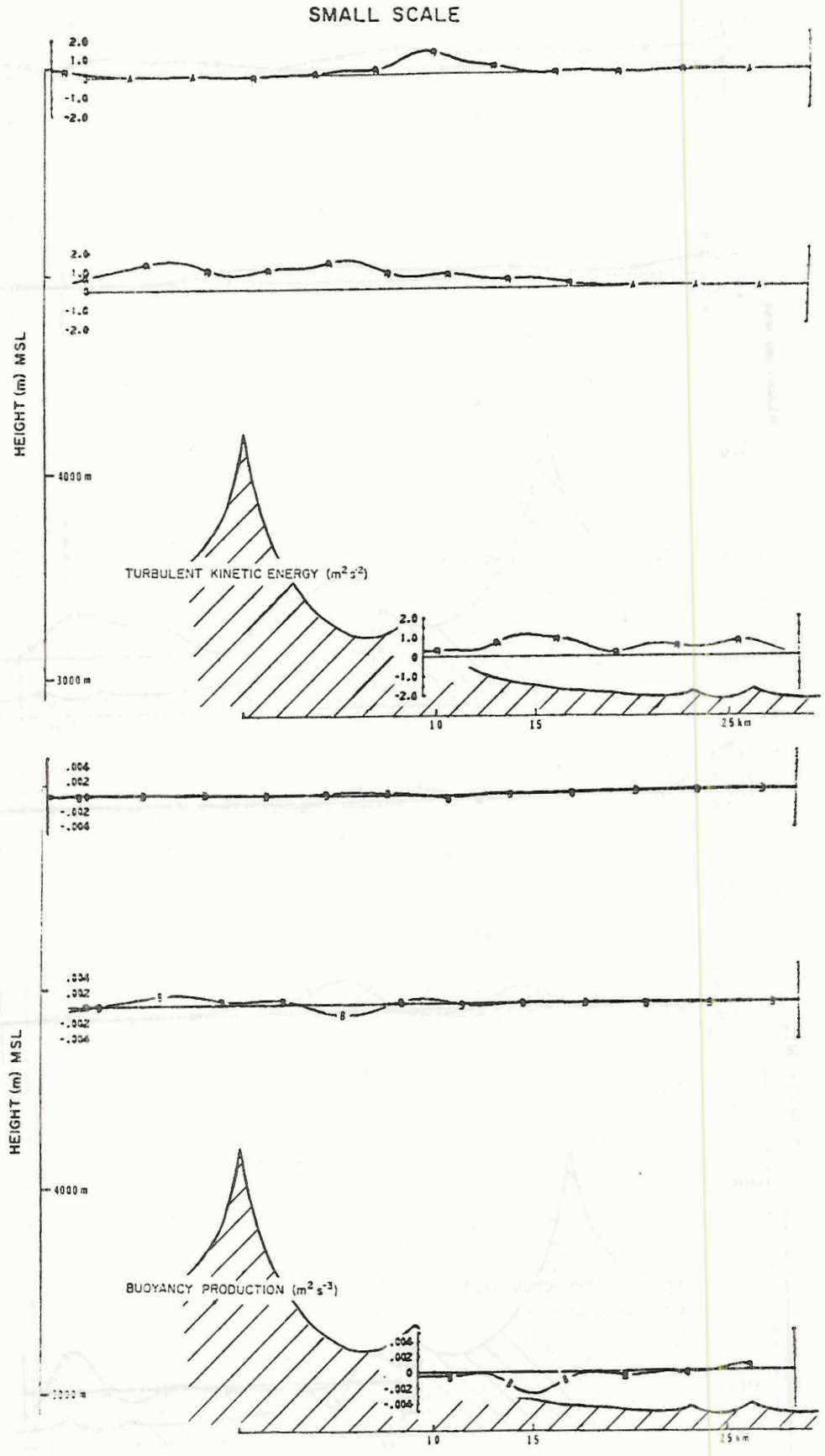

Fig. 4.5 14JUL TKE analysis (cont)

and smaller scale results are then smoothed with a low-pass filter that has a cutoff wavelength of about 4 km.

The larger scale TKE analysis is somewhat complicated due to the INS error associated with penetration of the cloud in the upper-level flight leg. Dissipation probably localizes the cloud much better. It is calculated at much smaller wavelengths (less than 250 m) so that the INS error does not affect the calculation. Buoyant production is positive in this area.

Stronger buoyant production is evident in the middle-level flight leg. The region above the mountain crest is supplying the area above with warm moist air and possibly allowing subsequent cloud development. The central maxima located away from the mountain is more precisely associated with the rainshaft already noted and possibly with downward moving, less turbulent air from aloft. Most of the dissipation was occurring near the mountain. The general lack of smaller scale motion in this area might suggest that the buoyancy was due to larger scale motion.

The lower flight leg is dominated by two highly turbulent areas resulting from the diverging cool air from the rainy area. It should be pointed out here that due to the nature of the way resolved scale turbulence is calculated different masses of surface air moving in different directions result in large turbulent values. The actual placement of the flight leg relative to different air masses will thus have a tremendous effect on the values of turbulence calculated by this method. A longer flight leg would be more desirable. This has occurred because the scale of motion is nearing the size of the flight leg.

Finally, buoyant production of TKE can be noted at the terminal edges of the diverging air. Dissipation is evident over the base station.

The smaller scale analysis showed that about one-tenth of the TKE occurred on scales of motion less than 1 km. Note the change in scales used.

The cloud in the upper-level flight leg is more easily discernible in the TKE analysis because effects of the INS error are not as pronounced. This effect was noted with dissipation as well. Since they are both calculated from smaller wavelengths, this would be expected. Indeed, both plots of dissipation and smaller scale TKE look very similar. The TKE over the mountains appears to be associated with buoyancy production, but at the lower level by other means not calculated. Recall that it was raining at the surface.

4.2 July 15

The general synoptic conditions on 15JUL were also favorable for cumulus convection. Like 14JUL, a surface low was analyzed over the Utah-Colorado border. A region of high pressure was also analyzed to the south over New Mexico. These conditions again provided a favorable surface pressure pattern for low-level moisture. The 50 kPa pattern was effectively the same as on 14JUL and provided upper-level moisture from the south. And again the winds were light at about 3 m/s from the surface up to 50 kPa. The day was to a large extent synoptically undisturbed. The first cumulus clouds were observed shortly after 0920 MDT. The aircraft entered the Park at about 1030 MDT and had detected precipitation by 1110 MDT. By 1340 MDT numerous cells were observed to be precipitating.

The cross sections of potential temperature and mixing ratio for 15JUL are presented in Fig. 4.6. The flow features, like 14JUL, are dominated by the presence of a cloud over the mountains. Mixing ratios 2 gm/kg higher than the surrounding air show that the air was derived from lower surface levels. The potential temperature cross section implies that air is being forced up the mountain (as noticed from data in the upper-level flight leg). The 1021 MDT rawinsonde detected winds generally out of the east at 3 m/s up to 2000 m AGL above which they turned westerly at 245°. The 1318 MDT rawinsonde also detected these winds though more turbulence was noted as well. It appears that there is forced low-level flow up the mountain barrier, possibly

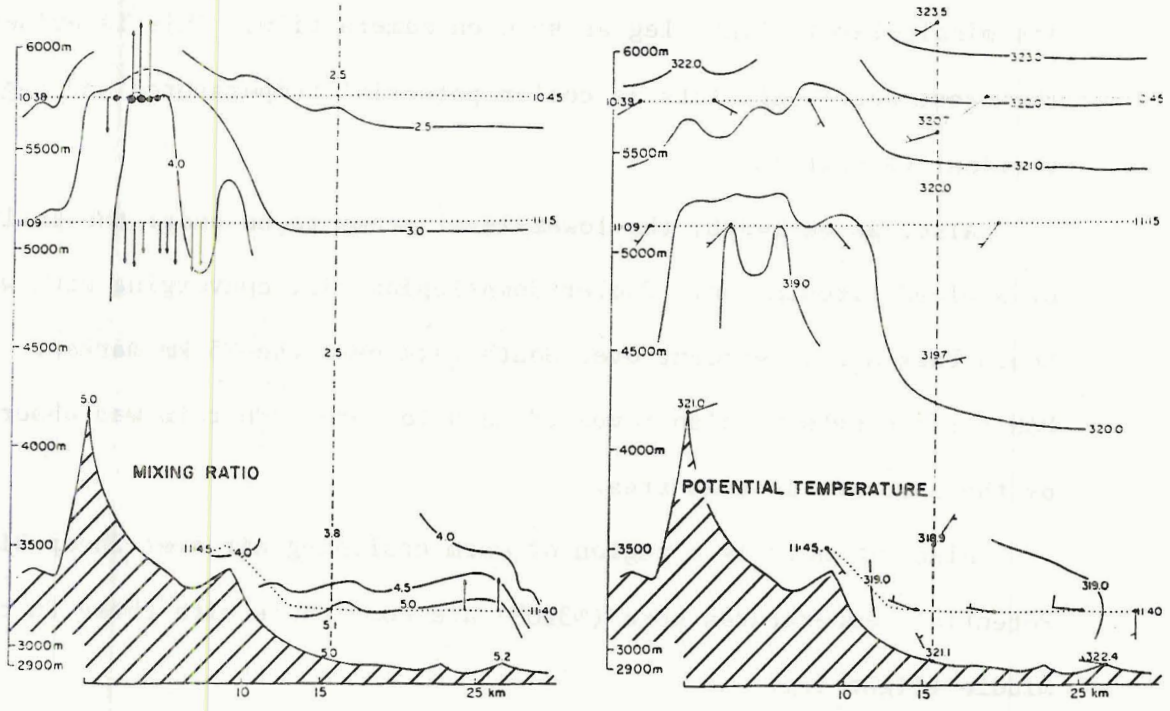

Figure 4.6 Cross sections of mixing ratio and potential temperature for July 15. Same as Fig. 4.3. The 1021 MDT rawinsonde is used here. Additional data points at the 0, 16, and 27 km markers are PAM surface station observations coincident with the nearest flight leg.

the result of a favorable pressure gradient. Both PAM surface stations at the apex of the mountain range recorded winds generally out of the east averaging about 2 m/s throughout the day. Thus it appears that easterly flow is aiding in the initiation of convective activity. Also the upsloping air is seen to carry with it an easterly component of momentum into the WSW winds detected in the upper two flight legs. Note the two winds barbs associated with the cloudy air in the upper flight leg. July 23 (not specifically in this study) also showed this potential temperature feature under similar light wind conditions. The wind on this day was out of the east at 140° up to 20 kPa and averaged about 2.5 m/s in the boundary layer, suggesting that forced flow up the mountain barrier was aiding the initiation of convection on this day as well.

Like 14JUL the aircraft passed through a precipitation shaft on its middle-level flight leg as seen on camera film. This is evident on the cross-sectional plots as cooler potential temperatures and negative vertical velocities.

Also, as on 14JUL, the lower-level seems to be under the influence of a cloud circulation. Cooler downsloping air, converging with warmer South Park air is evident over South Park near the 25 km marker. The PAM surface network also revealed this feature. No rain was observed by the aircraft in this area.

Also of note is a region of warm upsloping air over Sheep Ridge. Potential temperatures here (~320°) are comparable with those in the middle flight leg.

The development of the boundary layer on 15JUL is displayed in Fig. 4.3b with features similar to 14JUL. The air near the surface begins warming before 10 MDT so that a superadiabatic layer forms. The

cooler air above it seems to suppress cumulus activity over the Park area as no clouds were evident here at this time. By 1300 MDT the air throughout the boundary layer appears well-mixed.

The turbulent kinetic energy analysis for 15JUL is displayed in Fig. 4.7. The TKE maximum associated with the upper-level flight leg is representative of the turbulent cloud motion which had vertical velocities averaging over 5 m/s. Dissipation is also apparent in this region. Yet buoyancy production on the larger scale was primarily negative. The Rosemount temperature sensor (used here) showed no significant deviation compared to the reverse-flow sensor supposedly more reliable for in-cloud measurements. The strong updraft may partly be due to a non-hydrostatic pressure field created by cloud-scale dynamics, but accurate statements about this feature are difficult to make due to the decreased capability of in-cloud temperature measurements mentioned in Chapter 3. Errors of $1^{o}C$ can occur at typical Queenair speeds flown in South Park.

The TKE maximum associated with the middle-level flight leg just downwind of the cloud represents the subsequent drift of the cloud to the east and formation of a precipitation shaft. It then shows up as a production of TKE by buoyancy. More precisely, it is associated with the downward movement of cooler air possibly due to cloud dynamics or the evaporative cooling effect of the precipitation and drag of the falling rain.

The lower-level flight leg maxima of TKE occurring on the larger scale were similar to 14JUL and seem to result from the same mechanism. That is, potentially cool downsloping air, apparently associated with the cloud, was diverging out over the Park.

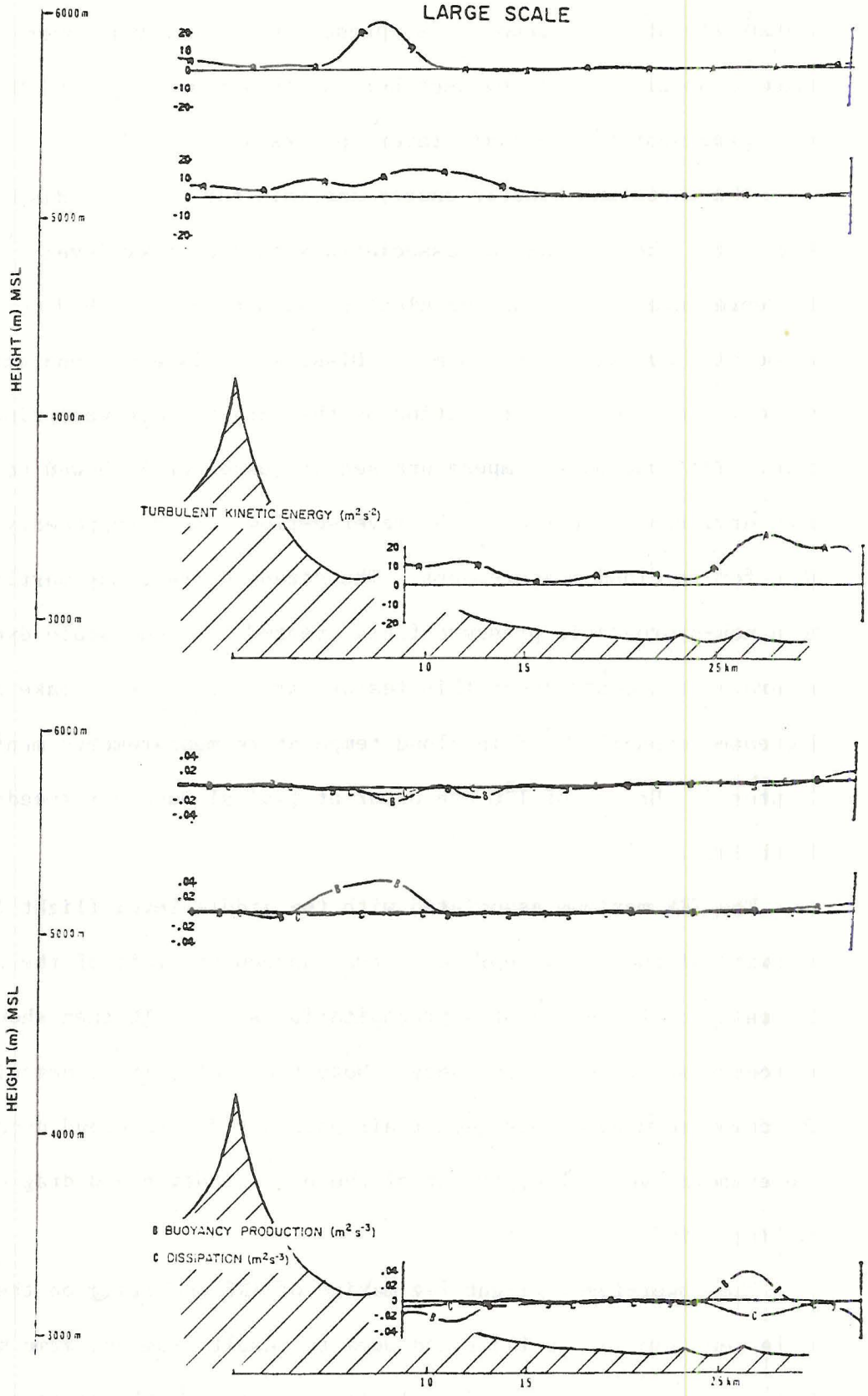

Fig. 4.7 15JUL TKE analysis.

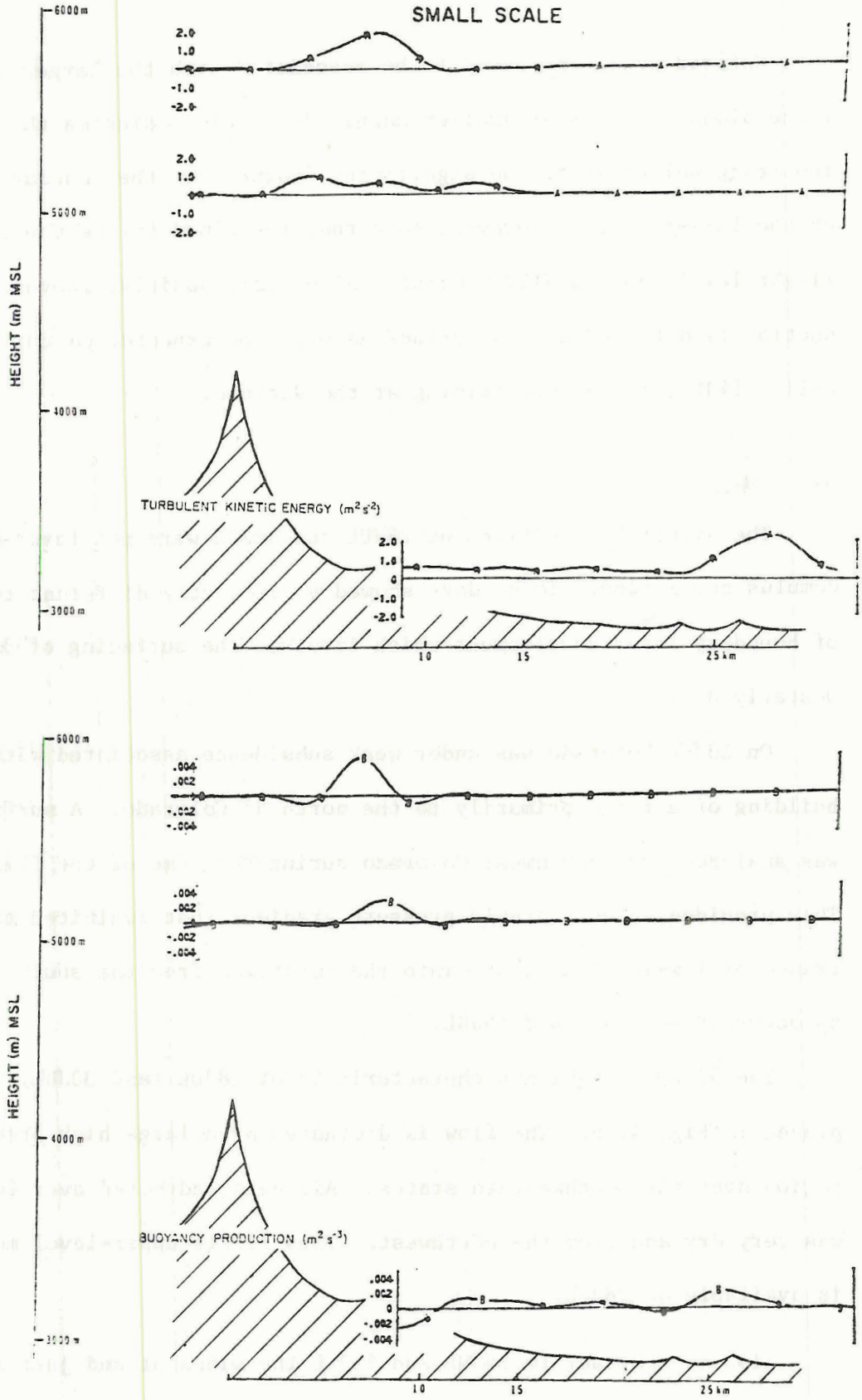

Fig. 4.7 15JUL TKE analysis (cont).

Subgrid scale TKE seems to be associated with the larger scale turbulence although it is of smaller magnitude. This indicates that we are isolating well most of the significant features of the boundary layer on the larger scale. However, note that the cloud in the upper-level flight leg is now locally buoyant. Also, more positive buoyancy production is detected at the surface as might be expected on this day. Unlike 14JUL, it was not raining at the surface.

4.3 July 28

The synoptic conditions on 28JUL and 30JUL were not favorable for cumulus convection. These days showed a distinctly different type of boundary layer development which involved the surfacing of dry westerly air.

On 28JUL Colorado was under weak subsidence associated with the building of a ridge primarily to the north of Colorado. A surface high was analyzed over northwest Colorado during the time of the flight legs. This provided an unfavorable pressure gradient that inhibited the entrance of low-level moisture into the mountains from the south or east as occurred on 14JUL and 15JUL.

The 50 kPa height map characteristic of 28JUL (and 30JUL) is displayed in Fig. 4.1b. The flow is dominated by a large high pressure region over the southwestern states. Air being advected over Colorado was very dry and from the northwest. Thus little upper-level moisture is available on 28JUL.

Also in contrast to 14JUL and 15JUL the winds at and just above ridgetop were very strong. The 1000 MDT rawinsonde measured 50 kPa winds

of 17 m/s at 300°. The two PAM surface stations at the top of the mountain range measured winds from this same direction averaging about 8 m/s during the time the aircraft was in South Park. Thus, none of the criteria cited for cumulus convection were satisfied on 28JUL.

Despite these differences, the actual state of the boundary layer air in South Park during the morning hours is not as different as the above features might imply. In fact, the total moisture content of the Park area extending up to ridge top at 60 kPa was similar on all case study days, averaging about 4 gm/kg. This is evident from averages of both 0600 MDT and 1000 MDT rawinsondes. The precipitable water as calculated from the rawinsondes was quite similar for all case study days (Table 4.1).

Also, general features of the developing boundary layer are similar to the other days as Fig. 4.4c shows. Heating of the surface has produced an adiabatic layer by 1000 MDT. Surface winds are out of the east at this time at about 2 m/s suggesting that upsloping is occurring on 28JUL as well.

Table 4.1 Precipitable water of case study days based on averages of 0600 MDT and 1000 MDT rawinsondes.

Case Study Day	Averaged Precipitable Water
14JULY	1.02 cm
15JULY	1.14 cm
28JULY	0.98 cm
30JULY	0.85 cm

The stable layer of air above 3000 m AGL, especially acute on 28JUL and 30JUL, was frequently observed over South Park primarily on the early morning rawinsondes. It is usually assumed to be the remains of the previous days boundary layer height. A sharp drop in moisture is usually present on the rawinsonde plots at this level. Holzworth (1964) has calculated monthly mean maximum mixing depths over the United States at upper air sounding sites based on the height of the dry adiabatic layer. For Grand Junction, about 200 km to the west, the maximum mixing ratio depth is 3200 m for mid-July and about 3100 m for the end of July. This corresponds well with the observed height of the stable layer over South Park despite the fact that Grand Junction is so far to the west and at a much lower elevation (1500 m ASL).

Tennekes (1973) has shown that a potential temperature discontinuity may exist at the top of the boundary layer due to the turbulent entrainment of air into the mixed layer. We further suggest that nighttime radiational cooling at the moisture discontinuity will add to the magnitude of the stable layer or inversion. Additionally, George (1979) has suggested that mesoscale cold air drainage from the mountains and valleys may accentuate the inversion over the mountains due to the compensating subsidence of the air above it.

Specifically, on 28JUL and 30JUL, the early morning rawinsondes showed strong inversions at 45 kPa and 49 kPa persisting until mid-afternoon and midmorning, respectively. They were 1.2^{o} and 1.7^{o} over a 1 kPa interval. Their presence seemed to inhibit or delay the development of large cumulus sytems. On 28JUL the inversion strengthened before its dissipation in the afternoon. This was probably associated

with the building of a ridge over Colorado and the advection of warmer air aloft.

Curiously, the Denver soundings (just 115 km to the northeast) did not show these inversions. Instead, they showed an absolutely stable layer at this height. The relative magnitudes of the layers as measured by the potential temperature changes, were very similar. This suggests that the mountains were somehow causing an accentuation of the stable layer. In addition to previously suggested causes by George (1979), it is possible that the sounding path may have been under the influence of a gravity wave. In subsequent analysis the presence of a gravity wave on 30JUL is demonstrated at the lower levels traversed by the aircraft. This, and conditions suitable for its development suggest that a gravity wave may also have been present at the inversion height. The rawinsonde was launched just 15 km downwind of the mountain barrier and may have had its ascent affected by the wave.

The early morning soundings on 14JUL and 15JUL showed isothermal and stable layers at 45 kPa, respectively. Since upper-level winds are very light and there is little synoptic subsidence, we expect these stable layers to be the results of the previous days boundary layer top altered possibly by radiational cooling and mesoscale drainage.

The cross-sectional plots of potential temperature and mixing ratio for 28JUL are displayed in Fig. 4.8. The most notable feature on this day is the tremendous localization of heat flux over Sheep Ridge. The highest potential temperature measured in the entire cross section occurred near the surface of Sheep Ridge. This area appears to be acting as a localized source of buoyant energy production. Strong

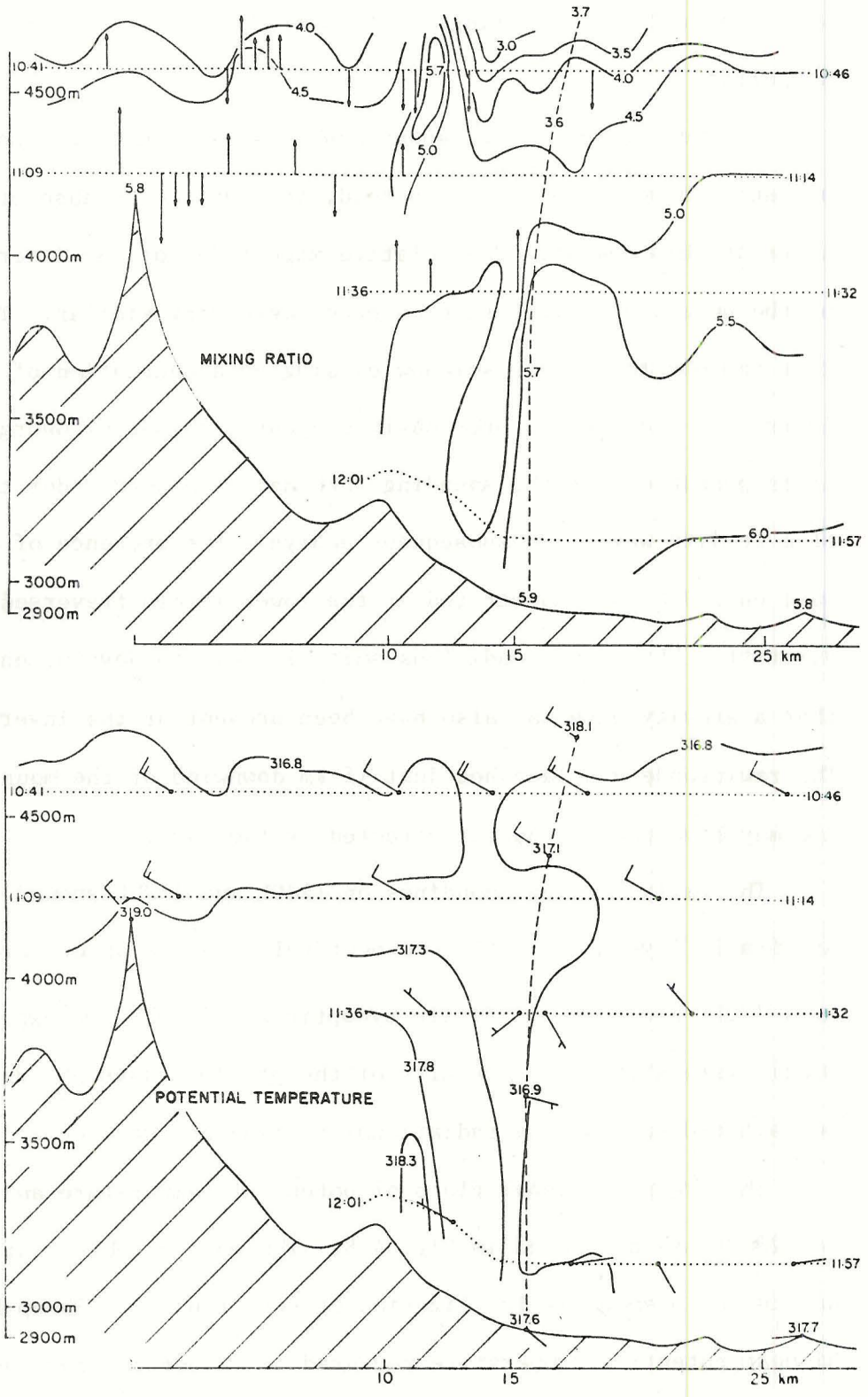

Figure 4.8 Cross sections of mixing ratio and potential temperature for 28JUL. Same as Fig. 4.6. The 1007 MDT rawinsonde is used here.

vertical velocities are also present and most notable in the lower middle flight leg. The lower edge of a ragged cloud was intercepted on the upper flight and is apparently associated with this area of heat flux. Mixing ratios near the cloud indicate that the air was derived from surface levels over the lower-lying terrain of the Park.

Strong vertical velocities are also present near Horseshoe Mountain. They indicate the presence of forced flow over the mountain barrier. Recall on this day ridgetop winds were on the order of 10 m/s. There are many other areas of strong vertical velocity indicative of the tremendous mixing of the lower atmosphere.

The lowest flight leg shows the presence of a cool and moist layer of air over the Park. Winds in this area were light at the time and tended to be easterly (upslope). This layer of air was apparently not yet affected by the upper level flow. Later in the day, the winds were strong and westerly throughout the Park at the surface indicating that the surface layer air had become well-mixed.

Cross-sectional plots of the various TKE parameters are displayed in Fig. 4.9. In addition to TKE, buoyancy production of TKE, dissipation and shear production is included. The vertical wind profiles used in calculating it for 28JUL (and 30JUL) are given in Fig. 4.10. The 0600 MDT and 1000 MDT rawinsonde calculated wind values are given along with the flight leg average of the wind component. Generally, the 0600 MDT rawinsonde was more comparable to the flight leg averages than the 1000 MDT rawinsonde despite the fact that the 1000 MDT sonde would have been more temporally consistent. This was attributed to the path the sounding took. There was a localized flux of lower momentum buoyant air mixing

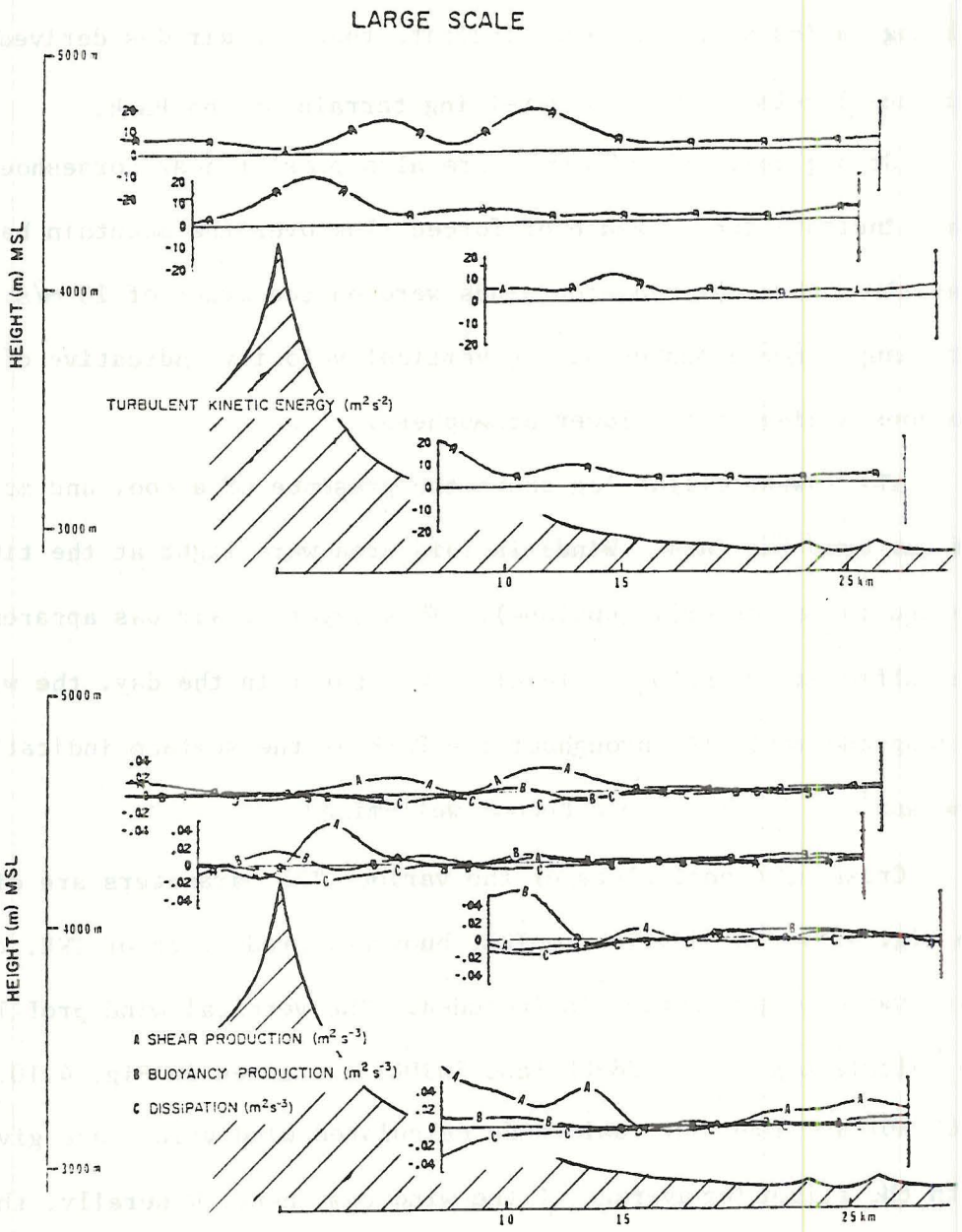

Fig. 4.9 28JUL TKE analysis.

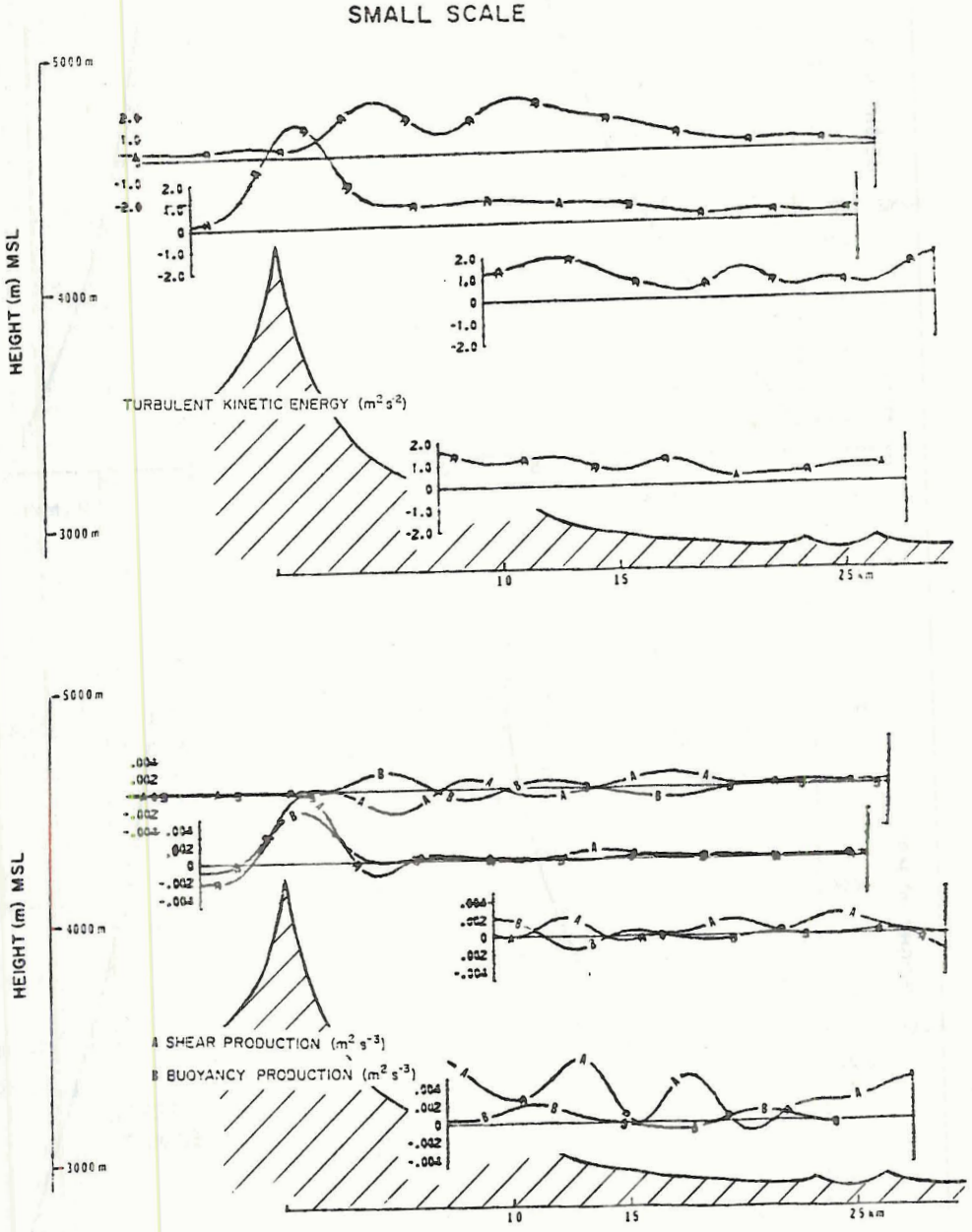

Fig. 4.9 28JUL TKE analysis (cont).

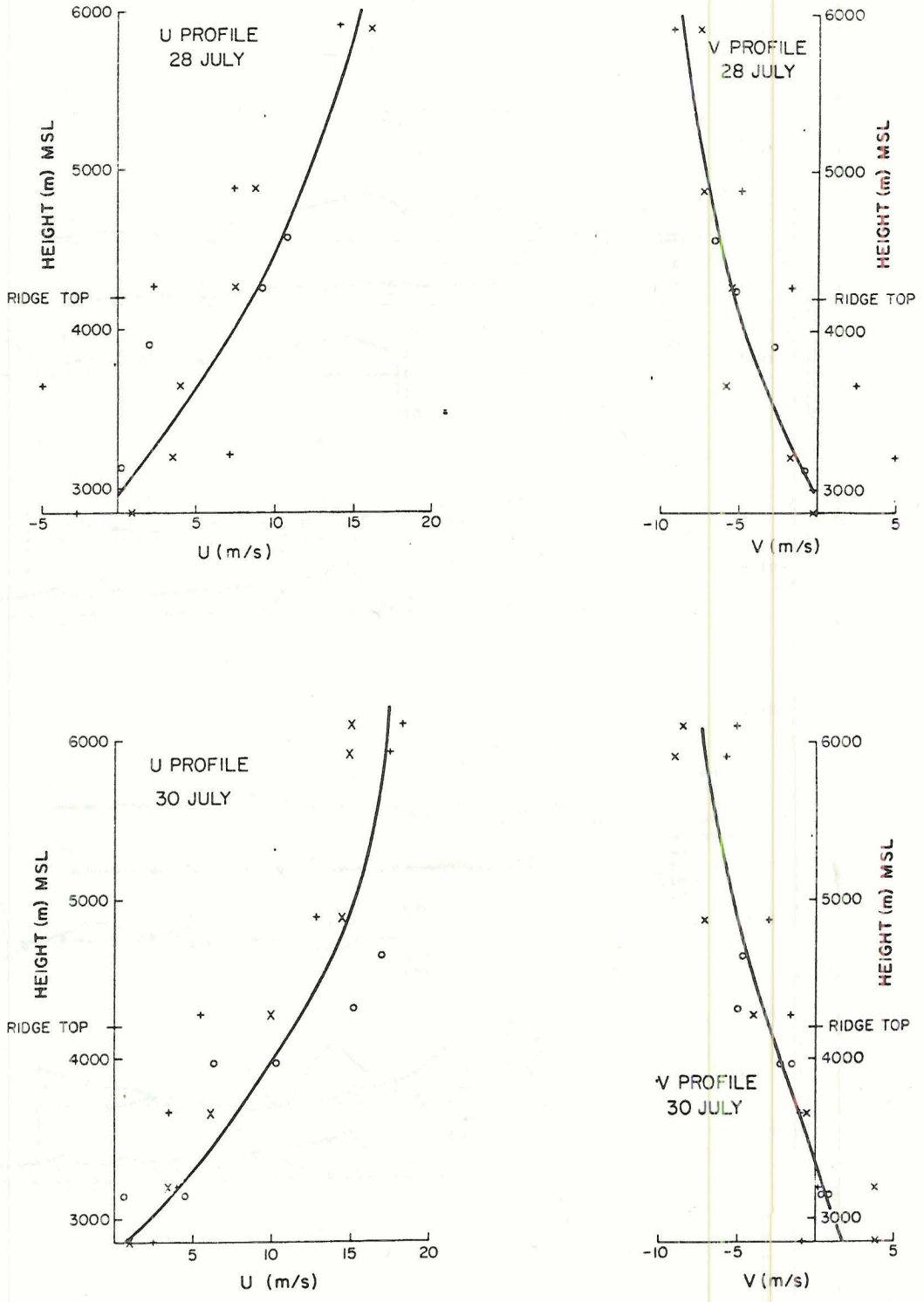

Figure 4.10 Vertical wind profiles for 28JUL and 30JUL. Data are taken from the 0600 MDT rawinsonde (x), the 1000 MDT rawinsonde (+), and the averaged aircraft measured component (0).

with the upper-level flow above the sounding site. The increased amount of turbulence and general tendency for upstream flow are apparent at and below ridgetop.

The cross-sectional plots of TKE revealed large isolated regions of turbulence downwind of the mountain crest. Shear productional cross sections were well correlated with the TKE cross sections indicating that shear production was the primary source of TKE. This is in contrast to previous studies of the unstable boundary layer performed over flat terrain and under lighter wind conditions where buoyancy was the primary productive source of TKE.

Buoyancy production was generally positive, but of smaller magnitude than shear production. As might be expected, it was of higher magnitude in the lower levels and became more neutral in the upper-level flight leg (where it even tended to compensate slightly for shear production). This general trend is apparent in other studies over flat terrain.

A localized area of positive buoyancy is evident in the lower-middle flight leg over Sheep Ridge (the small hill located to the lee of the mountain crest). Presumably, the area above the ridge is devoid of the pooled downslope air which has drained further out into South Park and takes less heating time to produce warm thermals. Therefore, the large buoyancy maximum seems to be the result of buoyant production from the ridge below. However, it is probably aided by the flow aloft which is starting to reach the surface.

Dissipation generally tended to compensate for the production modes calculated. Note also that it is of generally larger magnitude than calculated for 14JUL and 15JUL.

Smaller scale buoyancy production was often a better indicator of true heat flux from the surface. The effect of essentially different air masses interplaying at the lower levels (that is, warmer mixed air near Sheep Ridge and cooler South Park air) was not important on this scale due to the definition of this operator (an exception to this, of course, occurs at the boundary of the air masses.) Buoyancy production near the surface of Sheep Ridge is positive. Thus we see that there is heat flux associated with this area. Another maximum located above the mountain crest is also apparent.

Shear production on the subgrid scale was generally positive, expecially near the surface suggesting that entrainment of faster turbulent mixed flow from above was accelerating (slowing down the upslope flow) the air near the surface.

4.4 July 30

As mentioned previously, the synoptic conditions on 30JUL did not generally favor cumulus convection. Although a surface low was analyzed at 0600 MDT, which would tend to favor convection, the winds aloft were dry and very strong. The 50 kPa map was similar to 28JUL with winds of 18.5 m/s at 280°. Ridgetop winds were also very strong. The two PAM surface stations located at ridgetop measured winds averaging above 10 m/s at 280° throughout the morning. By 1200 MDT the surface low was no longer present.

Small cumulus clouds were observed to form at 0930 MDT which was towards the end of the aircraft flight. By 1100 MDT clouds had covered the entire sky, but never developed to any significant size. No precipitation was observed during the day.

As seen in Fig. 4.4d, the boundary layer was becoming well-mixed by 1000 MDT. This is earlier than on any of the other case study days. It will become apparent that this was a result of the close proximity to the mountain range and not indicative of the entire South Park area.

Cross sections of potential temperature and mixing ratio for 30JUL are displayed as two separate sets of plots (Fig. 4.11). The aircraft flew six flight legs on this day, of which the two lower ones were repeated. This allowed a more thorough sensing of the evolving boundary layer. Note that the upper two flight legs are the same on both sets of figures. The contours, however, are drawn to be more consistent with data appropriate for the lower two levels.

The most obvious flow feature on 30JUL was the wave-like nature of potential temperature and mixing ratio shown best earlier in the morning. Vertical velocities agreed well with this assumption. Some turbulent activity was evident near the crest of the wave over South Park but elsewhere the flow seemed to be somewhat laminar.

The lower-level flight leg allowed a comparison to be made with the boundary layer profiler in operation at this time and at the same height. Temperature, mixing ratio, wind speed, and direction all agreed remarkably well. The air below the level of the flight leg was stable at this time, but turbulence was still evident as fluctuations in horizontal wind. Gusts up to 7 m/s were observed between 150 m and 200 m AGL. Possibly the turbulence noted above this layer was being felt near the surface as well.

As the day progressed, a strong area of heat flux was noted over Sheep Ridge similar to 28JUL. Warm potential temperatures and strong positive vertical velocities were well correlated. The upper level

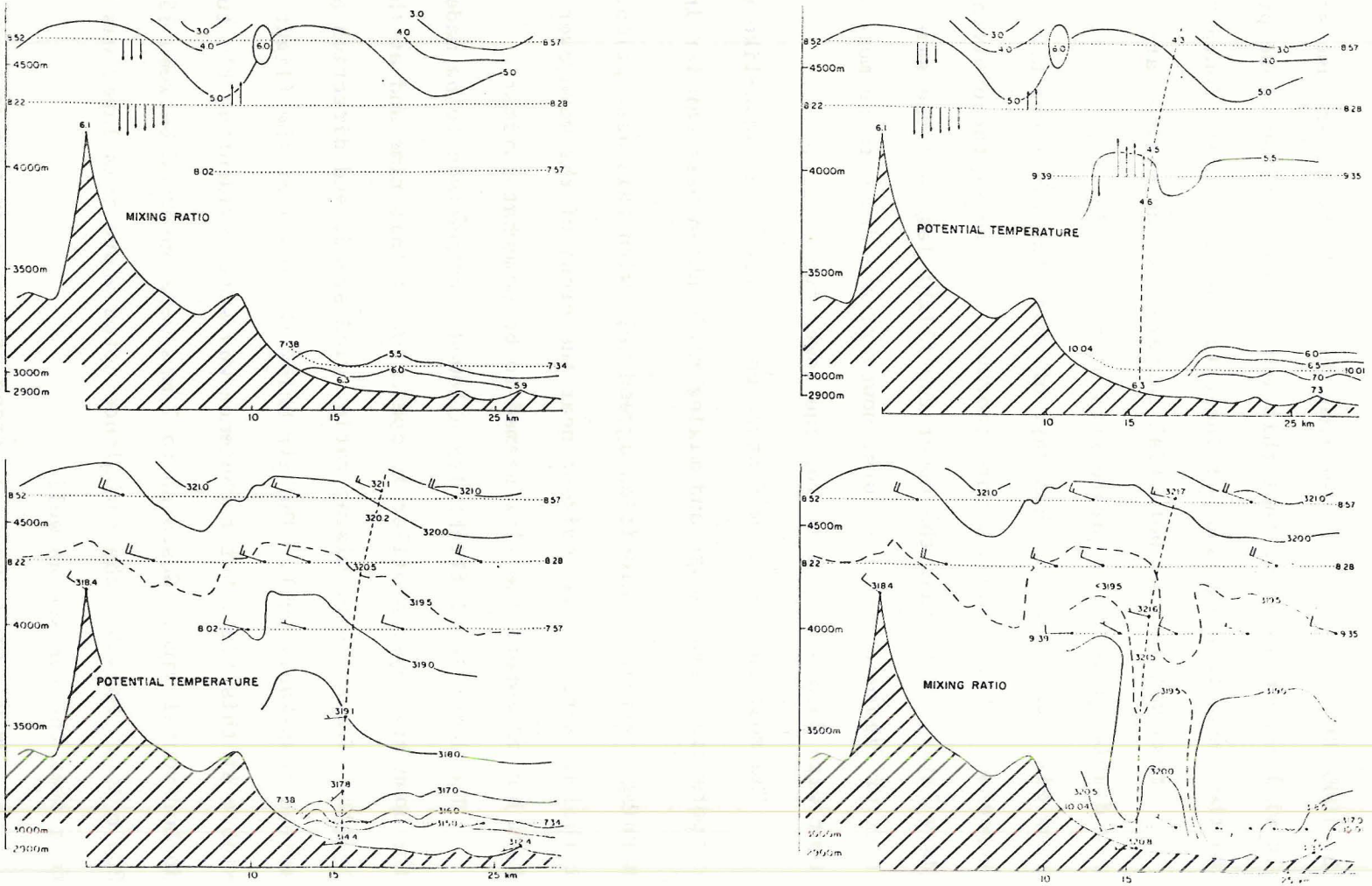

Figure 4.11 Cross sections of mixing ratio and potential temperatures for 30JUL. Same as Fig. 4.6. The 0620 MDT rawinsonde is used for the earlier plot and the 1021 MDT rawinsonde for the later plot.

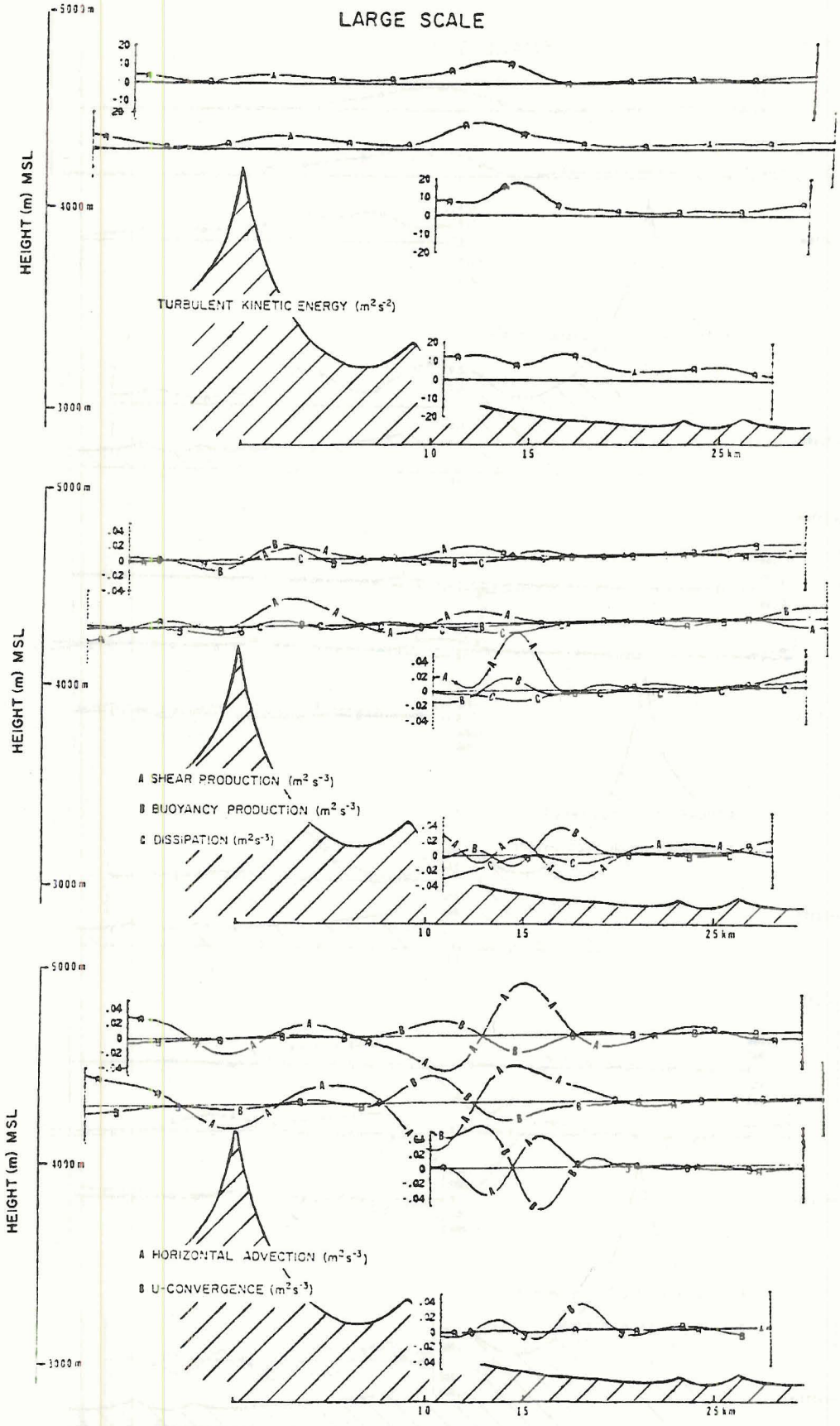

Fig. 4.12 30JUL TKE analysis.

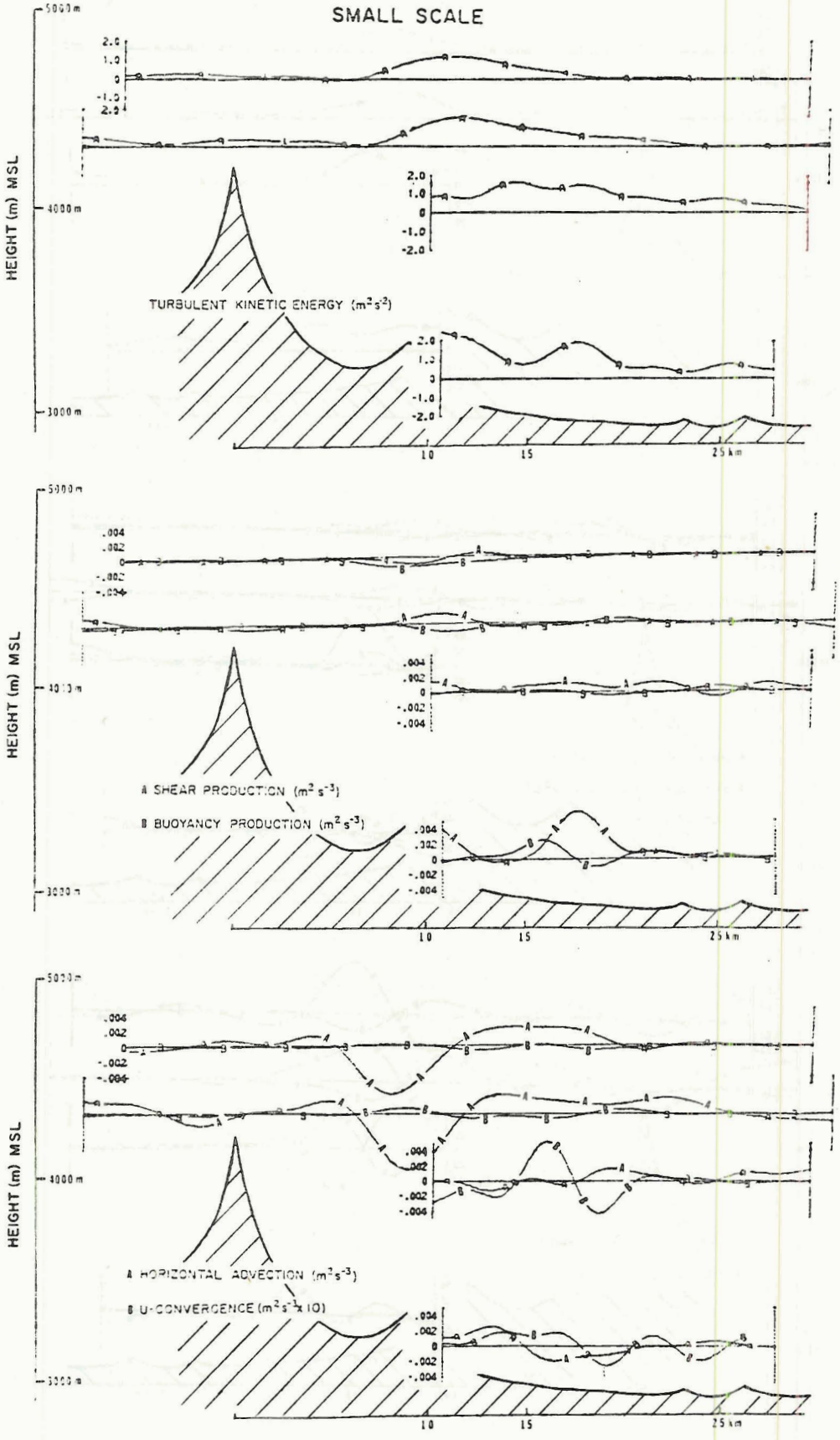

Fig. 4.12 30JUL TKE analysis (cont).

winds appeared to be working their way down to the surface where temperatures had risen to comparable amounts.

A cool and moist layer of air is evident, as on 28JUL, over the Park area at about 1000 MDT. Again winds were light and predominantly south-easterly (upslope). Later in the day, the westerlies surfaced and the air became dry and well-mixed throughout the study regime.

Cross-sectional plots of the various TKE parameters for the latter four flight legs are displayed in Fig. 4.12. In addition to previously calculated parameters, two TKE transport terms are calculated including the horizontal advection of TKE and the horizontal convergence of TKE.

The larger scale TKE maximum was located nearly 15 km downwind of the mountain crest. As on 28JUL, it was primarily due to shear production. Negative buoyancy production and dissipation tended to compensate for it in the upper two flight levels. In the lower levels, buoyancy production contributed to TKE, but also seems to be the result of the descending upper-level flow. The symmetrical sink-source buoyant region and shear production region located over the mountain crest is more precisely associated with forced flow over the mountain barrier. Also the negative maximum of shear production and the positive maximum of buoyancy production in the lowest level can be associated with the descending of the upper-level flow, which is warm, well-mixed, and rising in this region.

The transport terms calculated for 30JUL were generally of larger magnitude than shear production or buoyancy production. Advection of TKE was the largest measured term of the TKE equation indicative of the high winds and localized nature of the turbulence. It was approximately 2-3 times larger than the production terms. However, it was to a large extent compensated for by the horizontal divergence of TKE which was

approximately one-half of the advection. This was explainable by the fact that in the reference frame of the mean wind the slower-moving air ($u' < 0$) associated with this area was working its way upstream. This comes about partially through the system of TKE operators used, but serves to illustrate the more steady-state nature of the turbulent field not evident in the transport cross-sections. This effect was also noted on 28JUL although the cross-sections are not displayed.

An estimate of the vertical divergence in the positive horizontal convergence area was possible. The average vertical velocity (equivalent to w') at the lower boundary of the convergence maximum was 3 m/s. The TKE associated with this area was about 19 J/kg. Assuming average zero vertical motion in the upper-level flight leg, a convergence of 0.09 $m^2 s^{-3}$ results and the net transport in this area becomes small. Somewhat lower magnitudes of vertical motion associated with the downstream advection maximum suggests that in this area advection is important and larger than the compensating convergence.

The most notable feature of the smaller-scale TKE cross sections is the general lack of turbulence associated with the mountain crest. The flow in this area is somewhat laminar over the mountain so that small-scale turbulence is minimal. The scale of motion is effectively greater than 1 km. Shear production is generally positive as it was on 28JUL. It is a maximum in the lowest level where the upper-level flow is converging with the cooler South Park air. Buoyancy is positive where the well-mixed air has surfaced.

The smaller-scale transport of turbulence revealed again the large magnitudes of advection noted on 28JUL. The horizontal convergence of

TKE was generally much smaller and could not compensate for the advection. Note the change in scale necessary to display horizontal convergence with advection. Although it was of very small magnitude in the two upper-level flight legs, convergence was noted upwind of the turbulent areas and divergence within these areas. This effect can also be noted in the lower-middle flight leg where TKE is diverging from the two TKE peaks and converging between them. In the lowest flight leg a broad area of convergence occurs where the upper-level mixed flow has surfaced. Divergence results when the cooler South Park air is entrained into the flow aloft. It must be kept in mind, however, that divergence of TKE is a three-dimensional phenomena and we have only calculated it in one direction. Vertical divergence, for example, is usually of primary concern in most boundary layer studies.

5.0 DISCUSSION

Many of the turbulent features of the boundary layer over the mountains are explainable by various mechanisms peculiar to mountainous topography. A description of TKE without reference to these features is incomplete. Both the localization of turbulence and the causal mechanisms of its formation are considered in this chapter.

5.1 July 14 and July 15

July 14 and July 15 were days characterized by light winds from the surface to above 50 kPa and a favorable moisture supply. These conditions have been observed to support the development of cumulus convection over South Park. Clouds are generally observed to form over the mountains between 0930 MDT and 1000 MDT. On 14JUL convection began at 0900 MDT and on 15JUL shortly after 0920 MDT.

As observed from the aircraft data, there was an apparent localization of heat flux over the mountains. Both 14JUL and 15JUL show turbulent cloud development above the mountain crest in an otherwise undisturbed flow. Presumably this is due to converging upslope flow resulting from local heating with larger scale forcing provided by the pressure gradient induced by the heating of the mountain slopes. Banta and Cotton (1979) have presented a summary of the characteristics of this upvalley flow relying on four case study days from South Park in August. Their results suggest nighttime drainage (westerly to northwesterly) of cool air into South Park gives way to the upvalley (southerly to southeasterly) flow generally between 0730 MDT and 0930 MDT. Sunrise is about 0600 MDT. The upvalley winds are generally 200-300 m thick and typically approach magnitudes of 2-5 m/s. Consistent with these results

this temporal development is observed on our case study days. The condition of the winds in South Park after the upvalley winds were established is displayed in Fig. 5.1 for 14JUL and 15JUL. On 14JUL upvalley winds were about 190 m thick and had magnitudes approaching 5 m/s. Upvalley winds on 15JUL were a little more difficult to detect on the rawinsonde which had easterly flow up to and above ridgetop. This was apparently due to a favorable large-scale pressure gradient resulting from a low centered over the Utah-Colorado border approximately 250 km to the west. The transition from morning downvalley winds to upvalley winds near the surface was, however, observed shortly after 0300 MDT. The temporal development of the surface wind regimes for 14JUL and 15JUL (also 28JUL and 30JUL) are summarized in Fig. 5.2. The results are based on looking at successive plots of winds such as those seen in Fig. 5.1 and obtaining an average condition of the winds over South Park.

Upvalley winds converge over the mountains and result in cloud formation typically seen in South Park at from 0930 MDT to 1000 MDT. Clouds are generally not present in South Park at this time. The boundary layer has not had sufficient time to mix up. Also, subsidence over the Park, due to mass conservation, would effectively strengthen any stable layers and further delay the formation of a mixed layer over South Park.

Cloud formation is frequently observed in this region just downwind of the mountain crest. Two additional days (not included in this study) under similar meteorological conditions also showed this tendency. Other clouds were present above the mountain range to the north and south, but this local region seemed to be preferred. Huggins (1975), using an M-33 (10 cm) radar in his climatological study of first echoes in the central Colorado mountains indicated the presence of preferred

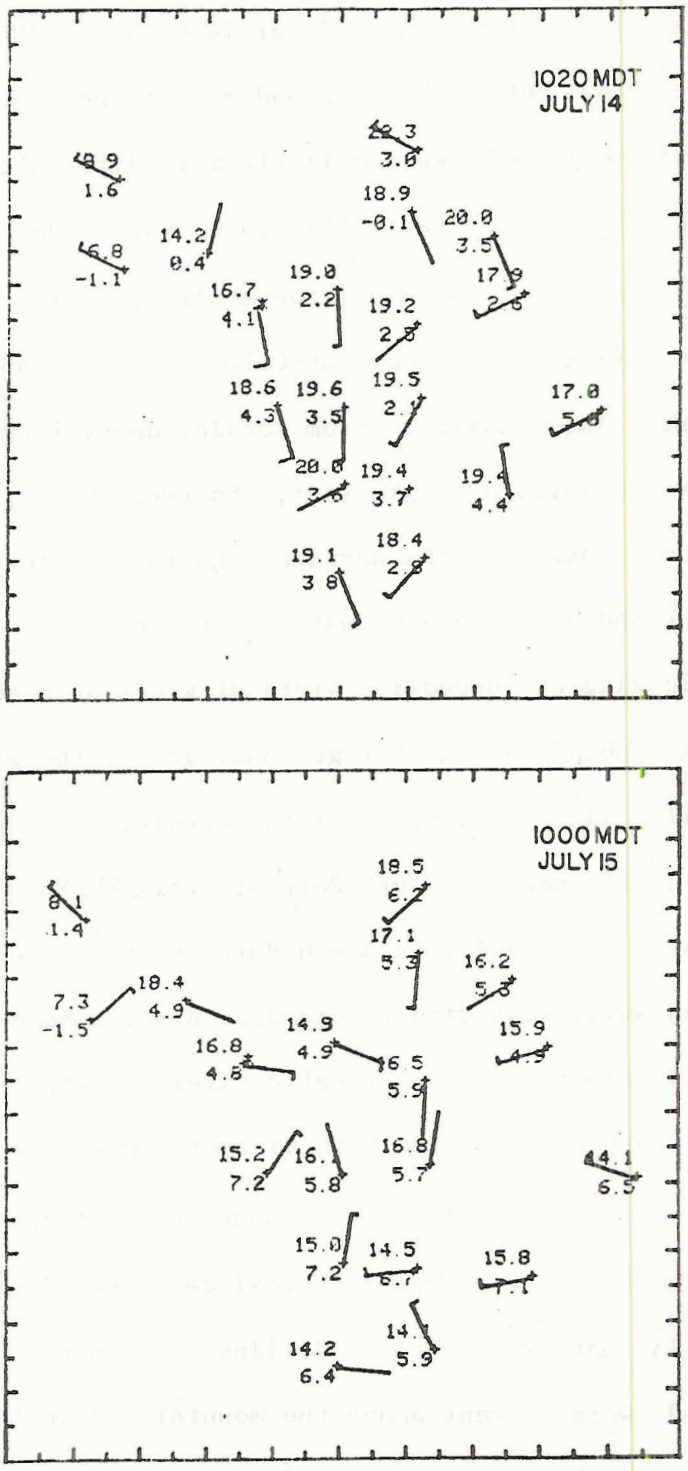

Figure 5.1 Surface winds on 14JUL and 15JUL. The surface winds as measured by the PAM system are in knots. Temperatures and dewpoint temperatures are in ^{o}C. Refer to Fig. 3.1 for placement of the PAM sites.

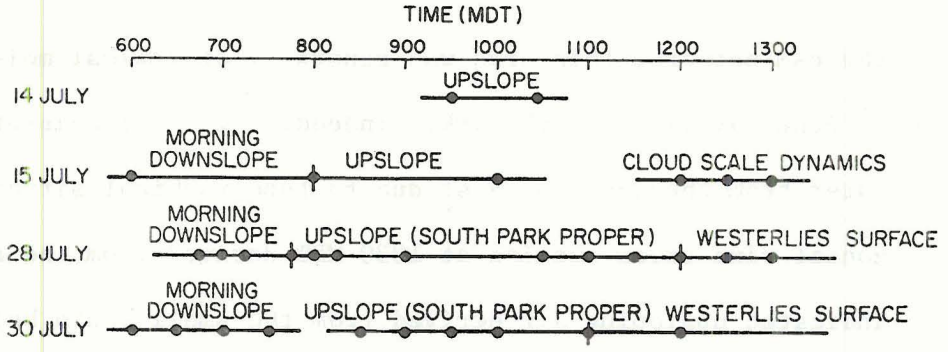

Figure 5.2 Time development of wind regimes from PAM data.

mountain thunderstorm genesis areas. He locates one maxima in the South Park area associated with the Mosquito Range. This occurred at Fairplay approximately 14 km to the east and 6 km to the north of where the clouds were typically observed. Huggins' maximum may be associated with our local maximum. Possibly, he could not pick up the small cumuli which were near Horseshoe Mountain (∿mountain crest) until they had reached a later stage of development and drifted further to the east. Two of the four above-mentioned examples were precipitating by the time they had reached Sheep Ridge. The M-33 radar would probably have been capable of picking them up. However, the westerly winds were anomalously low (∿3 m/s) on these days suggesting slower advection downwind.

Henz (1974) has also shown this "hotspot" effect for Front Range cumuli. He concluded that their importance was influenced by 1) favorable slope, 2) aspect, and 3) access to low-level moisture. These requirements seem to be locally satisfied in this area. The bowl where the clouds formed faces to the ESE and has a slope that will intercept a maximal amount of solar radiation. The area apparently derives its moisture from the larger valley facing to the southeast. As shown by

the PAM network, this area was generally of maximal moisture relative to other areas in South Park. Indeed, low-level moisture must generally enter from the south or east due to topographical situations. The horizontal wind cross section at 1030 MDT derived from the aircraft data indicated upsloping air derived from the small basin below Horseshoe Mountain. The topographical features of this area and location of the cloud are shown in Fig. 5.3.

In general, the size of the turbulent (cloud) area, although somewhat variable, seemed to be closely coupled with the topography below. Orville (1967), using an extremely steep mountain (1 km high and 2 km wide) simulated a cloud 1/2-2/3 the width of his mountain. The clouds present over Horseshoe Mountain were typically 5 km wide. The surrounding topography associated with this mountain is about 7 km wide and about the same height (1 km). This suggests a similar causal mechanism and hence is in agreement with our assumed cause of development.

As mentioned previously additional factors seemed to aid in the earlier development of clouds over the mountains. Cumulus clouds were observed to form by 0900 MDT on 14JUL and shortly after 0920 MDT on 15 JUL. This is slightly earlier than a more typical time of between 0930 MDT and 1000 MDT. On 14JUL we attributed the earlier cloud development to a weak cold frontal passage occurring at approximately the same time. On 15JUL forced upslope flow from the east in the lower 2000 m of the atmosphere probably aided in the slightly earlier time of first cumulus convection.

The potential temperature cross-section for 15JUL suggests that the air surrounding the cloud has been forcibly lifted. We have already

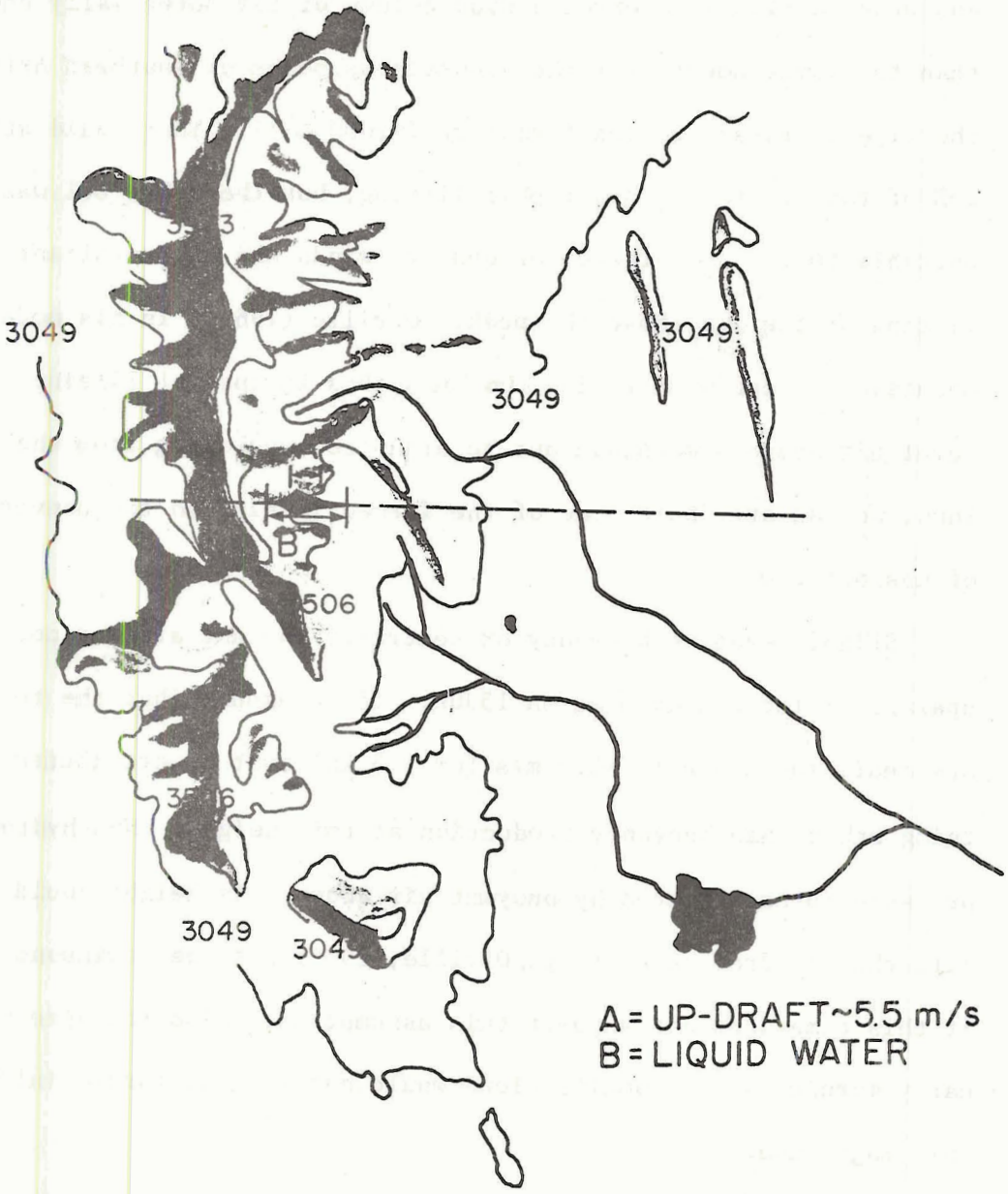

Figure 5.3 Shaded contour plot of the terrain over which the aircraft flew. The position of the cloud on 15JUL is also indicated.

attributed some of these cooler temperatures to the forced lifting resulting from easterly flow below 2000 m AGL. In addition, Braham and Dragins (1960) observed a wide column of air potentially cooler than the environment over the mountainous peaks of southern Arizona at the time of first cumulus formation (∿1000 LST). They could attribute 20% of this to forced orographic lifting, but the other 80% was attributable to the convergence of upslope winds and the resultant forced lifting of the air above the peak. Orville (1965), in his model of mountain upslope winds, also simulated this feature of lifting the upper level air above a mountain due to organized upsloping from the mountain. Thus, we can attribute some of the forced lifting to the convergence of upsloping winds.

Slight negative buoyancy or neutrally buoyant air was noted in the updraft of the cloudy area on 15JUL. If we assume that the temperatures are real, the updraft (∿5.5 m/s for 1.5 km) must be attributed to something other than buoyancy production at this height. Non-hydrostatic pressure forces created by buoyant air above this height could forcibly lift the air from below (e.g., Orville, 1965) but the rawinsonde taken at this time does not support this assumption. Also the size of this early morning small cumulus cloud would not suggest forced inflow of this magnitude.

It is possible that the Rosemount temperature sensor was measuring temperatures too low in this cloudy area which was below freezing. As mentioned before, errors as large as $1^{o}C$ can exist. This would easily account for the vertical velocities measured in the cloud. However, since both the Rosemount and reverse-flow sensors showed similar

responses and the reverse flow sensor is protected from cooling by cloud water we suspect that the measured values of temperature are reasonably accurate.

The vertical velocities may be attributed to warm thermals originating over the mountains. Indeed, thermals just 0.3°C warmer than the somewhat mixed air below the cloud approach vertical velocities of this magnitude. The cloudy air detected by the aircraft may have reached a level of neutral or slightly negative buoyancy and continue to rise due to inertial considerations. Further, some lifting may be the result of forced flow up the mountain barrier.

Definite conclusions are difficult without knowledge of the thermal structure of the air near the mountain which may be quite different than what the rawinsonde, taken over South Park, would indicate.

Finally, both clouds on 14JUL and 15JUL were precipitating soon after their formation. Small gust fronts associated with the evaporative cooling and drag of the rain formed over South Park. Thus it seems that by midday, cloud-induced dynamics were becoming important in the South Park area. PAM station data after these times tends to show more variable winds, indicative of cloud activity over South Park.

A summary of important features of the boundary layer development occurring on low wind days is presented in Fig. 5.4. It is based on data and inferences from both 14JUL and 15JUL. Initial cloud development (∿1000MDT) results from the convergence of upslope flow to the lee of the mountain. Warm parcels of air rise over the mountain, condense, and force their way into more stable flow aloft. The cloud is drawn

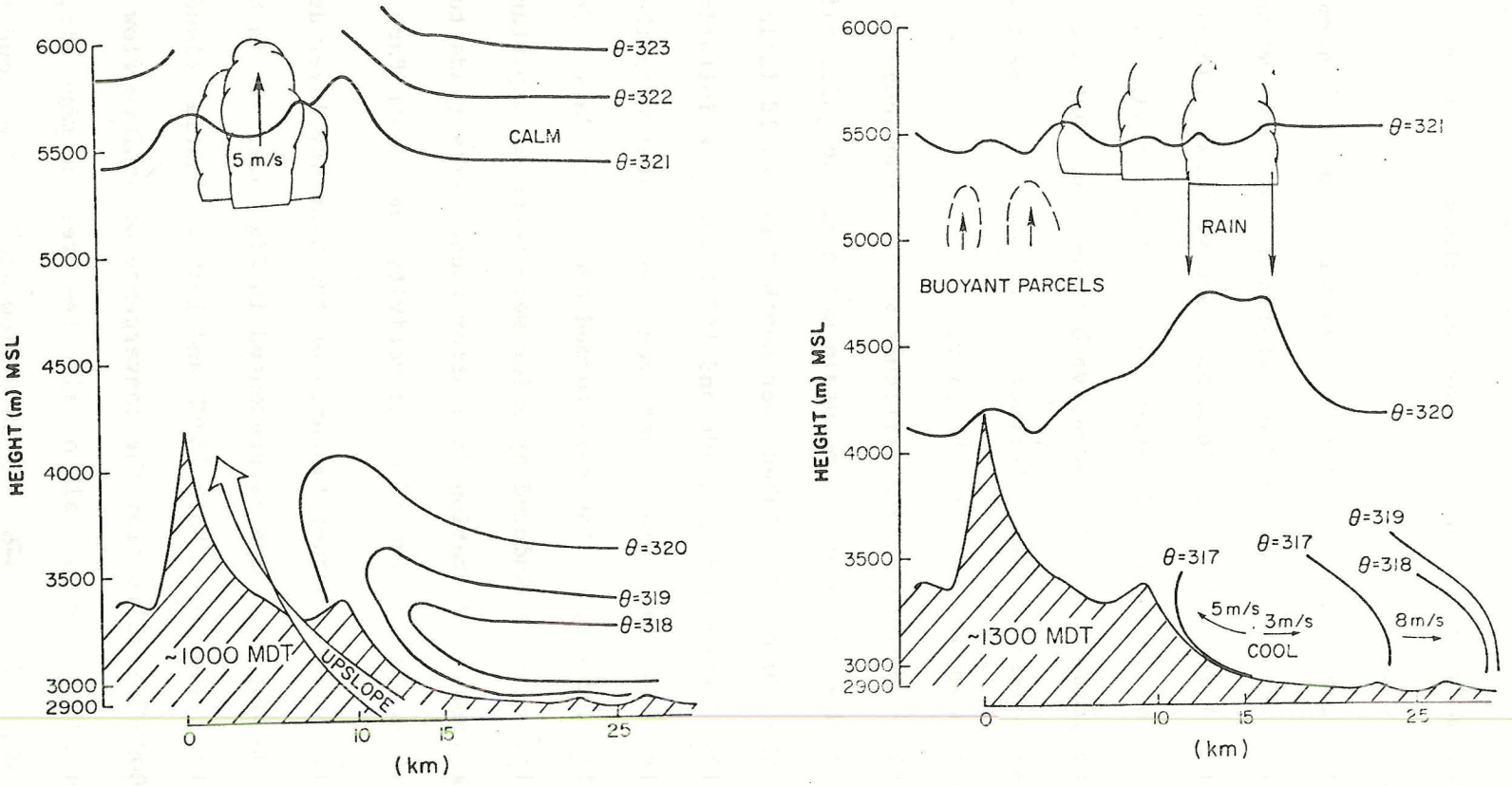

Figure 5.4 Model of development for convective days. See text for details.

so as to be neutrally buoyant. Potential temperature lines below ridgetop are drawn to indicate some forced lifting of the air up against the mountain which also advects moisture in from the east. A super-adiabatic layer forms near the surface. By early afternoon (~1300 MDT) the cloud is precipitating and cloud-scale dynamics begins to take over. Higher momentum air, presumably derived from higher levels, has reached the surface as a small gust front. The continued generation of cloudy material by buoyancy production is indicated over the mountain crest.

5.2 July 28 and July 30

July 28 and July 30 were days characterized by strong westerly winds in the troposphere including the lower levels at ridgetop. The air was generally dry aloft and the surface pressure gradient did not favor the flow of low-level moisture into South Park. These conditions have been generally observed to be unfavorable for cumulus convection. On 28JUL and 30JUL, clouds were observed to form at 0930 MDT but generally failed to develop to any significant size. Only a few isolated clouds were observed to precipitate.

The strong winds at mountain ridgetop level on 28JUL and 30JUL allowed for a dynamical interaction with the westerly airstream. Cross-sectional plots of locally averaged wind direction were made to discern the character of flow on these days. Evidence to be presented will show that many of the upper-level features observed in the energetics study for 30JUL are explainable through the action of an unstable wave-like phenomenon caused by the mountain crest. This feature is less evident on 28JUL.

Cross-sectional streamline analyses done for 30JUL are presented in Fig. 5.5. Wind vectors in the xz plane were plotted every 500 m and projected vertically by drawing parallel wind barbs. A best fit streamline was then drawn through the vector field parallel to the local wind direction. The streamlines revealed the presence of a wave-like phenomena to the lee of Horseshoe Mountain.

The cross-sectional plots are considered to be accurate representations of flow on these days. The large horizontal velocity component makes the INS drift error relatively small. The flight legs are considered to be long enough (15-35 km) to accurately measure absolute vertical velocities relative to assumed zero mean motion. It was possible to follow constant lines of potential temperature through large regions of the flow suggesting that a great deal of it was laminar and interpretable as trajectory paths, especially on the earlier analysis done for 30JUL. The three upper-level flow patterns aligned very well with each other indicating a somewhat steady-state flow and further supporting our ability to follow isentropes representative of parcel trajectories. A slight cooling trend, arising from cold air advection, is evident.

The 30JUL 1010 MDT rawinsonde indicates a stable layer of about 4.6^{o} θ/km just above the upper flight leg. This layer is evident on the cross-sectional wind analysis in the troughs of the wave. Assuming the air has been initially displaced upwards, it is possible to calculate a frequency of buoyant oscillation (Brunt-Väisälä frequency) of the stable air, advect it downstream, and arrive at an estimate of its wavelength. If stability is estimated from the sounding, a wavelength of about 9.5 km is calculated. However, this is not necessarily a good estimate of the stability of the air 1.5 hrs earlier and at a

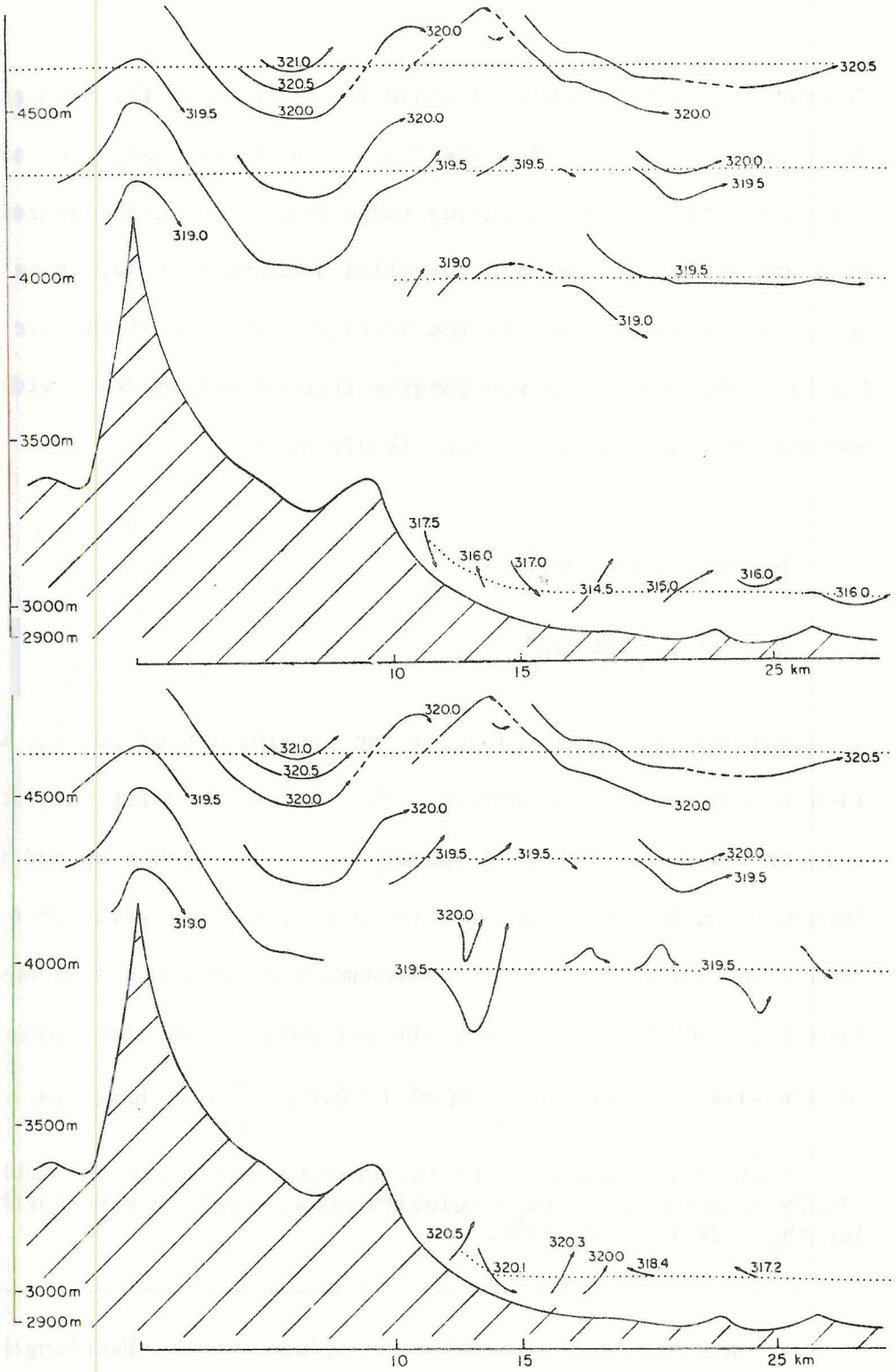

Figure 5.5 Streamline analysis for 30JUL. The earlier aircraft flights are on top and the later flights on the bottom. The lines indicate streamlines indentifiable from both the UW wind component and potential temperature. They are drawn relative to each flight leg which are represented by dotted lines. Note that the streamlines are not consistent with respect to temperature from flight to flight. They were separated in time by ∿½-hour and cooling trend is evident.

lower(flight leg) height. Instead we use a potential temperature line representative of the flow field at a particular height to calculate a wave amplitude. By comparing ridge and trough temperatures with this amplitude, and assuming parallel isentropic flow, it is possible to arrive at an estimate of the average stability of the air at that height. The calculated wavelengths then correspond well with the spectral estimate of wavelength (Table 5.1).

The Scorer parameter

$$\ell^2 = \frac{g}{\theta} \frac{\delta\theta}{\delta z_o} / U_o^2 \quad ,$$

is often used as a criterion for the possibility of gravity wave formation to the lee of 2-D terrain. "... waves can exist only if there is a layer low down in which ℓ exceeds its value higher up and the lee wavelength is such that k is equal to an intermediate value of ℓ." (Scorer, 1954). The parameter k is the wavenumber defined as k = 2π/wavelength. From the 1000 MDT rawinsonde, the estimated ℓ for the stable layer at 56 kPa gives a value of k equal to 6.0×10^{-4} m^{-1}, based on a mean wind

Table 5.1 Estimation of the gravity wavelength on 30JUL. Sensitivity of both $\partial\theta/\partial z$ and U velocity measurement to wavelength. $\text{Wavelength}_x = 2\pi U(g/\overline{\theta}\ \partial\theta/\partial z)^{\frac{1}{2}}$.

U	$\overline{\theta}$	$\partial\theta/\partial z$	Wavelength
18m/s	320°	4.6°θ/km	9.5 km
18m/s	320°	3.0°θ/km	11.8 km
16m/s	320°	3.0°θ/km	10.5 km

of 16 m/s; the aircraft derived value is 5.3×10^{-4} m^{-1}, based on a mean wind of 18 m/s. Above this layer ℓ is obviously small due to the minimal potential temperature gradient evident on the sounding which satisfies the first criterion. The value of k (5.3×10^{-4} m^{-1}) satisfies the second requirement based on the sounding and comes close based on the aircraft derived value of ℓ. Thus, the possibility of a gravity wave exists.

It is also possible that this wave flow feature is due to topographic forcing. Another east-west flight leg occurred farther to the north of the study regime and at the same altitude as the upper-level flight leg. This allowed for a comparison. After plotting wind vectors of the UW plane, it was obvious that the flow corresponded to the topography. The terrain was higher and more mountainous, however, which meant the aircraft was often within 400 m of the peaks. Topography would then be expected to be more influential on the flow in this case.

Referring back to Fig. 5.5, it appears that the flow in the 30JUL case study regime also corresponds with the terrain. The wave-like flow appears to deform near Sheep Ridge at the 9 km marker. Hence, it is possible that much of the flow pattern is due to topographic forcing.

On 30JUL, the flow becomes unstable near its crest over South Park. TKE maxima have previously been noted in this area. We suggest that it may be due to shear instability arising from a low Richardson number and resulting in Kelvin-Helmholtz billows. They are a commonly observed atmospheric phenomena (e.g., Gossard et al., 1970; Hicks et al., 1968). The criteria for their onset is generally considered to be a Richardson number less than 0.25 (e.g., Miles and Howard, 1964). Radar observations and aircraft data have revealed detailed structure of the billows (e.g.,

Browning et al., 1973). Our somewhat limited observations suggest a wavelength of about 2.5 km and an amplitude of over 300 m. This is consistent with observed structure and size noted in previous observations.

Richardson numbers for the laminar flow regions (where it was possible to estimate stability) were calculated and shown to be slightly greater than this criterion (i.e., Ri $\sim$ 1). Hence we would not expect billows to form in these regions. It proved difficult to obtain an accurate estimate of stability in the turbulent regions although its magnitude was low. Scorer (1967) has shown that the distortion of an otherwise stable linear flow can alter the local Richardson number and allow the formation of billows in certain areas. Contrary to expectation, the most stable layers develop the smallest Richardson numbers in waves, and so billows are most likely to develop there. The effect arises from the tilting of a stable layer of air and the resulting gneration of vorticity due to solenoidal considerations. Also deceleration causes a decrease in Richardson number. Generally, billows are most likely to form at a wave crest. We suggest that the turbulence appearing on the early morning of 30JUL at the upper three levels arises from shear instability. It does not appear to be induced by lower-level buoyant activity since the early morning air at the lower-middle height is cooler under the wave crest (Fig. 4.11).

However, some forcing may be present by 0830 MDT from upsloping air over Sheep Ridge. The convergence of air above the ridge may be initiating some of the turbulence by perturbing the flow above. Up-valley winds in South Park appear to have become established by the time the two upper-level flight legs were flown. Generally lower momentum air

is present in this area suggesting that the flow is mixing somewhat with the lower momentum air below.

A streamline analysis was also done for 28JUL. The airflow was less organized than on 30JUL, especially over South Park where the turbulence was more transient. This was apparently due to the very low stability of the air and high vertical wind gradient at the time. Recall that the flight legs occurred later in the day than on 30JUL and hence the boundary layer was more developed. Forced laminar flow was apparent over the mountain crest but it gave way to turbulence downwind over South Park. It is possible that a gravity wave existed earlier in the day and that we were observing a later stage of development. The 1007 MDT rawinsonde generally supports this assumption. However, the angle of the wind was approximately 30^{o} normal to the ridgeline. Recall that angles greater than this are not normally conducive to the formation of gravity waves. Therefore it is possible that a wave was present earlier in the day when the boundary layer was more stable and that we observed only a remnant of this feature.

On all four case study days, there is evidence of the diurnal variation of morning upslope winds following nighttime drainage. However, unlike 14JUL and 15JUL, the upslope on 28JUL and 30JUL was confined to the low-lying South Park area (Fig. 5.6). Higher PAM surface stations to the west (e.g., Fourmile and Horseshoe Mountain) show no evidence of upslope. The air is dry and probably associated with the upper-level flow.

The lower-level aircraft flight legs on both 28JUL and 30JUL show a large convergence of cooler and moister South Park air and much drier downsloping air associated with the forced flow over the

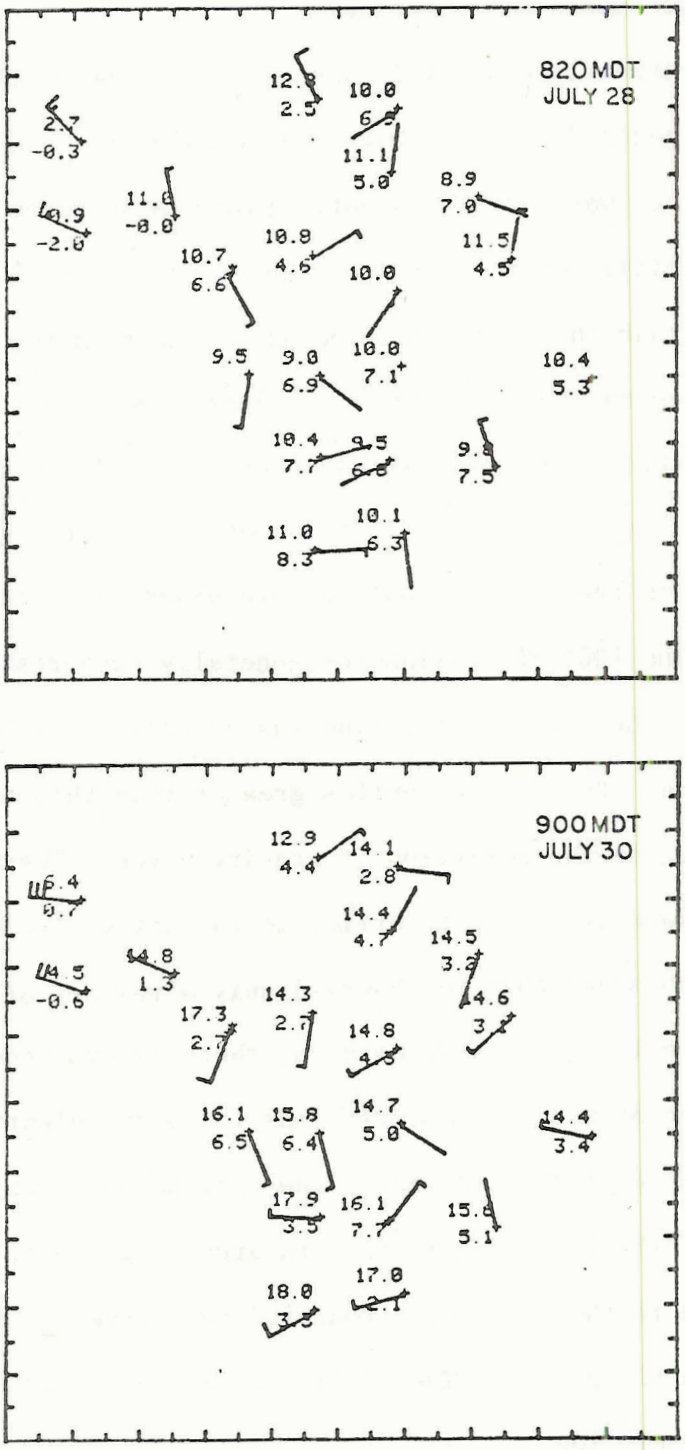

Figure 5.6 Surface winds on 28JUL and 30JUL. Same as Fig. 5.1.

mountain barrier. The aircraft measured magnitude of the upsloping air's westerly component was about 2 m/s, but the possible INS drift error is also of this magnitude. The results could not be considered as meaningful by themselves. However, between the hours of 0735 MDT and 1000 MDT on 30JUL, the mixing ratio of the air, as measured by the surface flight leg, increased from 5.5 gm/kg to 7.0 gm/kg (Fig. 4.11). The source of this increased moisture, as suggested by the PAM data, apparently was associated with the upslope advection of more moist air from the southeast. We therefore conclude that upslope activity was generally present but underdeveloped to its usual extent due to the wave aloft.

On 28JUL and 30JUL heat flux was largest over Sheep Ridge. Anomalously high potential temperature (1-2^{o}C) with respect to the upper levels are evident in the two lower flight legs. July 28 had higher temperatures over Sheep Ridge, but this may be attributable to the fact that the flight legs were later in the day. The ridge had received more solar insolation and hence was a better source of heat flux.

Both the larger scale and the smaller scale showed significant buoyant production near Sheep Ridge. However, the larger-scale production can be somewhat misleading. There are three reasons for this: 1) The elevation of the lowest flight leg is not constant due to terrain consideration. Any potential temperature gradient near the surface would accentuate the magnitude of measured production. 2) There appears to be a potentially cooler and more moist area over the Park proper (as revealed by potential temperature and mixing ratio considerations) which also tends to magnify the actual production term. 3) Thirdly, wind direction plots suggest the possibility of an interaction with the upper-level

flow. High vertical velocities near the surface may be attributable to the effects of the descending wave.

The smaller-scale buoyancy production showed significant localization of production near Sheep Ridge. Since each of these points is not directly dependent on the larger-scale situation, they are considered more representative of true heat flux. On both days, fluctuating scale buoyant production localized itself over Sheep Ridge. Two reasons are suggested for this particular localization of buoyant production. First, the slope is of favorable aspect for the interception of morning solar radiation. Secondly, it is devoid of cooler, drained, downslope flow from the previous night. On 30JUL, potential temperatures were about 2^{o} warmer in the early morning on the east side of Sheep Ridge, 20-50 m higher than the rest of the flight leg flown near the surface of South Park.

The cross-sectional wind pattern for both days suggests the possibility of an interaction of upper-level flow with "buoyantly active" Sheep Ridge. Generally high horizontal and vertical wind speeds were evident near the surface in this area. Potential temperatures are higher than could be derived from the upper-level flow and generally more moist. There must be some mixing before the effects of the wave are felt at the surface. Apparently, the two factors are interacting to produce the above-mentioned flow features. We suggest that the entrainment of small buoyant plumes or bubbles above Sheep Ridge allows the faster upper-level air to approach the surface and subsequently aid in the washing out of cooler South Park air. Evidence of entrainment comes from two sources. First, small regions of moist air, apparently derived from the lower boundary layer, are evident above

Sheep Ridge in the cross-sectional plots of mixing ratio. These plots have been redone to accentuate this effect (Fig. 5.7). Note also the large updraft velocities associated with the boundary of moist surface air over the Park. This seems to suggest a deviation of the surfacing wave by the rising and subsequent entrainment of low-level moist parcels of air. Hence, some of the energy noted in this area seems to be derived from the upper-level flow. Secondly, chaff was observed by radar to be entrained into three clouds slightly downwind of the ridge. It had been released in a low flight leg near Sheep Ridge. The ridge seems to be a focus of convective motion localized by the upper-level flow.

By early afternoon on 30JUL and late afternoon on 28JUL the winds throughout South Park had become dry and shifted to the direction of the upper-level flow. Apparently, the boundary layer over the Park had warmed to a sufficient extent to allow vertical mixing with the more rapid, upper-level flow. The lower, more moist layer, could then be pushed out of the Park through the turbulent exchange of momentum. The pressure gradient (a high to the west) could also aid in this process.

A summary of important features of boundary layer development occurring on high wind days is presented in Fig. 5.8. It is based on data and inferences from both 28JUL and 30JUL. The formation of a wave-like flow conforming with the topography is immediately obvious. It becomes unstable at the western edge of South Park and forms billows that aid in the mixing of air at this level. As early as 0800 MDT upslope is beginning and further perturbs the upper-level flow. Upslope flow is still present by 1100 MDT and continues to bring potentially cooler and moister air in from the lower-lying areas to the southeast.

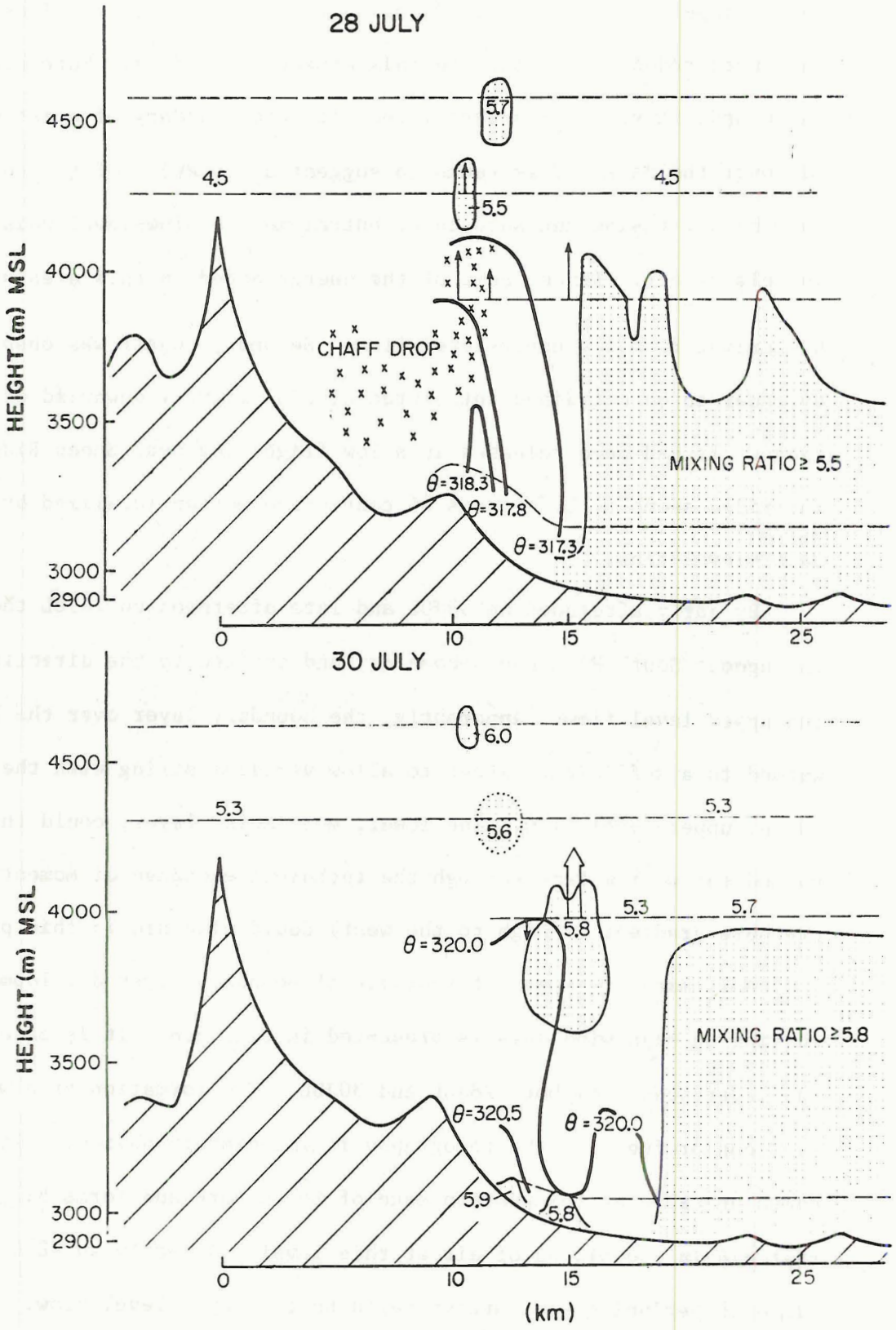

Figure 5.7 Cross sections of mixing ratios for 28JUL and 30JUL. Potential temperature lines are drawn near Sheep Ridge where warm air was detected. Arrows indicate regions of strong vertical velocities associated with this area. 1 cm = 4 m/s.

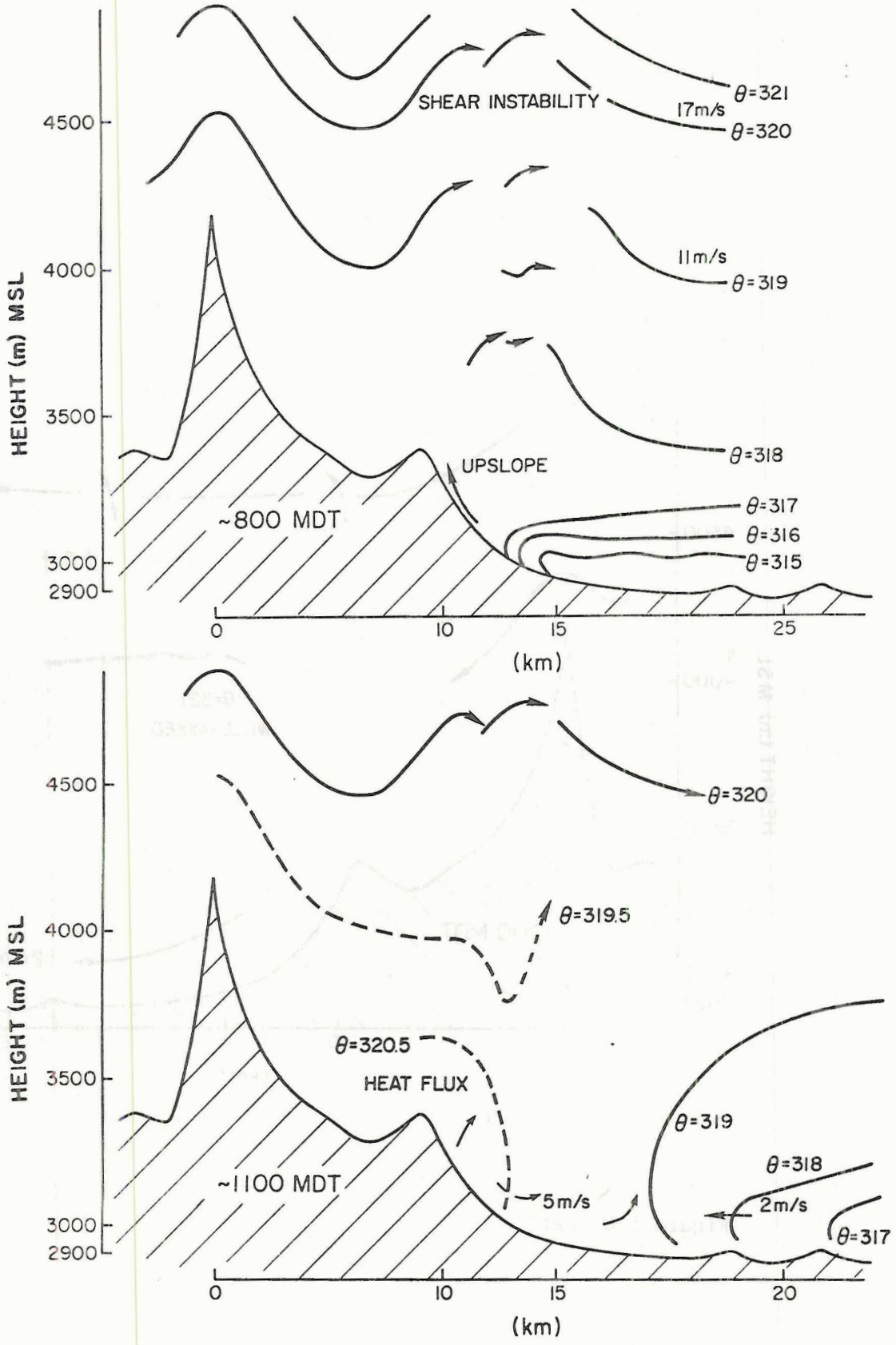

Figure 5.8 Model of development for dry and windy days. See text for details.

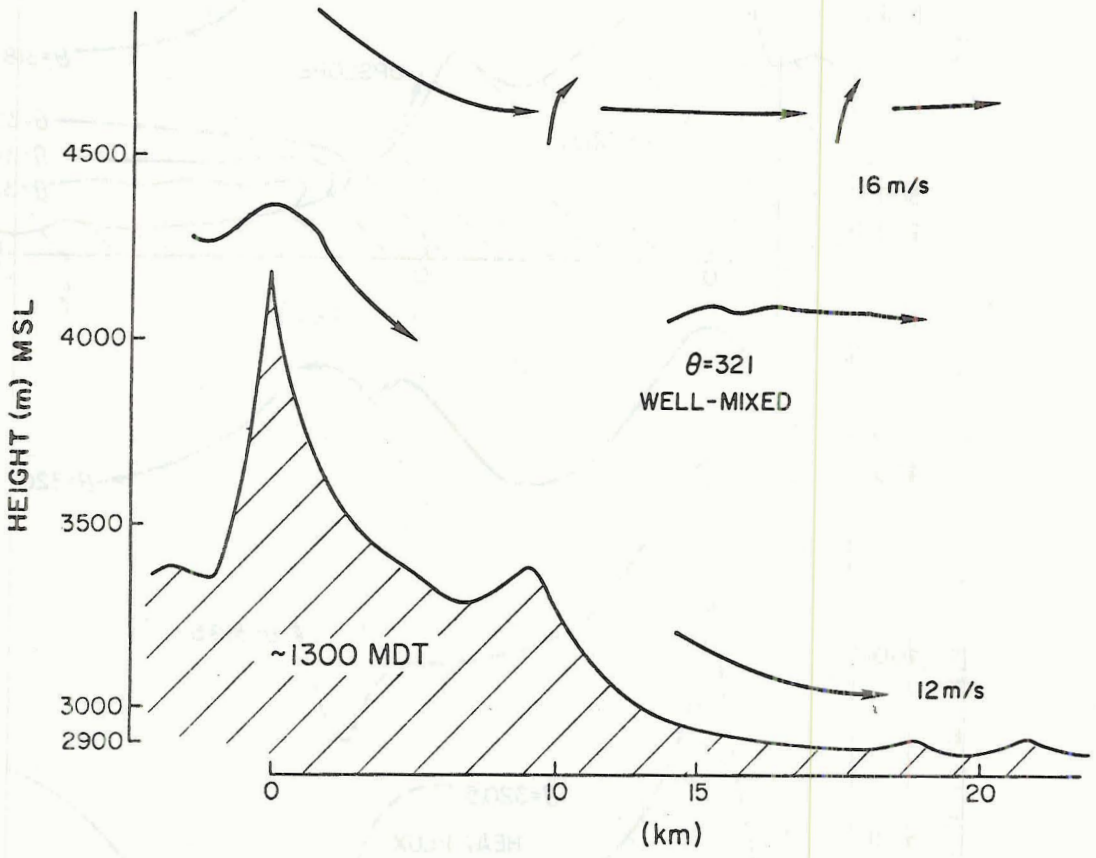

Figure 5.8(cont)

Heating continues and the strong morning inversion diminishes. Over Sheep Ridge a strong area of heat flux is noted. Subsequent rise of this potentially warmer air into the westerly airstream aids in bringing the faster well-mixed air down to the surface through an exchange of momentum. The potentially cool and moister South Park air is entrained into the upper-level flow as it advects in from the east. Later in the day, as surface heating continues, the dry westerly airstream surfaces and seems to wash out the remaining cool pool of air out of South Park. The air throughout the Park becomes dry and well-mixed.

6.0 CONCLUSION

Two different types of case study days, one characterized by light winds and mid-level moisture, and the other by strong and dry mid-level winds, illustrated features of boundary layer development over mountainous terrain in the summertime. Among these features was the surfacing of higher momentum, upper-level flow which was noted on both types of days but occurred by different mechanisms. Analysis of the spatial variability of TKE terms, cross-sectional plots of potential temperature and mixing ratio, and other sources, helped to reveal the presence of these features.

On days characterized by low winds throughout the lower levels of the atmosphere, buoyancy production of turbulent kinetic energy occurred in localized areas due to organized upslope winds. It is inferred that this occurs in certain preferred hot spot areas that have a favorable slope and access to low-level moisture. Initial cloud development ($\sim$1000 MDT) seems to be the result of convergence of upslope winds which, once organized, can advect low-level moisture in from lower-lying areas to the southeast. Warm thermals rise over the mountains and force their way into the more stable air aloft. Initially the clouds are neutrally or slightly negatively buoyant. Later in the day positive buoyancy at cloud levels allows more vigorous and extensive cumulus cloud growth. As the clouds reach the upper levels of the atmosphere, turbulent mixing and associated evaporational cooling creates downdrafts which allow for the downward movement of higher momentum air aloft. The resulting winds at the surface are of a magnitude comparable with those aloft at 40 kPa in this case.

On days characterized by high vertical wind shear in the boundary layer, the formation of turbulent areas downwind of the mountain crest

occurs. The turbulence is caused by shear instability, expressed as a low Richardson number, and results in the mixing of air at that level. A buoyantly-driven, well-mixed region over the lower-terrain levels of the Park, deepens as a consequence of surface heating. The upper-level momentum can reach the surface when the upper-level air, being well-mixed due to shear instability, and the lower-level air, being well-mixed due to surface heating, approach the same potential temperature. The higher momentum air can then reach the surface through an exchange of momentum throughout the deep layer of nearly constant potential temperature. This occurs first to the lee of mountain crests. The shear instability arises downwind of the mountain due to the formation of an unstable flow pattern, possibly an unstable gravity wave. Strong areas of buoyancy production occur over the lower mountain slopes to the lee of the mountain peak on the sunny side. This area is devoid of the potentially cooler air present over South Park in the morning. The air above the lower mountain slopes can heat to a higher temperature earlier in the day. When the potential temperatures of these two areas reach a comparable magnitude the strong upper-level winds rapidly descend to the surface.

On both types of days, the initial state of the boundary layer was quite similar. A potentially cool layer of air exists in South Park, presumably the result of nighttime drainage and radiational cooling. Moisture in the boundary layer was about the same on both types of days. Upslope-upvalley winds formed on both days. Flow above mountain ridge-top levels remained distinctly decoupled from the below ridge-top levels throughout the early morning period. By late morning, however, the two days became grossly different.

On days characterized by strong winds and dry air above ridge-top levels, the coupling between the above-ridge-top and below-ridge-top air masses resulted in the washout of moisture out of the Park and only minimal cloud development. On days characterized by low-speed winds and moist air above ridge-top levels, the coupling between the two air masses resulted in the formation of surface gust fronts and convergence zones and their concomitant precipitating cloud systems.

REFERENCES

Alaka, M.A., ed., 1960: The airflow over mountains. WMO Tech. Note No.34, 135 pp.

Banta, R., and W.R. Cotton, 1979: Horizontal and vertical structure of diurnal boundary layer flow patterns over mountainous terrain. Preprints, Fourth Symposium on Turbulence, Diffusion, and Air Pollution, Reno, NV., AMS, Boston, 217-224.

Braham, R.R., and M. Draginis, 1960: Roots of orographic cumuli. J. Meteor., 17, 214-226.

Browning, K.A., G.W. Bryant, J.R. Starr, and D.N. Axford, 1973: Air motion within Kelvin-Helmholtz billows determined from simultaneous Doppler radar and aircraft measurements. Quart. J. R. Meteor. Soc., 99, 608-618.

Caughey, S.J., and J.C. Wyngaard, 1979: The turbulence kinetic energy budget in convective conditions. Quart. J. R. Meteor. Soc., 105, 231-239.

Cotton, W.R., D.C. Hahn, and R. Banta, 1978: Air turbulence measurements in and below cumulus congestus over mountainous terrain. Preprints, Conf. on Cloud Phys. and Atmos. Elect., Issaquah, Wash., AMS, Boston, 408-415.

_____, and R.L. George, 1978: A summer with PAM. Preprint, Fourth Symposium on Meteor. Observations and Instrumentation, Denver, Colo., April 10-14, 1978, 87-92.

Danielson and Cotton, ed.: Space Log 1977. Dept. of Atmos. Sci., Colo. St. University.

Defant, F., 1951: Local winds. Compendium of Meteorology, T.F. Malone, ed., AMS, Boston, 655-672.

Gossard, E.E., J.H. Richter, D. Atlas, 1970: Internal waves in the atmosphere from high resolution radar measurements. J. Geophys. Res., 75, 3523-3536.

Henz, J., 1974: Colorado high plains thunderstorm systems - a descriptive radar-synoptic climatology. M.S. thesis, Dept. of Atmos. Sci., Colo. St. Univ., Fort Collins, Colo.

Hicks, J.J., and J.K. Angell, 1968: Radar observations of breaking gravitational waves in the visually clear atmosphere. J. Appl. Meteor., 7, 114-121.

Holzworth, G.C., 1964: Estimates of mean maximum mixing depths in the contiguous United States. Mon. Wea. Rev., 92, 235-242.

Huggins, A.W., 1975: The precipitation sequence in mountain cumulus. M.S. thesis, Dept. of Atmos. Sci., Colorado St. Univ., Fort Collins, Colo.

Kaimal, J.C., J.C. Wyngaard, D.A. Haugen, O.R. Cote' and Y. Izumi, 1976: Turbulence structure in the convective boundary layer. J. Atmos. Sci., 33, 2152-2169.

Lanczos, C.: Applied Analysis, Prentice Hall, Englewood, N.J., 539 pp.

Lenschow, D.H., 1970: Airplane measurements of planetary boundary layer structure. J. Appl. Meteor., 9, 874-884.

_____, 1974: Model of the height variation of the turbulence kinetic energy and temperature variance in the atmospheric surface layer. J. Atmos. Sci., 28, 190-201.

_____, and W.T. Pennell, 1974: On the measurement of in-cloud and wet-bulb temperatures from an aircraft. Mon. Wea. Rev., 102, 447-454.

_____, C.A. Cullian, R.B. Friesen, and E.N. Brown, 1978: The status of air motion measurements on NCAR aircraft. Proceedings of Fourth Symposium on Meteorological Observations and Instrumentation, April 10-14, Denver, Colo., 433-438.

_____, B.B. Stankov, and L. Mahrt, 1979: The rapid morning boundary-layer transition. J. Atmos. Sci., __, 2108-2124.

Lumley, J.L., and H.A. Panofsky, 1964: The Structure of Atmospheric Turbulence. New York, Interscience, 239 pp.

McCarthy, J., 1973: A method for correcting airborne temperature data for sensor response time. J. Appl. Meteor., 12, 211-214.

Miles, M.W., and L.N. Howard, 1964: Note on heterogeneous shear flow. J. Fluid Mech., 20, 331-336.

Moores, W.H., S.J. Caughey, C.J. Readings, J.R. Milford, D.A. Mansfield, S. Abdulla, T.H. Guymer, and W.B. Johnston, 1979: Measurements of boundary layer structure and development over SE England using aircraft and tethered balloon instrumentation. Quart. J. R. Meteor. Soc., 105, 397-421.

National Center for Atmospheric Research, 1976: Airborne humidity measurements. NCAR Research Aviation Facility, Bulletin No. 22.

Nicholls, J.M., ed., 1973: The airflow over mountains. WMO Tech. Note No. 127, 73 pp.

_____, 1978: Measurements of turbulence by an instrumented aircraft in a convective atmospheric boundary layer over the sea. Quart. J. R. Meteor. Soc., 104, 653-676.

Orville, H.D., 1965: On mountain upslope winds. J. Atmos. Sci., 22, 684-699.

_____, 1967: Ambient wind effects on the initiation and development of cumulus clouds over mountains. J. Atmos. Sci., 25, 385-402.

Peterson, E.W., 1972: Relative importance of terms in the turbulent-energy and momentum equations as applied to the problem of a surface roughness change. J. Atmos. Sci., __, 2108-2124.

Scorer, R.S., 1954: Theory of airflow over mountains: III - Airstream characteristics. Quart. J. R. Meteor. Soc., 80, 417-428.

_____, 1967: Causes and consequences of standing waves. Proceedings of the Symposium on Mountain Meteorology, CSU, Fort Collins, Colo., 75-95.

Tennekes, H., 1973: A model for the dynamics of the inversion above a convective boundary layer. J. Atmos. Sci., 30, 558-567.

Wood, N.L.H., 1977: A field study on the representativeness of turbulent fluxes of heat and water vapor at various sites in southern England. Quart. J. R. Meteor. Soc., 103, 617-624,

Wyngaard, J.C., and O.R. Cotè, 1971: The budgets of turbulent kinetic energy and temperature variance in the atmospheric surface layer. J. Atmos. Sci., 28, 190-201.

Zangvil, A., 1977: On the presentation and interpretation of spectra of large-scale disturbances. Mon. Wea. Rev., 105, 1469-1472.

Zubkovskiy, S.L., and B.M. Korprov, 1970: On the turbulent energy balance in the boundary layer of the atmosphere. Izo. Atmos. Oceanic Phys., 6, 989-995.

APPENDIX A

Filtering

The data have been filtered on several occasions with weights derived from the formula

$$w_k = \begin{cases} \nu_c \text{ for } k = 0 \\ \\ \frac{1}{2\pi k} \sin(2\pi\nu_c k) \quad \cos(\tfrac{1}{2}\pi k/M) \text{ for } 0 < |k| \leq M \end{cases} \tag{A1}$$

where the subscript k identifies the weight, M is half the total number of weights minus one, and ν_c is the half-amplitude point in cycles per data interval. This is the complement of a Lanczos (1956) high pass filter. Depending on the desired effect and sampling rates of the instruments, different values of M and ν_c have been used. A summary is given in Table A.1.

Table A.1 Filtering Parameters

Desired Effect	Cutoff Wavelength	Data Sampling Rate	M	ν_c
low pass filter	4km	8Hz	512	.0025
"	"	1Hz	64	.02
"	1km	8Hz	128	.01
"	"	1Hz	16	.08
high pass filter	.25km	8Hz	64	.04

The high pass filter weights are simply calculated by changing the sign on all of the weights and adding 1 to the central weight. Also the values of ν_c have been determined by assuming the aircraft was flying at 80 m/s. This was not always the case so that the actual filtered wavelength may vary. Occasionally, the plane would fly up to 90 m/s.

Whenever filtering is performed on the data, a small portion is of necessity lost at the terminal ends of the series. There are many different artificial techniques employed to preserve this data. For purposes of this study, a least squares linear fit is added to the prefiltered terminal ends. The fit is based on the same amount, or length, of data that would be lost at the ends. For example, if a set of weights is used containing 1001 points, 500 points would normally be lost at each end of the data set. To prevent this complete loss of data, the least squares linear fit is calculated for the terminal 500 points and the data are extended by 500 points using the linear trend.

All of the data is smoothed to about 4 km and hence is necessarily somewhat artificial within 2 km of the terminal ends. Caution must be used on interpretations in this region.

APPENDIX B

Estimate of the Dominant Scales of Motion

Spectral properties of the aircraft data were analyzed using NCAR's FFT package for all four case study days. Emphasis was on defining dominant scales of motion through the use of wind, temperature, and humidity data. This allowed the choice of an appropriate averaging scale that would resolve the majority of turbulent motion in the TKE analysis.

Method

Spectra of vertical motion, kinetic energy, potential temperature, and humidity were plotted using area-conserving coordinates. For the purpose of defining major scales of motion a "no dominant scale" null hypothesis was used. As described by Zangvil (1977) this is effectively a simplified version of the red noise hypothesis for degrees of persistence between 0.3 and 0.7. Most atmospheric spectra resemble red noise. The raw data are detrended and the raw spectra are conservatively smoothed using a 9-point Hamming filter. Due to the nature of the type of display used, only the longer wavelengths show up as being smoothed, and only to a small degree. However, most of the motion will be shown to occur at these longer wavelengths and the plots considered accurate.

General Characteristics of Results

Generally the results showed a tendency for most of the significant variance to occur at wavelengths greater than 1 km. Contrastingly, vertical turbulent motion spectra associated with the lowest flight legs

typically showed a maximum variance near 1 km wavelengths with significant variance below this wavelength. This was probably indicative of the close proximity to the surface of the South Park area (∿200 m) and possibly the size of the local topography.

Potential temperature, mixing ratio, and TKE spectra were often dominated by an air mass effect in the lowest flight legs. On 28JUL and 30JUL potentially cool and moist air was converging with warm downslope air such that the spectra represented a step function of these parameters. Additionally, potential temperature spectra of the lowest flight leg tended to be meaningless due to the fact that the plane followed the contours of the topography which in some cases meant a 200 m elevation change at the western edge of the flight leg. A relevant mean value from which deviations occur is difficult to define.

It is generally considered beyond the capability of the temperature sensors to measure meaningful temperature fluctuations in a cloud. This meant that potential temperature spectra were inaccurate on 14JUL and 15JUL for the upper flight leg which had cloud penetrations. Also, humidity, as measured by the microwave refractometer, is inaccurate in a cloud so that these spectra are also subject to error. The dewpoint hygrometer, with a better estimate of in-cloud humidity, has a response time too slow for accurate spectra.

In general, vertical velocity spectra were very useful for isolating the sizes of different scale of vertical motion. This was partly due to the fact that they were most compatible with our cross-sectional analyses and easily interpretable considering the topography, but also

due to the fact that much turbulent motion arises from instabilities in the vertical direction. TKE spectral plots had a tendency to be too complicated for interpretation. Most showed a dominance of motion at the longer wavelengths, but were difficult to interpret near the surface apparently due to the relative increase in magnitude of the horizontal winds.

28JUL and 30JUL

On 28JUL and 30JUL, spectral plots of vertical velocity, potential temperature and mixing ratio showed two separate turbulent regimes in the upper flight levels of the data set. The vertical velocity spectra are given in Fig. B1. The first longer wavelength peak was associated with forced flow over the mountain barrier, the second with smaller scale turbulence noted over the Park. July 30 spectra showed a relatively small amount of variance in the small-scale regime. This was apparently due to the earlier state of boundary layer development under study.

Additional analysis for 30JUL in the upper flight legs showed potential temperature and vertical velocity fields to be 90^{o} out of phase (Fig. B2). The quadrature spectrum of these two variables was negative in the wave-like region and of significantly greater magnitude than the cospectra. This is what would be expected in a gravity wave situation because vertical velocity should lead the temperature change by 1/4 of a wavelength. The cospectral analysis done on 28JUL showed that only 1/3 of the w, θ correlations could be attributed to a wave-like flow. The remaining 2/3 was caused by some sort of forced lifting, which is attributed to shear instability over the Park.

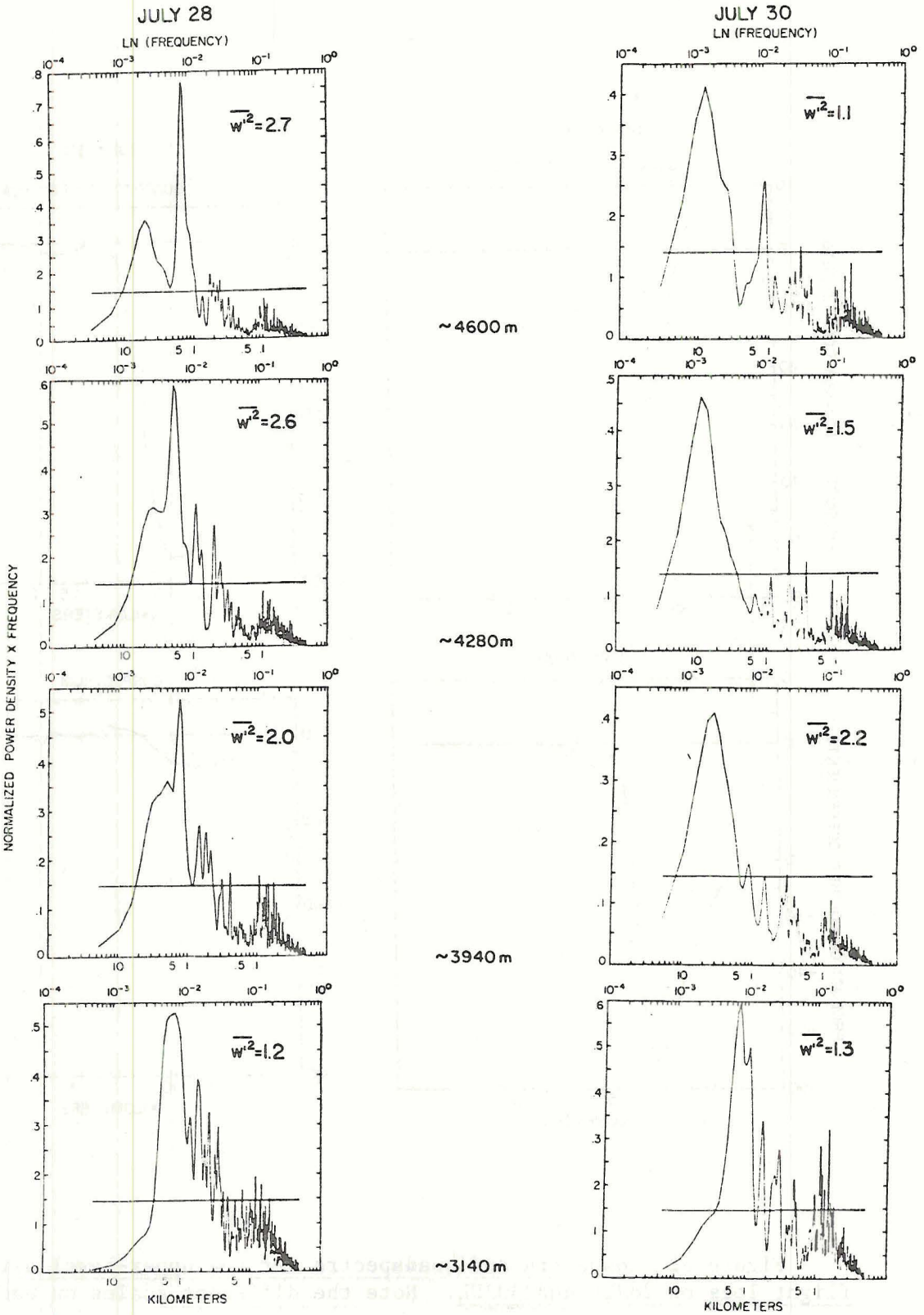

Figure B1 Power spectra of vertical velocity for 28JUL and 30JUL. Aircraft heights, from which the data are taken, are indicated in the center. All plots are normalized. The horizontal line in each plot represents the "no dominant scale" point below which the variance is considered to be insignificant.

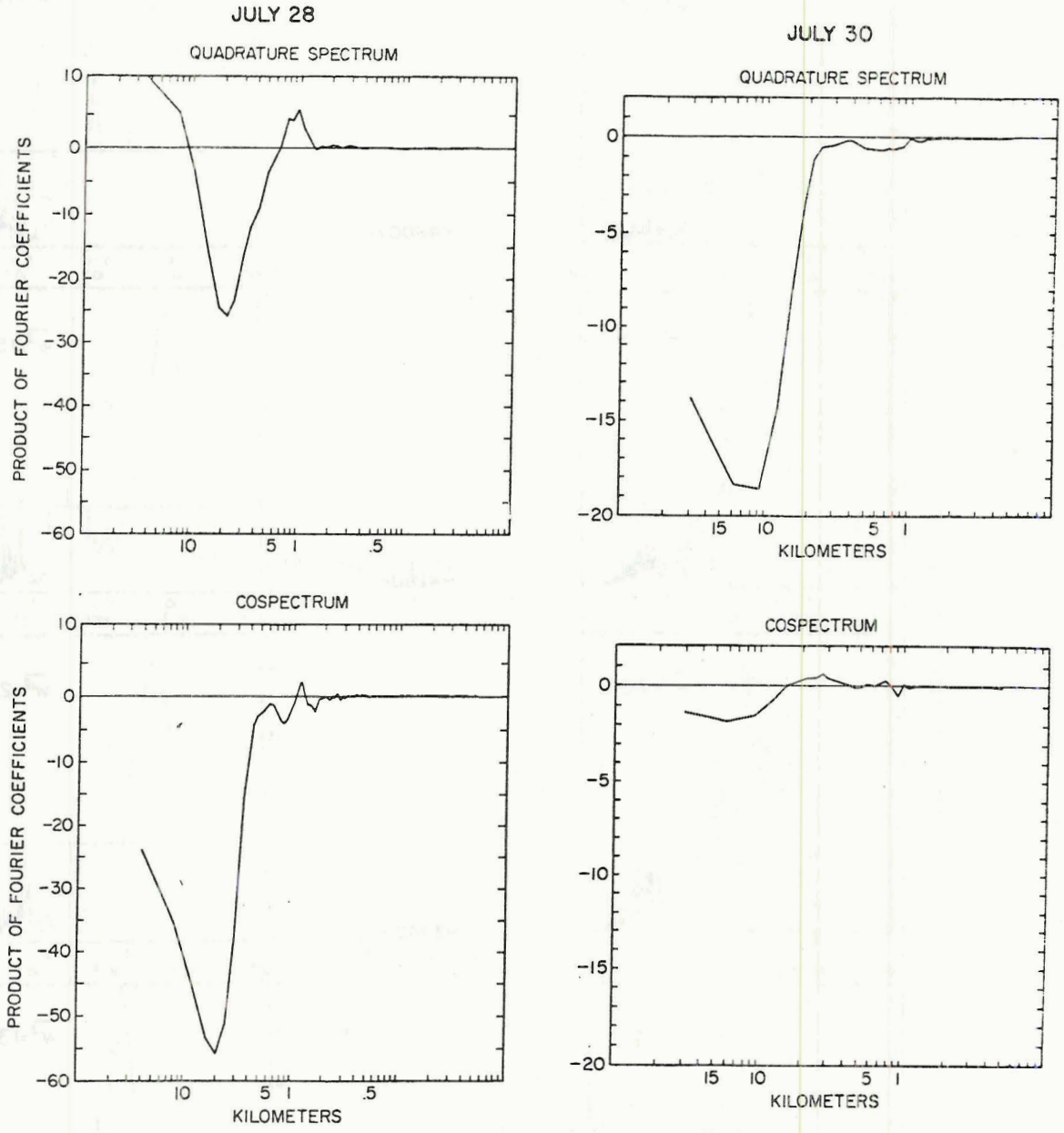

Figure B2 Cospectra and quadspectra for the upper-level aircraft flight legs on 28JUL and 30JUL. Note the different scales on each day.

The spectra of the lowest flight legs were similar in shape and magnitude on both days. A broad well-defined maximum at 1.25 km is apparent. Most of the variance was associated with the turbulence of the well-mixed air near Sheep Ridge.

14JUL and 15JUL

The vertical velocity spectral analyses for 14JUL isolated the cloud associated turbulence very well (Fig. B3). Despite the previously mentioned gust probe error on 14JUL, a spectral peak of 8.8 km seemed indicative of the cloudy area. Liquid water was observed by the Johnson-Williams (J-W) for about 6.5 km. Remembering that the J-W only measures cloud water drops and the actual turbulence associated with a cloud is of necessity larger than the visible cloud, this observation makes sense. Further, we are approximating a cloud form with a sine form and

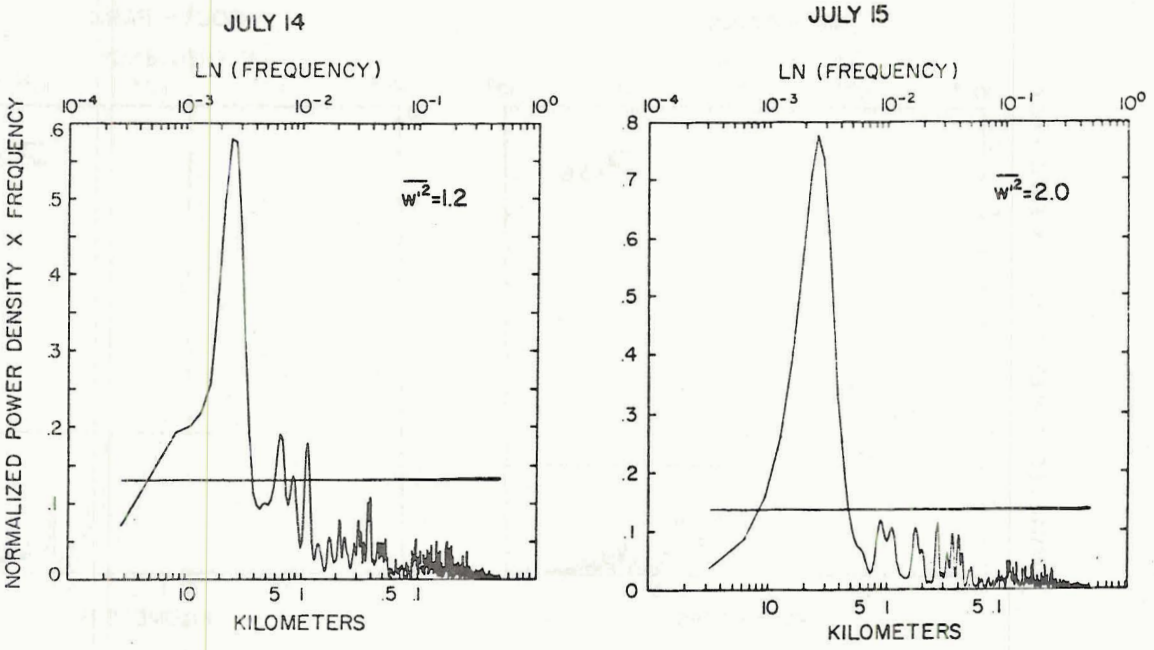

Figure B3 Power spectra of vertical velocity for the upper-level aircraft flight legs on 14JUL and 15JUL. See Fig. B1 for details.

the two are not necessarily the same. The vertical velocity spectrum on 15JUL is also capable of showing the cloud. It isolates a spectral peak at 4.2 km. Liquid water is observed for 3.5 km.

A comparison of above mountain vs. above Park variance was done for 15JUL indicating the tremendous point to point variability in statistical parameters on these days. While the general forms were similar (the dominance of energy at longer wavelengths) variance over the mountains, associated with the cloud, was 36x greater than over the Park (Fig. B4).

The mountainous sections, including the cloud area, typically contained over 90% of the total variance associated with vertical velocity. Contrasting 28JUL and 30JUL showed a different localization

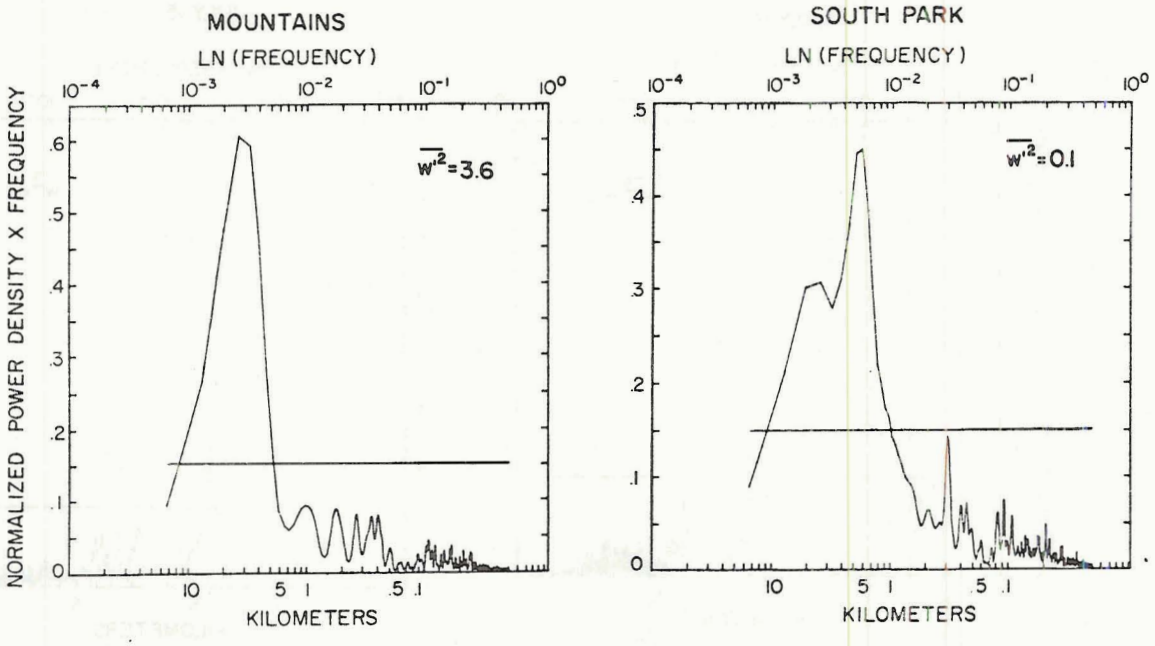

Figure B4 Power spectra of vertical velocity comparing turbulence above the mountains with turbulence over South Park on a convective day. The upper-level aircraft flight leg on 15JUL is used here. A cloud was present over the mountains.

of turbulence. Much of the turbulence was located downwind of the mountain crest.

The lowest-level spectra were difficult to interpret on both days. This was apparently due to the presence of a larger scale circulation pattern. However, a common peak near .85 km (containing most of the variance on 15JUL and a large portion on 14JUL) was noted. This might be more indicative of the boundary layer at this height as opposed to 1.25 km noted on 28JUL and 30JUL. The peak on 28JUL and 30JUL was under the influence of upper-level flow.

In summary, the power spectrum analysis showed that most of the vertical air motion, as measured by the variance, occurred on scales of motion greater than 1 km. Near the surface ($\sim$200 m AGL) significant motion was noted below 1 km as well. In order to resolve this motion, and attribute it to specific causes through use of the TKE equation, it is necessary to average on an appropriate scale of motion. We have chosen 1 km.

APPENDIX C

Method of Calculation of TKE Terms

Shear Production, Buoyancy Production, Advection & Horizontal u-Divergence

The TKE data are displayed for two scales of motion. The larger scale, which represents all wavelengths measurable by the aircraft, and the smaller scale which represents wavelengths less than 1 km.

The fluctuating quantities associated with the two scales of motion are calculated in different ways. For the larger scale, deviations are taken with respect to the entire flight leg mean. On the smaller scale, deviations are taken from the smoothed time series in which a cutoff wavelength of 1 km was used. The calculated terms, with the same definitions as were given for equations 1 and 2, are displayed below in Table C.1.

Table C.1 Calculated Terms of the TKE Equation

TKE terms	from Eq.2	Calculated Terms: all wavelengths	Calculated Terms: wavelengths less than 1 km
shear production	$-\overline{uw}\,\frac{\partial U}{\partial z}$	$-\{uw\}\,\frac{\partial U}{\partial z}$	$-\{u_s w_s\}\,\frac{\partial U}{\partial z}$
buoyancy production	$\frac{g}{T_v}\overline{wT'_v}$	$\frac{g}{T_v}\{wT'_v\}$	$g\left\{\frac{w_s T'_{vs}}{\{T_v\}}\right\}$
advection	$-\frac{U}{2}\frac{\partial \overline{q^2}}{\partial x}$	$-\frac{U}{2}\left\{\frac{\partial}{\partial x}\{q^2\}\right\}$	$-\frac{1}{2}\left\{\{U\}\frac{\partial}{\partial x}\{q_s^2\}\right\}$
horizontal u-divergence	$-\frac{1}{2}\frac{\partial \overline{uq^2}}{\partial x}$	$-\frac{1}{2}\left\{\frac{\partial}{\partial x}\{uq^2\}\right\}$	$-\frac{1}{2}\left\{\frac{\partial}{\partial x}\{u_s q_s^2\}\right\}$

A subscript s has been added to the smaller scale quantities to distinguish between the two types of fluctuating quantities. The brackets indicate smoothing to a cutoff wavelength of 4 km. Note that the overbars used in (2) have effectively been replaced by smoothing. That is, the local average is calculated as opposed to the entire flight leg average used in (2). Remember that the quantities calculated represent time series whereas the terms of (2) represent one value each.

Dissipation

It is possible to obtain an estimate of dissipation from the variance in the inertial subrange. Presumably the variance of the wind, as a function of aircraft measured frequency, is describable by the Kolmogorov equation

$$E(f) = \alpha(TAS)^{2/3} (2\pi)^{-2/3} \varepsilon^{-2/3} f^{-5/3} , \qquad (C1)$$

where $E(f)$ is the variance of a velocity component per unit frequency, α is a constant, TAS is the true air speed of the aircraft sensor, and f is the frequency. This should be true for scales of motion less than a wavelength of about 250 m. By considering a range of small scale motion corresponding to wavelengths from 20 m to 250 m, and knowing the variance of this range, an estimate of dissipation is possible. The variance accounted for in this range can be obtained by integration.

$$\int_{f=0.32}^{f=4} E(f)df = \alpha(TAS)^{2/3}(2\pi)^{-2/3}\varepsilon^{2/3} \int_{f=0.32}^{f=4} f^{-5/3}\, df \qquad (C2)$$

f=0.32 corresponds to a wavelength of 250 m, and f=4 to 20 m, for an aircraft speed of 80 m/s. The left side of (C2) is the variance accounted for by the range of the integration. Dissipation does not depend on the frequency so can be removed from the integral. The equation for dissipation becomes:

$$\varepsilon = 4.2 \frac{V^{3/2}}{TAS} \quad , \tag{C3}$$

where V is the variance, and an α of 0.5 has been used corresponding to the longitudinal velocity component.

An estimate of the variance at each data point can be obtained by high pass filtering the longitudinal velocity time series so that only frequencies greater than .32Hz are passed, and then squaring the terms. Dissipation is then calculated by applying (C3). Note that each data point is assumed to contain a spectrum of frequencies, predictable by (C1), that contribute to the variance. The data are then smoothed with the same filter used for the other TKE variables.

BIBLIOGRAPHIC DATA SHEET	1. Report No. CSU-ATSP-332	2.	3. Recipient's Accession No.
4. Title and Subtitle OBSERVED CHARACTERISTICS OF TURBULENCE IN THE ATMOSPHERIC BOUNDARY LAYER OVER MOUNTAINOUS TERRAIN			5. Report Date December, 1980 6.
7. Author(s) David C. Hahn			8. Performing Organization Rept. No. CSU-ASTP-332
9. Performing Organization Name and Address Department of Atmospheric Science Colorado State University Fort Collins, Colorado 80523			10. Project/Task/Work Unit No. 11. Contract/Grant No. NSF ATM-83361
12. Sponsoring Organization Name and Address National Science Foundation, 1951 Constitution Ave., NW., Washington, D.C. 20550			13. Type of Report & Period Covered Masters Thesis 14.

15. Supplementary Notes

16. Abstracts

The location and development of turbulence in the morning hours of boundary layer development over mountainous terrain is examined. NCAR QueenAir aircraft data is the primary source of data. The days are analyzed by making use of cross-sectional plots of potential temperature, mixing ratio, and various terms of the TKE equation. Four case study days are presented which illustrate important features on two types of days observed on a broad and elevated plain, bordered by relatively high mountain ranges, in central Colorado. One type of day is characterized by moist light winds above ridgetop. Clouds originating over the mountain slopes, apparently the result of the convergence of upslope winds, can act as a coupling mechanism between the above-ridge-top and below-ridge-top air masses. Higher momentum air aloft can be brought down to the surface as a gust front by turbulent mixing and evaporational cooling. The second type of day is characterized by strong dry westerly winds at mountain ridgetop that, by midafternoon, work their way down to the surface and the boundary layer becomes well-mixed and dry. The strong winds aloft reach the surface when below-ridge-top air, being well-mixed due to surface heating, and the above-ridge-top air, being well-mixed due to shear instability, approach the same potential temperature.

17. Key Words and Document Analysis.

1) Convective Boundary Layer, mountainous terrain
2) Turbulent Kinetic Energy Analysis
3) Upslope-Upvalley Winds

18. Availability Statement	19. Security Class (This Report) UNCLASSIFIED X	21. No. of Pages 104
	20. Security Class (This Page) UNCLASSIFIED	22. Price

FORM NTIS-35 (Rev. 3-72)